Design of a magnetometer using multiple COTS sensors for attitude control

T.Buijs

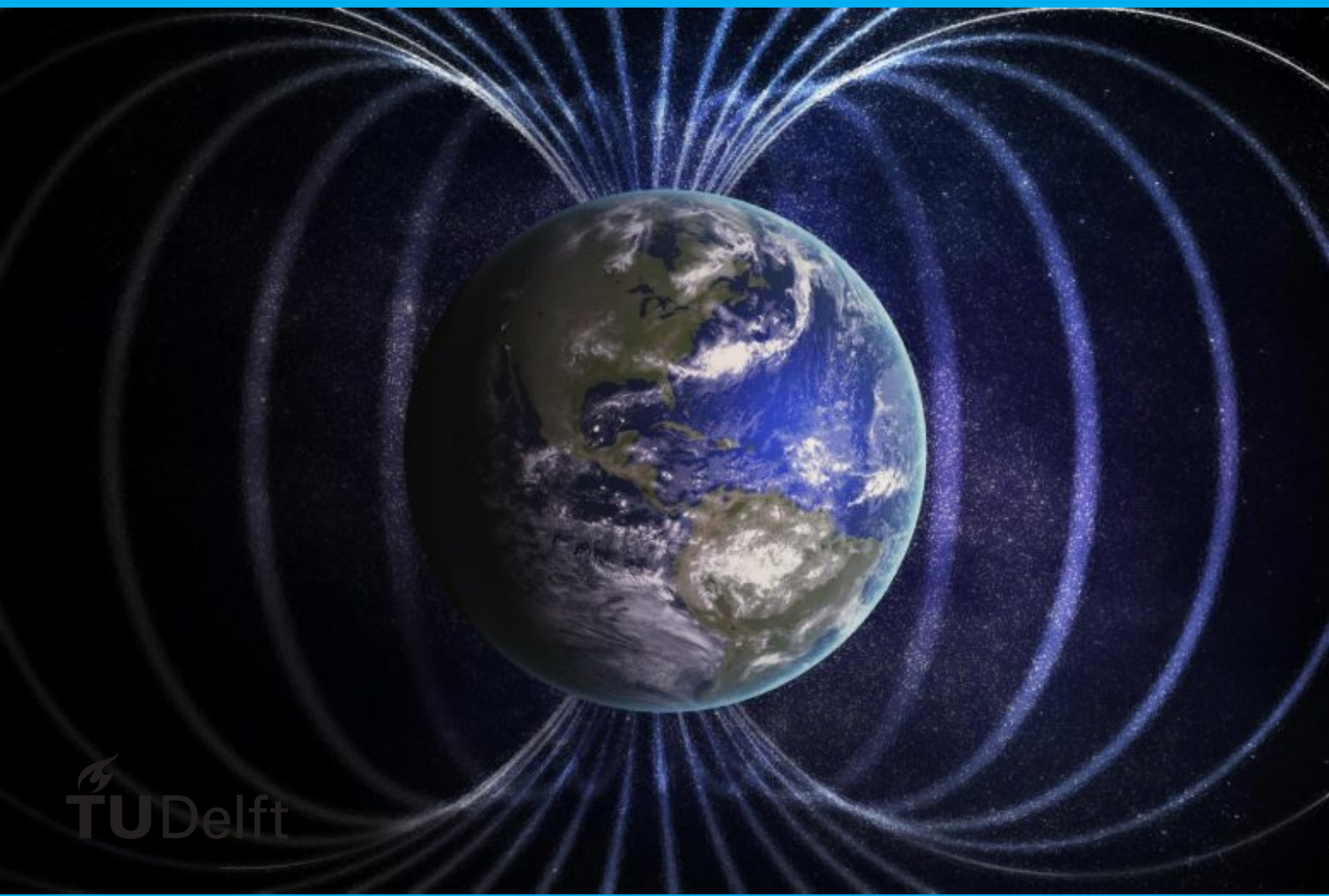

Design of a magnetometer using multiple COTS sensors for attitude control

by

T.Buijs

to obtain the degree of Master of Science
at the Delft University of Technology,
to be defended publicly on Friday July 16, 2021 at 9:00 AM.

Student number:	1506811	
Project duration:	March 19, 2020 – July 16, 2021	
Thesis committee:	Ir. J. Bouwmeester,	TU Delft, supervisor
	Prof. Dr. E.K.A Gill,	TU Delft
	Dr. ir. W. van der Wal,	TU Delft
	Ir. S. Speretta,	TU Delft

TU Delft

Abstract

The Earth magnetic field is used in many applications such as navigation. Magnetic field sensors are mainly used on satellites for attitude control and in limited missions as scientific instruments. These magnetic field instruments are: specifically designed for the mission, expensive and/or require knowledge of the magnetic noise sources present in the complete satellite. Therefore a proposal was made of a magnetic field instrument consisting of multiple COTS sensors that doesn't require knowledge of the satellite and could be placed inside the satellite. Two measurement processing methods were used to test the effectiveness of such a system. Both methods were tested simultaneously testing if an ideal sensor placement exists and the effect of the number of sensors was considered.

The requirements for a sensor system to be used for attitude control and/or scientific purposes are as follows. Firstly for both kind of systems (attitude or scientific) a measuring frequency of at least 10 Hz is preferred. Secondly the sensitivity for an attitude control instrument needs to be 50 nT or less and for a scientific instrument 0.5 nT or less. Lastly the accuracy for an attitude control instrument needs to be 50 nT and/or 3 degrees or less and for a scientific instrument 0.5 nT or less.

The two measurement processing methods used in this research are the averaging method which averages the measurements of multiple sensors and the SOE method which uses a system of equations to determine the location, direction and magnetic strength of the noise sources. It was found that the SOE method can maintain an accuracy of less than 50 nT if a determined or overdetermined system of equation could be realized. This can only be the case if the number of sensors is $3\frac{1}{3}$ times as much as the noise sources which is not feasible for a satellite. Another limitation of the SOE method is the computational time which is at least 7 order of magnitude bigger than the computational time of the averaging method. The averaging method can produce better accuracies than 50 nT and/or 3 degrees but is very dependent on the sensor placing and less dependent on the number of sensors. An increase in accuracy can only be gained if all sensors are placed far from the biggest noise sources and there should be a minimum distance from small noise sources. If one of the sensors doesn't adhere to this then there is a decrease in accuracy and a single sensor could perform better. The sensitivity of a sensor system improves when multiple sensors are used.

Preface

From a very young age I got interested in engineering and always tried to investigate each device or construction to determine their workings. My first fascination with space engineering started while reading the TinTin comic destination moon and seeing the rocket blueprint. I didn't even consider another study and chose for aerospace engineering and a master related to space engineering even before I began my studies. During my studies I came up with some difficulties but the constant support of my parents and eventually my girlfriend and future wife helped me push through and finally finish this thesis. I also like to thank Jasper Bouwmeester who guided me during my thesis even though some difficulties arose.

T.Buijs
Dordrecht, July 2021

Contents

List of Symbols

Symbol	Description	Default Unit
A	Amplitude dipole change	Am^2
A	Correction matrix	-
B	Magnetic field strength	T
C	Bias correction	T
C	Calibrated magnetic field vector	T
D	Measured magnetic field	T
K	Kallman gain	-
N	Number	-
M	Correction matrix	-
P	Extrapolated estimated uncertainty	T
R	Distance	m
S_{on}	On/off state constant (1 or 0)	-
V	Induced voltage	V
a	Correction factor	-
b	Multiplication factor	-
b	Correction vector	-
c	Constant	H*m
f	Angular frequency	$\frac{rad}{s}$
i	Current	A
n	Unit vector	-
m	Dipole moment	Am^2
q	Process uncertainty	-
r	Radius	m
r	Measurement uncertainty	T
t	Time	s
x	Distance	m
x	Predicted value	T
y	Distance	m
z	Distance	m
z	Measured value	T
θ	Polar angle	°
μ_0	Magnetic constant	$\frac{Tm}{A}$
ϕ	Azimuth angle	°

List of Abbreviations

Abbreviation	Description
ADCS	Attitude Determination and Control System
AHP	Analytic hierarchy process
AMR	Anisotropic Magnetoresistance
B.C.	Boundary conditions
COTS	Custom Of The Shelf
DOT	Design Option Tree
GMR	Giant Magnetoresistance
LEO	Low Earth Orbit
SOE	System of equations
SPI	Serial Peripheral Interface
SEOMM	System of equations using multiple measurements
SQUID	Superconducting quantum interference device
TMR	Tunnel Magnetoresistance

List of Figures

List of Tables

1 Introduction

The Earth magnetic field has been important for humankind for a long time. One of the most important uses is for navigation, which started with the use of a compass. Since satellites were sent to space, the Earth magnetic field is also used for satellite attitude control. To accomplish this, a magnetic field instrument is placed on a satellite to measure the Earth magnetic field and then compare the measurements to a database with known magnetic field values. The database is created with multiple measurements over time using scientific magnetic field instruments on Earth, in the sky and in space.

The database needs to be updated regularly because the Earth magnetic field is constantly changing. Big changes of the Earth magnetic field can be related to the internal working of the planet itself and happen over a long period of time and small changes which are caused by natural phenomena such as solar particle radiation (space weather) and manmade phenomena such as satellites happen in a small time period. To measure these effects, accurate measurements need to be done by scientific magnetic field sensing instruments. Several missions that use scientific magnetic field instruments have been or are in orbit. The few missions out there provide a good static model of the magnetic field, which is used for attitude control but more satellites are needed to create a dynamic model.

Satellites themselves produce an electromagnetic field and thus produce interference. To avoid this, most scientific magnetic field instruments are placed on booms outside of the satellite and/or the satellites are designed for magnetic cleanliness. This makes these missions to measure the magnetic field, expensive and thus only a handful of missions are in use today. Satellites are also getting smaller like cube and picosats. Due to this fact electronics are closer to each other and solar cells which can cause large magnetic interferences are more often on the body of these small satellites. Magnetic cleanliness is therefore harder to achieve because every current produces an electric field. These reasons would result in a necessity of a Magnetic field instrument that is low cost in both financial and technical resources and should be easy to install. In this research an instrument will be designed and tested to fulfill this necessity.

The thesis starts with a problem statement in Chapter 2 which introduces the current technologies and ends with a research question and requirements for the sensor system. Chapter 3 discusses the available sensors and the sensor selection for the magnetic field instrument after which a configuration is discussed in Chapter 4. Two different processing techniques for the measurement data are discussed in Chapter 5. Both the methods are verified with a simulation in Chapter 6 after which a thorough simulation of the sensor system is performed in Chapter 7. The calibration of the sensors is done in Chapter 8. The test set-up and the test results of the complete system are discussed in Chapters 9 and 10 respectively. The results of the research are detailed in the conclusion, followed by recommendations for future research in Chapter 11.

2

Problem analysis

Magnetic field instruments have been used for many goals. In satellites they are mainly used for attitude control or as scientific instruments. This means there already exists similar instruments to the one that will be designed in this report. Therefore this Chapter will first discuss the current technologies and techniques after which a research question will be presented finalizing the chapter with some high level requirement for the magnetic field instrument.

2.1. Current technologies

The magnetic field instruments used on satellites are primarily used to measure the Earth magnetic field (EMF), of which the magnetic field strength is very small. The measuring range needed for a magnetic field sensor to be able to sense the complete EMF should be +/- 60000 nT as stated by Miles Et al.[7] and Friis-Christensen Et al. [8]. These articles also mention that a sensitivity of 0.5 nT is necessary for a scientific research instrument in LEO (Low Earth orbit), which is also mentioned by Diaz-Michelena [9]. LEO is mostly used for measuring the EMF because the magnetic field strength decreases exponentially with increasing distance from Earth, this would mean more sensitive equipment would be needed at higher altitudes. The sensitivity of an attitude sensor will be between 6.7 and 50 nT, the actual sensitivity depends on the pointing accuracy needed for a satellite. The sensitivity for the attitude instrument is derived from Table 2.1, which shows the magnetic instruments used in previous missions. Single three-axis magnetometers should be able to achieve an attitude accuracy between 0.5 and 3 degrees as proven by Psiaki [10], Ma Etal [11] and Sugimura Etal [12]. The accuracy for a scientific instrument is 0.5 nT which is based on the Magsat instrumentation [13]. The accuracy of the attitude control instrument is assumed to be 50 nT if the same ratio between attitude and scientific sensor sensitivities is used.

Table 2.1: Reference missions.

Mission	sensor / developer	purpose	kind	resolution	range [+/-]	sample rate [1/s]	source
ZDPS-1A	Honeywell HMC2300	attitude control	magneto-resistive	6.7nT	0.2 mT	10-154	Xiang Et al. [14]
Ex-Alta1	custom design	Scientific	fluxgate	35 pT	65536nT	100	Miles Et al. [7]
Ulysses	custom	scientific	vector helium	32 pT	65.52 nT	2	Balogh Et al.[15]
Ulysses	custom	scientific	fluxgate	3.9 pT 31.2 pT 1000 pT	8 nT 64.00 nT 2048 nT	2	Balogh Et al.[15]
Swarm	DTU Space	scientific	fluxgate	0.0625 nT	65536 nT	50	Swarm [16]
Swarm	CNESS	scientific	Optically pumped	0.3 nT	65000 nT	50	Swarm [16]
MagSat	custom	scientific (vector)	fluxgate	3 nT	64000nT	-	Acuna Et al.[13]
DTUsat	Honey well HMC1021	attitude control	magneto-resistive	50 nT	100000nT	-	Krogsgaard Et al. [17]

A problem that occurs is that the magnetic noise can be bigger than the sensitivity of the instrument. The magnetic noise can be caused by multiple sources but the main source is usually the satellite itself. The magnetic interference caused by the satellite depends heavily on the design of the satellite and the equipment present inside of the satellite. For the ZDPS-1A satellite an extensive research was done into the magnetic interference caused by different elements present in the satellite (Xiang Et al. [14]). In the research by Xiang Et al. the noise was split in three different categories. The first category is the total static noise which has a value between 3040-7200 nT. The second category is the dynamic magnetic field which was in the order of 10 to 50 nT. Lastly is the noise generated due to solar cells which could be as much as 3774.8 nT/A as can be seen in Figure 2.1. Note that in Xiang's research the word bias is used which in this research is considered noise. In this case the ZDPS-1A is a picosat where every system is close to each other and the sensor was placed close to a solar cell which caused most of the noise. Although this is a specific case and as mentioned above the amount of interference depends largely on the power consumption of the other systems and their distance to the instrument, these values give a good indication of the expected size of the magnetic interference's and the problem that the signal to be measured is smaller than the noise level. The noise discussed is only one of the sources that can be encountered. Although there are many noise sources, the one caused by the satellite itself is one of the biggest and most varying. The noise sources can be divided in different categories:

- Environmental Noise: All interference generated outside the satellite.
- Static systems: This includes measurement bias and systems that have a constant power usage.
- Dynamic systems: Magnetic field changes caused by other systems due to changing power needs.
- Permeable material: These materials have a magnetic field of their own or assume a magnetic field in the presence of another field
- Temperature: Measurement errors caused by the temperature of the sensor

mG

Bias vector		X	Y	Z
Static bias $\boldsymbol{b}_{sta}$		72.0	52.0	30.4
Dynamic bias $\boldsymbol{b}_{dyn}$	TTC A/B switch	0	−0.1	0.5
	OBC A/B switch	−0.2	0	0
	Sensor II on/off	0	−0.1	0.1
	Payload on/off	0	0	0.1

(a) Different systems

mG/A

Solar panel	Magnetometer axis		
	X	Y	Z
$+X$	−6.315	1.707	−3.029
$-X$	2.064	−0.394	−1.640
$+Y$	4.701	−0.125	3.155
$-Y$	6.026	−2.982	5.068
$+Z$	−37.748	−3.960	−1.257
$-Z$	2.786	0.833	0.872

(b) Solar panels

Figure 2.1: Noise generated by ZDPS-1A satellite ([1])

To minimize the effects of the noise sources different techniques and designs are being used. A design option that is frequently used for scientific measurements, is placing the magnetic field instrument on a boom away from the satellite. An example of such a system is present on the swarm ([16]) and Ulysses mission ([15]). Another way to minimize the noise is to place the sensors away from other equipment within the satellite, if this is possible. In some cases two different sensors are used for the same purpose as seen in the Ulysses mission. The magnetometer can also be modified with feedback coils to generate a noise compensation field. This is done to suppress ambient magnetic fields with higher spatial frequencies as discussed by Krogsgaard Et al. [17].

All the techniques mentioned are solutions based on hardware but there are also techniques that involve software. Measurement compensation can also be performed as shown by Xiang Et al.[1] and Miles Et al. [7]. In both cases an extensive research is performed to identify all the noise sources present in the satellite, Figure 2.1 shows an example of the results. The knowledge gathered will be combined with the measurement to filter noise. To have an accurate reading the study of the components needs to be done both on earth and space.

2.2. Research question

Magnetic instruments can be used in different ways and for different purposes as stated in the previous section. For scientific instruments this often means that the instrument is outside the satellite and attitude sensors are mostly inside. The sensors themselves are often specifically designed for each mission (more for scientific instruments than for attitude control). Even if COTS are used, they need to be modified, are expensive or an extensive research of all other components will be necessary to accommodate the COTS. An example of a COTS magnetometer would be the NMRM-Bn25o485 which costs €15000 [6], which is used for attitude control. While the use of multiple magnetometers is used in the medical field ([18]), in satellite missions at most two sensors are used for the same purpose.

All of this leads to the following research question:

Is it possible to create a magnetic field instrument consisting of multiple magnetometers from low cost COTS components which can provide relevant data for attitude control and/or scientific data and can be positioned inside a satellite without special modifications?

Some of these points need to have some explanation which are:

- Low cost COTS: The price for the total instrument should be low. For an attitude control instrument the cost should be lower than €2000 and for a scientific instrument it should be lower than €10000.
- Position: Some instruments are placed outside the satellite to reduce the noise effects (especially scientific instruments) but because this technique is already used on current missions this location will not be of interest to the research and is closely related to the next point.
- Special modifications: In this research question special modifications are measures taken in the design of the satellite itself to reduce noise by placing instruments on a boom. Also techniques that involve extensive research of the satellite will be considered in this category.

The research question can be divided in the following parts:

- The number of sensors:
  - What is the effect of multiple sensors?
  - Is there a number of sensors at which adding more won't affect the outcome?
- The position of the sensors:
  - What is the effect of sensor placement?

2.3. Primary requirements

The research question is introduced in the previous section and gives the goal of the research, but to be able to verify or validate the question it will be broken up in different parts as requirements for the magnetic field instrument. Every requirement will be given a code for traceability and ease of reference. All requirements can be found in Appendix A. The highest level are the main requirements where all subsequent requirements will relate to. The main requirements are as follows:

- NAMG: The magnetic field instrument should be able to measure the Earth magnetic field in space
- NMAG-1: The magnetic field instrument should be able to measure the Earth magnetic field in space in a technical feasible manner
- NMAG-2: The magnetic field instrument should be able to measure the Earth magnetic field in space within constraints

The highest requirements just relate to the ability of creating a working magnetic field instrument within the time limit and budget. These are elaborated in the sub-main requirements:

- NMAG-1a: The magnetic field instrument should be able to measure both direction and the size of the magnetic field

- NMAG-1b: The magnetic field instrument should be made using only COTS products
- NMAG-1c: The magnetic field instrument should be able to fit in a microsat
- NMAG-2a: The magnetic field instrument should have a low cost
- NMAG-2b: The creation and testing of the instrument should comply with the designated deadlines

Note that NMAG-1c is underlined, this is because it is a possible goal if the results of the research will allow it. To do a good verification of the instrument actual numbers are needed. These values can be derived from the information presented in Section 2.1. The requirements for both the attitude control and scientific instrument will be presented separately so that both systems can be verified separately. These lead to the instrument level requirements:

- NMAG-1a-INSTR1: The magnetic field instrument should have a measuring range of +/- 100 μT
- *NMAG-1a-INSTR2: The magnetic field instrument should have a sensitivity of a maximum 50 nT if used for attitude control*
- *NMAG-1a-INSTR3: The magnetic field instrument should have a sensitivity of a maximum 0.5 nT if used as a scientific instrument*
- NMAG-1a-INSTR4: The magnetic field instrument should be able to perform at least 10 samples per second
- NMAG-1a-INSTR5: The magnetic field instrument should have a pointing accuracy of atleast 3 degrees if used for attitude control
- NMAG-1a-INSTR6: The magnetic field instrument should have an accuracy of atleast 50 nT if used for attitude control
- NMAG-1a-INSTR7: The magnetic field instrument should have an accuracy of atleast 0.5 nT if used as scientific instrument
- NMAG-2a-INSTR1: The magnetic field instrument should cost less than €10000 if it is used as a scientific instrument.
- NMAG-2a-INSTR2: The magnetic field instrument should cost less than €2000 if it is used for attitude control

2.4. Methodology

The research question presented in Section 2.2 relates to the design of a magnetic field instrument. Designing an instrument by itself can be done using multiple methodologies but for this research the instrument needs to adhere to certain criteria, the ability to be used as an attitude and/or scientific sensor. The criteria can be found in Section 2.3. To make a good analysis actual values are needed and thus a Quantitative method will be used.

The research question mentions that multiple magnetometers will be used. For the final instrument design it is intended to have eight sensors, one for each corner of the satellite. Assuming that the satellite has a box shape this would fill each corner, which most cube and nanosats have. The corners are chosen because most of the equipment is usually on the sides or middle of the satellite and therefore not close to major noise sources. This is a preliminary design and will be finalized when the effect of the number of sensors and their location is tested.

The instrument consists of a hardware and a software part. The software uses the measurements gathered from the hardware to calculate the ambient magnetic field and eliminate the interference from the magnetic field caused by the noise sources. A main part of the magnetic field instrument is the sensors which will be chosen from existing magnetometers. To choose a sensor research will be performed of the existing magnetometers after which a comparison will be done. This research is performed in Chapter 3. The selection of the other components will be discussed in Chapter 4.

The next step is designing the software, for this several methods for filtering the ambient magnetic field will be proposed. An experimental approach in the form of simulations will be used to select a method/methods

for the final design. Except for the method selection, the simulations will be used to analyze the effects of the number of sensors and their location. This can be found in Chapters 5 to 7.

The results of the simulations will be used to make a final design for the magnetic field instrument and afterwards to construct it. The final design will be tested with an experimental approach with a physical test set-up. The test set-up and the test itself will be discussed in Chapters 8 to 10.

The methodology used during this research is therefore a hybrid between two quantitative methods. Namely using existing data to select the sensors and experiments to prove the effectiveness of the magnetic field instrument.

3

Sensors

The magnetic field sensor also named magnetometer, will be the main component of the instrument. Therefore research is performed, on the different types of sensors available in Section 3.1. Thereafter in Section 3.2, a search is performed for relevant available sensors that comply to the requirements set in Section 2.3 finishing the chapter with trade-off between optional sensors in Section 3.3.

3.1. Types of sensors

Magnetic field sensors can be divided into different categories depending on the principle used to measure a magnetic field. Figure 3.1 displays all the available types of sensors in a design option tree.

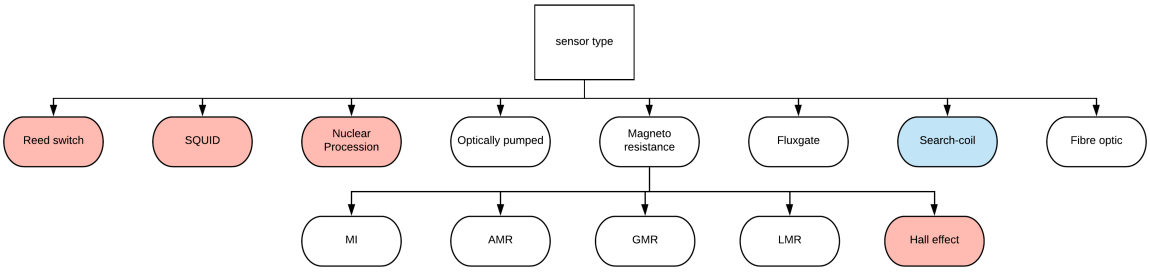

Figure 3.1: Design option tree showing the different magnetic sensor families

Some of the options shown in Figure 3.1 are displayed in different colours. The red coloured sensor options will not be viable for this research. The Search coil magnetometer is coloured blue because it can't be used as a standalone sensor but might be used in combination with others. The other types of sensors should be able to function within the boundaries of the requirements of the instrument, as described in Section 2.3. The following sections discuss the strengths, weaknesses and usefulness of the different sensors.

3.1.1. SQUID

Superconducting quantum interference device (SQUID) is one of the most sensitive flux detectors and is able to detect fields as small as 10^{-15} T. As stated in the name, it makes use of superconductivity, a state that is only achieved at low temperatures. These low temperatures depend on the materials used, but the highest temperature at which the sensor works is around 90 K as mentioned by Katila [19]. Therefore the sensors need to be cooled, which is usually done by compounds such as liquid helium. The cooling system needed for SQUID sensors makes these sensors not applicable for this research because a cooling system will increase complexity and mass.

3.1.2. Nuclear precession magnetometer

Nuclear precession magnetometers polarize the atomic nuclei of a substance, causing the nuclei to precess temporarily around a new axis. As the behavior of the nuclei turns to normal, the frequency of the precession

of the nuclei is measured, and can be correlated to magnetic flux density. Helium-3 or a hydrogen based liquid such as kerosene (proton precession) is used inside the sensor as mentioned by Waters Et al [20]. A proton precession magnetometer uses less power than a Helium-3 magnetometer. An example of a proton precession sensor is the GSM-8 which consumes 8 J per reading. According to requirement NMAG-1a-INSTR4 a sample rate of 10 Hz is needed, this means a power usage of 80 W is to be expected. This is not ideal for a micro-sat especially if multiple sensors are considered.

A third option is using the Overhauser effect, which makes use of a special chemical dissolved in a hydrogen-rich liquid. The electrons of the special chemical are exited using radio frequency magnetic field. Such a system uses only a couple of Watts to perform measurement ([21]). This option will be of limited use because of its size. For example the GSM-19 sensor unit is a cylinder with a height of 175mm and diameter of 75 mm. These properties of this sensor makes it not ideal for a micro-sat and thus this sensor will not be considered further.

3.1.3. Optically pumped

An optically pumped sensor uses a light source, a contained volume of vapour and a light detection system to measure a magnetic field. The light source is usually a laser and the detection system can be a photo-diode. The laser emits electromagnetic waves that establish a magnetically sensitive state in the vapour by transferring polarised light to the vapour. This state of the vapour is referred to as optical pumping. Once in this state the polarised light will pass through the vapor and becomes detectable by the sensor instead of being absorbed by the gas. The optically pumped state is very sensitive to magnetic fields and the optically pumped state needs to re-establish with every change in this field, causing fluctuations in the output of the sensor. These sensors are able to measure very weak magnetic fields: they have a femtotesla sensitivity as described by Tierney Et al [22].

The sensor will be able to achieve the sensitivity necessary for the instrument but is dependent on a vapour. The vapour properties for magnetic sensing depend on the kind of molecule, the temperature and pressure. The last two properties lead to a strict temperature requirement and/or good knowledge about the thermal properties of the gas in combination with a thermal sensor. Swarm used such a sensor in their mission [16].

3.1.4. Fluxgate

A fluxgate magnetometer consists of two highly permeable alloy cores with copper wires wound around it. These wires are wound in a mutually opposite direction as seen in Figure. In this example the cores are ring cores. Alternating currents are driven through these winding's, also called drive windings. This causes the generation of alternating magnetic fields which are mutually opposing. A secondary winding called the sense winding is wound around both cores to generate a current in the presence of an external magnetic field. In the absence of an external magnetic field there will be no current. The current is generated because an external magnetic field will reinforce the magnetic field in one core while simultaneously weakening the other one resulting in a net non-zero flux as described by Banerjee Et al [2].

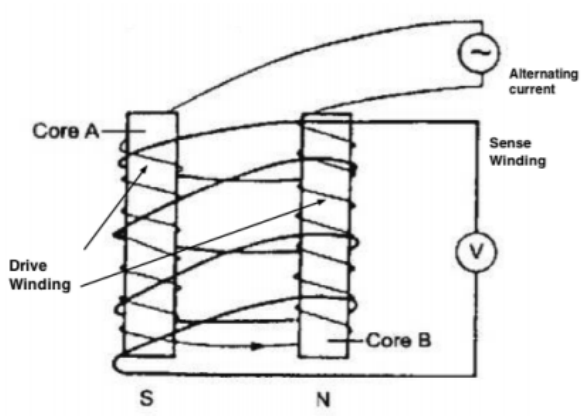

Figure 3.2: Workings of a fluxgate magnetometer [2]

Fluxgate magnetometers are able to measure variations in the order of 0.01 nT and can have a large measuring range as can be seen in Table 2.1. The Table also shows that these sensors are used on multiple missions for magnetic field sensors as is needed in this research.

3.1.5. Search-coil

A search-coil magnetometer is one of the easiest sensors to produce because it consists of a wire turned in a loop creating a spiral. The spiral consists of a great number of loops even thousands of loops with or without a high permeability core in the middle. Comparatively a coil with a high permeability core needs a shorter length to have same measuring results. A search-coil antenna works due to Faraday's law of magnetic induction which states that a loop of wire with a time-varying magnetic field passing through it will have a time-varying voltage induced around it. The induced voltage can be calculated using Equation 3.1 and 3.2 where the latter is a rewritten version of the former. ([23], [24])

$$V = -c\frac{d}{dt}(\boldsymbol{B} * \hat{\boldsymbol{n}}) \tag{3.1}$$

$$V = -c(\boldsymbol{B} * \frac{d\boldsymbol{n}}{d\boldsymbol{t}} + \boldsymbol{n} * \frac{d\boldsymbol{B}}{d\boldsymbol{t}} + \boldsymbol{u} * \nabla[\boldsymbol{B} * \boldsymbol{n}]) \tag{3.2}$$

In these equations V is the induced voltage, c is a constant that depends on the area of the loop and on properties of the core material, $\boldsymbol{B}$ is the magnetic field vector, $\boldsymbol{n}$ is the unit vector along the axis of the coil and $\boldsymbol{t}$ denotes the time.

The induced voltage in the coils is an effect of a time varying magnetic field as seen in the equations. Equation 3.2 can be divided into three parts. The first term represents the voltage induced by the angular motion of the coil which is used on spinning spacecraft to measure the background DC magnetic field. The second term relates to the magnetic component of electromagnetic waves and the third term relates to the convective motion of a coil with velocity $\boldsymbol{u}$ relative to the magnetic field $\boldsymbol{B}$. The Earth magnetic field is mostly constant and therefore will have a negligible effect on the induced voltage. The constant part of the magnetic field can still be measured if a spinning satellite is considered, but this is only useful to satellites with instruments that don't need a static platform. Because of this search-coils will not be useful for this study as a main sensor.

3.1.6. Magneto resistance

Anisotropic magnetoresistance (AMR), and Giant magnetoresistance (GMR), and Hall effect, and Tunnel magnetoresistance (TMR), and Magnetic inductance magnetometer are based on the magnetoresistance as stated in the names. Magnetoresistance is the tendency of materials to change its electrical resistance in an external magnetic field. Ferromagnetic materials are usually used in one way or another.

While the basic principle is the same as explained in the aforementioned sensors, the way how it is applied is different. The AMR uses one layer of ferromagnetic material where a dependence of electrical resistance on the angle between the direction of electric current and direction of magnetization can be observed. This makes these kinds of sensors ideal to sense the direction of the magnetic field. Of course these sensors are also able to measure the strength of the field.

The GMR magnetometers are made up of several layers of ferromagnetic materials and between these layers non-magnetic conductive layers are used. Because of the multiple layers the sensor can achieve a higher resolution compared to the AMR but are less effected by the direction of the field. Although the GMR has giant in its name they are usually chip-sized components.

The TMR has almost the same design as the GMR, one of the main differences is that the TMR has an insulator film instead of a non-magnetic conductive layer. The sensitivity and accuracy of a TMR are better than the GMR.

The Hall effect sensors conduct a signal when an outside magnetic field passes a certain magnetic field density therefore they function mostly the same as a switch.

Magnetoresistive magnetometers are used in multiple space missions, some of them are mentioned in Table 2.1 where they mostly are used for attitude determination.

The development in MI (magneto impedance) sensors has produced more sensitive sensors but are not readily available at the time of writing this research as described by García-Arribas ET AL. [25]. In the future these kinds of sensors might replace the more conventional AMR and GMR sensors.

3.1.7. Fiber-optic

A fiber-optic magnetometer makes use of an optical fibre with a laser on one end and a light sensor on the other. The optical fibre is surrounded by a magnetostrictive jacket. A magnetostrictive material changes shape in the presence of a magnetic field. This means if a change of magnetic field happens near the magnetostrictive jacket, the optical fibre length changes. The change of length is measurable due to phase shifts of the light at the sensor end. A schematic diagram of a fiber-optic magnetometer can be seen in Figure 3.3. The diagram shown was used for the first successful tests on such a sensor done by Dandridge ET AL.[3].

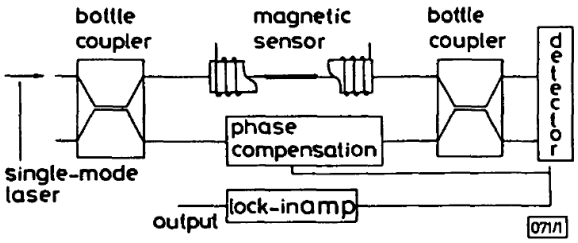

Figure 3.3: Schematic diagram of fibre-optic magnetic sensor system as visualized by Dandridge Et al [3]

Most of these available sensors are focused on the magnetic intensity and have a high sensitivity. In recent years investigations were done so that these sensors could also be used as vector-based sensors so that the intensity and direction of a magnetic field could be measured simultaneously. One of these investigations was successfully done by Yin Et al [26] and a sensor was created with a measurement error of $\pm 1.9^{\circ}$

3.1.8. Reed Switches

Reed switches are switches that react to the presence of a magnetic field. They consist of two rods of which at least one rod is made out of a ferromagnetic material in a closed glass tube. These rods come together when a magnetic field is applied. Because this is just a switch, it will not be of interest in this research.

3.1.9. Magnet

The simplest magnetic sensors is a compass consisting of a magnetized needle which can show the direction of a magnetic field. A compass is not able to determine the strength of a magnetic field. Thus it will not be considered for further research.

3.2. Available sensors

The possible types of magnetometers that can be used are identified in the previous section. A list of possible COTS sensors can now be created. For sensors to be applicable for the research they need to comply to some conditions. These conditions were derived from the requirements NMAG-1a-INSTR2 and NMAG-1b. The sensors must be COTS products and must be ready to use. The other condition would be that the sensor needs to have a sensitivity of 50 nT or lower so that the instrument would be able to achieve the NMAG-1a-INSTR2 requirement and can be used as an attitude sensor. The cost of the sensors cannot exceed the total cost requirement of the instrument, which is stated in the requirements NMAG-2a-INSTR1 and NMAG-2a-INSTR2 which state an instrument cost of €10000 for a scientific instrument and €2000 for an attitude control instrument respectively. Most of the cost will consist of the sensors but there must be room for other equipment, therefore only 80 % of the cost will be used for the sensors. The viable sensors that can be bought are displayed in Table 3.1. The last date of the search was in 05/2020, sensors available after this date are not considered.

During the search the names of the sensor types were used such as "Fluxgate" to find all available sensors also the general terms magnetic sensor and magnetoresistor were used. After that online stores such as Farnell were searched for all their magnetic sensors through their shop interface. The sensors included in the table comply to the requirements mentioned above. This means sensors that need to be specially ordered or still need a circuit designed around it are not included.

As can be seen in Table 3.1 the most readily available sensors are magnetoresistive. Other types of sensors are specially made products or don't comply to the aforementioned conditions. Also there can be seen that the best sensor sensitivity is 4 nT among the selected sensors, this might indicate that the magnetic field

Table 3.1: Possible sensors

Sensor name	Measuring range (+/- μT)	Sensitivity (nT)	Type	Price (€)
AK09940 [27]	1200	10	TMR	6.81
LSM303D [28]	200	8	AMR	9.08
	400	16		
	800	32		
	1200	47.9		
BM1422AGMV-ZE2 [29]	1200	42	MI	3.948
LSM9DS1TR [30]	400	14	MR	6.1
	800	29		
	1200	43		
	1600	58		
LIS3MDLTR [31]	400	14.6	-	1.44
	800	29.2		
	1200	43.8		
	1600	58.4		
QMC5883l [32]	200	8.33	AMR	4
	800	33.33		
HMC2003 [33]	200	4	MR	111.66

instrument will not comply with the NMAG-1a-INSTR3 requirement of 0.5 nT sensitivity will not be met with the magnetic field instrument designed in this research. To be able to prove that the designed instrument can be useful a comparative COTS attitude magnetometer was found, that is already used for space missions. The instrument is not included in the previous table because of its price which exceeds the NMAG-2a-INSTR1 requirement of €10000. As mentioned in Section 2.2 the NMRM-Bn25o485 magnetometer can be used as a reference sensor, of which some details can be found in Table 3.2. The sensors properties can be compared to the designed instrument to check if it is a viable sensor.

Table 3.2: Magnetic instrument for comparison, the NMRM-Bn25o485 [6]

	Value	Unit
Measurement range	+/- 60000	nT
Resolution	<8	nT
Update rate	<18	Hz
Noise density	<16	nT rms/Hz @1 Hz
Dimensions	99 x 43 x 17	mm
Mass	<85	g
Power	<750	mW
Price	15000	€

3.3. Sensor trade-off

With the list of magnetic field sensors presented in Table 3.1 a trade-off can be made to select a sensor that will be used in the final design. The trade-off will be done using the AHP method (Analytic hierarchy process) with sub-criteria. The criteria for the AHP are Power, Performance, Price and flexibility. The Power criteria relates to the power that the sensor consumes. The Price is the cost of the sensor. The Flexibility of a sensor is the ability to use multiple sensitivity settings. The Performance denotes the ability to achieve the requirements mentioned in Section 2.3, therefore it is divided in to the sub-criteria Attitude sensitivity, Measuring range and Scientific sensitivity each which relate into a requirement. Figure 3.4 shows a visual representation of the hierarchy.

To get the criteria weights the relative importance scale proposed by Saaty [34] is used. To check if the weighing factors are useful a low cr value is preferred, in this case the cr value should be below 0.05. This should be true for both the criteria and sub-criteria. The ability to use the sensor for attitude control and/or scientific data are related but separate things, therefore the final trade-off will be done for each separately.

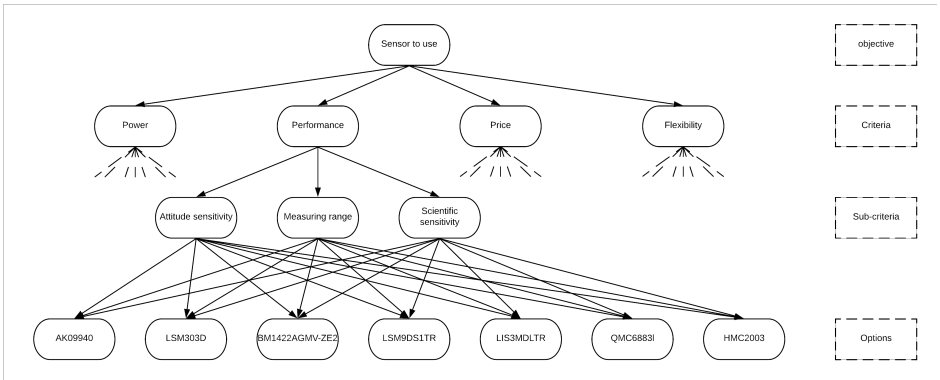

Figure 3.4: Hierarchy for the sensor AHP

3.3.1. Attitude control

Table 3.3 shows the relative importance and the related weighting factors for the main criteria. The Performance of the sensor will be of most importance because it would help prove the effectiveness of the system and theory. The power usage and flexibility of the sensor are at the same level of importance. The price will be of least importance because it will have the least effect on the research directly.

Table 3.3: The AHP criteria table

	Performance	Power	Price	Flexibility	Weighted sum	Criteria weight
Performance	1.00	5.00	7.00	5.00	2.616	0.627
Power	0.20	1.00	3.00	1.00	0.625	0.154
Price	0.14	0.33	1.00	0.33	0.256	0.064
Flexibility	0.20	1.00	5.00	1.00	0.627	0.155
Criteria weights	0.628	0.154	0.064	0.155	-	-
cr	0.0277					

The relative importance of the sub-criteria are displayed in Table 3.4. The measuring range determines the maximum and minimum values that a sensor can measure. All expected values of the earth magnetic field and noise sources should be in this range for the sensor to be effective. The measuring range is usually easier to achieve than the sensitivity, therefore it will be of lower importance. The score for the measuring range of all the sensor might end up being the same, for the small case where it will be different the Attitude sensitivity is the most important parameter. The results of both the sub-criteria and criteria is shown in Tables 3.3 and 3.4 in which the criteria weights used for the trade-off is noted.

Table 3.4: The AHP sub-criteria table for attitude control

	Attitude sensitivity	Measuring range	Weighted sum	Criteria weight
Attitude sensitivity	1.00	3.00	1.50	0.470
Measuring range	0.33	1.00	0.50	0.157
Criteria weights	0.75	0.25	-	-
cr	0.0			

Finally the trade-off can be done and is shown in Table 3.6. In the trade-off table the real values of the sensors are displayed on the left of the column and the corresponding score on the Right. The scoring is done on a 1 to 5 scale and explained in Table 3.5. This kind of scaling can be done because everything can be related to values. To have a clear primary candidate the difference between the sensor next in line while normalized needs to be bigger than 0.05. The LSM303D sensor will be the best choice for the experiment according to the trade-off. The LIS3MDLTR and QMC5883 are both a close second choice but by a very little margin.

Table 3.5: The Scoring for the trade-off explained for attitude control

Score		Attitude sensitivity (nT)	Measuring range (+/- μT)	Power (mW)	Price ($)	Flexibility (-)
1	bad	>50	>10000	>200	>1000	0
2	sufficient	50-30	10000-3000	200-50	1000-100	1
3	above sufficient	30-10	3000-1500	50-10	100-20	2-3
4	good	10-5	1500-200	10-0.5	20-5	4-5
5	very good	<5	100	<0.5	<5	>5

Table 3.6: Trade-off table for attitude control

name	Attitude sensitivity		Measuring range		Power		Price		Flexibility		Score	Normalized
Weight	0.470		0.157		0.154		0.064		0.155			
	value (nt)	score	value (+/- μT)	score	value (mA)	score	value ($)	score	value (number of modes)	score	2.877	0.850
AK09940	10	4	1200	4	1.44	4	6.81	4	1	2	2.853	0.902
LSM303D	8	4	200	4	0.75	4	8.95	4	4	4	3.162	1
BM1422AGMV-ZE2	42	2	1200	4	0.54	4	3.948	5	1	2	2.258	0.714
LSM9DS1TR	14	3	400	4	1.32	4	6.1	4	4	4	2.833	0.896
LIS3MDLTR	14.6	3	400	4	0.675	4	1.44	5	4	4	2.897	0.915
QMC5883	8.33	4	200	4	1.584	4	4	5	2	3	3.071	0.971
HMC2003	4	5	200	4	500	1	111.6	2	1	2	2.593	0.820

3.3.2. Scientific

The weight of the main criteria are the same as stated in Table 3.3 in the previous section. The relative importance of the sub-criteria are displayed in Table 3.7. The measuring range is less important than the sensitivity for the same reason provided in the previous section. The Scientific sensitivity is the most important parameter. The results of both the sub-criteria and criteria is shown in Tables 3.3 and 3.7 which show the criteria weights used for the trade-off.

Finally the trade-off is be done as shown in Table 3.9. In the trade-off table the real values of the sensors are displayed on the left of the column and the corresponding score on the Right. The scoring is done on a 1 to 5 scale and explained in Table 3.8. This kind of scaling can be done because everything can be related to values. The scaling in this table is a bit different than the scaling presented in Table 3.8. The biggest difference is in the power and price which both have higher values that are acceptable. This increase is a logical step because a more accurate instrument will often need more power and cost more. There needs to be a difference of at least 0.05 in the normalized values between the leading option and the next second best to have a obvious winner. The LSM303D, LSM9DS1TR and LIS3MDLTR sensors will be the best choice for the experiment according to the trade-off.

Table 3.7: The AHP sub-criteria table for Scientific data

	Scientific sensitivity	Measuring range	Weighted sum	Criteria weight
Scientific sensitivity	1.00	3.00	1.50	0.470
Measuring range	0.33	1.00	0.50	0.157
Criteria weights	0.75	0.25	-	-
cr	0.0			

Table 3.8: The Scoring for the trade-off explained for Scientific data

Score		Scientific sensitivity (nT)	Measuring range (+/- μT)	Power (mW)	Price ($)	Flexibility (-)
1	bad	>1	>10000	>2000	>5000	0
2	sufficient	1-0.1	10000-3000	2000-500	5000-500	1
3	above sufficient	0.1-0.01	3000-1500	500-100	500-100	2-3
4	good	0.01-0.001	1500-200	100-5	100-20	4-5
5	very good	<0.001	100	<5	<20	>5

Table 3.9: Trade-off table for Scientific data

name	Scientific sensitivity		Measuring range		Power		Price		Flexibility		Score	Normalized
Weight	0.470		0.157		0.154		0.064		0.155			
	value (nt)	score	value (+/- μT)	score	value (mA)	score	value ($)	score	value (number of modes)	score	2.877	0.850
AK09940	10	1	1200	4	1.44	5	6.81	5	1	2	1.962	0.864
LSM303D	8	1	200	4	0.75	5	8.95	5	4	4	2.272	1
BM1422AGMV-ZE2	42	1	1200	4	0.54	5	3.948	5	1	2	1.962	0.864
LSM9DS1TR	14	1	400	4	1.32	5	6.1	5	4	4	2.272	1
LIS3MDLTR	14.6	1	400	4	0.675	5	1.44	5	4	4	2.272	1
QMC5883	8.33	1	200	4	1.584	5	4	5	2	3	2.117	0.932
HMC2003	4	1	200	4	500	3	111.6	4	1	2	1.591	0.700

4

Configuration

The magnetic field instrument consists of multiple components. The magnetometer is one of the driving components of the system and is discussed in the Chapter 3. To identify the rest of the components an ideal hardware architecture is presented in the Section 4.1. Section 4.2 shows selected components and the hardware architecture of the prototype. The differences between both architectures are also discussed in this section. The chapter will be concluded with a flowchart for the software in Section 4.3

4.1. Basic hardware architecture

The basic architecture of the instrument will consist of the following parts:

- Magnetic field sensors
- Controller
- Power source
- Data storage device

The magnetic field sensors are the components that actually measure the magnetic field. These sensors are discussed in Chapter 3. The controller gathers the data obtained from the sensors and makes computations to get the earth magnetic field. The computed data is then stored in a storage device until it can be sent to other systems and/or users. Of course everything needs to be powered by a power source, a satellite usually has a separate system that can provide this. Figure 4.1 shows how the components are connected. The black arrows show the communication lines between components and the red lines show the power lines.The dashed line represents the connection to other systems and/or the user.

4.2. Architecture of prototype

Components will be selected for each part in the architecture presented in the previous section. As mentioned above the sensors are already selected. The data storage can be performed by a single part which is a SD-reader/Writer which can store the data on a SD-card.

4.2.1. Controller

The controller has two main functions as mentioned above. For the prototype these functions will be divided between two devices, a computer and a simple programmable controller. The controller will be an Ardiuno mega 2560 because of its easy accessibility and they are relatively cheap. This controller will gather the information from the sensors and store the raw information on storage device. This type of Arduino is chosen because of the amount of internal memory needed to control the whole system.

The computer will be used to analyze the data and perform computations with the raw data. The main reasons for this is the ability to use multiple methods with the raw data, easier to spot errors with these methods and testing time. Some of the computations can be time intensive, so to minimize the testing time in the field this separation is needed.

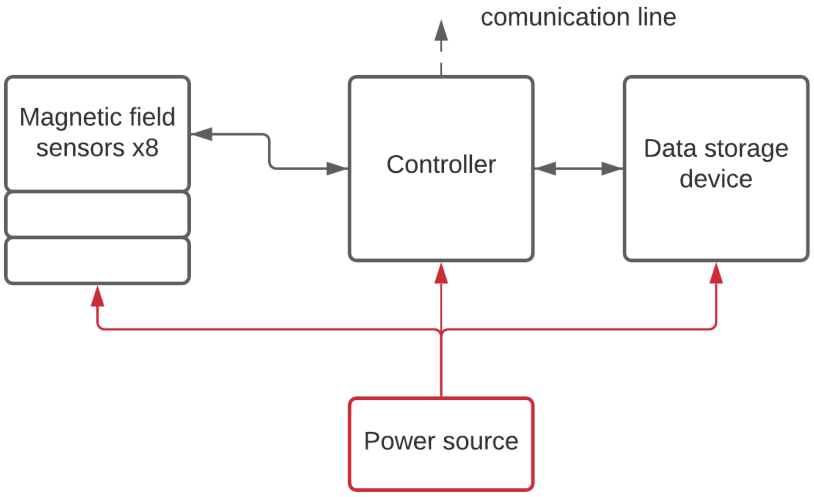

Figure 4.1: The basic hardware architecture

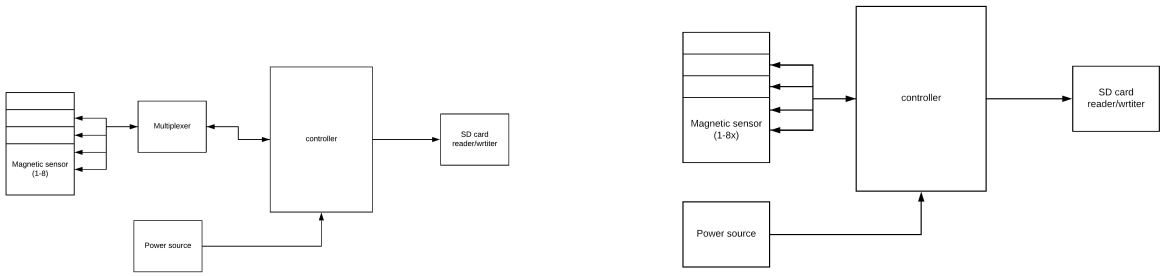

(a) I2C (b) SPI

Figure 4.2: The possible architectures

4.2.2. Internal communication

The necessity of using a multiplexer depends on the communication method used. The two communication methods considered are I2C and SPI because most sensors support both. For both methods an architecture is displayed in Figure 4.2. As can be seen in Figure 4.2a, the I2C communication method uses a multiplexer because for this kind of communication every slave (in this case the sensors) need a specific address. The sensor hardware usually has one to four different addresses, in this case the sensors can only have two different addresses. This also means that if there are enough addresses then the I2C will look the same as the SPI architecture because a direct connection can be made between the sensors and the controller.

The SD-card module only works with SPI and therefore this module will be connected using this communication method. For the sensors the I2C communication method will be used, which means a multiplexer is needed. Although another module is added the amount of wires used in the total system will be less and thus should create less magnetic noise. The SPI uses 4 wires per module and I2C 2 wires. The SPI method is usually faster than I2C but the later is less susceptible to noise as can be seen from a comparison by Myers [35]. The robustness of the system is valued more important and therefore I2C is chosen.

4.2.3. Power source

In the system presented in Figure 4.2 the power is controlled by the Arduino. To make the system more robust it would be better to supply the power without the help of the Arduino. Except for the Arduino every component needs a supply voltage of 5 V, therefore a power converter is needed. The power converter chosen is the MP1584. The Arduino Mega 2560 can have a supply voltage between 7-12V which means this can be connected directly to a battery pack. In this system there will be a battery pack of 12 V consisting of 8 AA batteries to supply power to all components except for the Arduino which has its own power supply in the

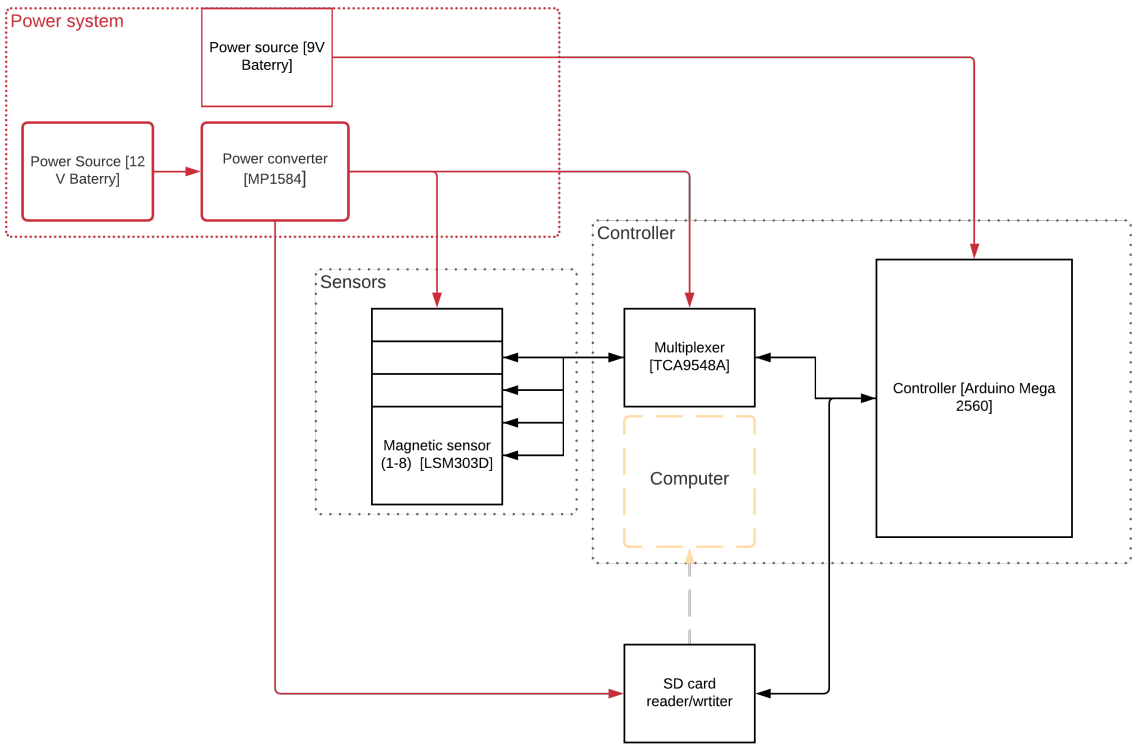

Figure 4.3: The architecture of the magnetic sensing instrument

form of a 9 V battery.

4.2.4. Final design

The complete architecture of the Magnetic field instrument can be found in Figure 4.3. In the figure the red lines relate to the power of the system and the black part to the data movement. Except for the function of the parts and their numbers, the names of the specific parts are also mentioned in the figure.

The parts used for the magnetic field instrument are the following:

- Magnetic field sensors: LSM303D
- Controller: Arduino mega 2560
- Power source: 9V and 12 V baterry
- Power converter: MP1584
- Data storage device: Adafruit MicroSD card breakout board+
- *Multiplexer*: TCA9548A

4.3. Software flowchart

The software for the magnetic field instrument is as important as the hardware. The workings of the software can be seen in Figure 4.4. The flowchart is divided in two parts. The first part is related to the prototype sensor itself and will be programmed using the Arduino software. While the system is turned on it gathers the information of each sensor on the controller and then writes the data to the SD-card. This sequence is chosen because connecting to the SD-card takes time and would slow the system down if this needs to happen for every sensor measurement.

The dashed part denotes the transition to the computer which is done using a SD-card. The block Analyze data relates to all computations that will be performed on the computer. The methods used for analyzing the data are explained in Chapter 5.

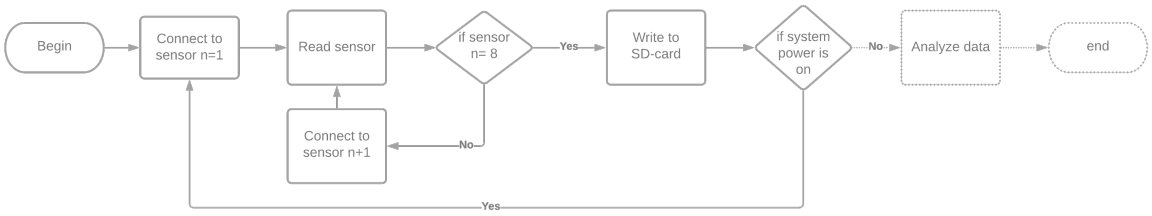

Figure 4.4: Software flowchart

5

Sensor data processing methods

There are multiple methods of manipulating the measured data, as discussed in Section 2.1. All methods mentioned in this section are based on a single sensor or in rare cases two and involve extensive research of the whole satellite system. The magnetic field instrument designed in this paper will use multiple sensors without further knowledge of the system therefore the methods mentioned in Section 2.1 will not be used. Possible methods will be discussed in Sections 5.1 to 5.4.

5.1. Averaging method

The first method that will be considered is averaging the measurement from all sensors with the same time index. This is a simple method which doesn't use a lot of calculations and therefore can be fast.

5.2. System of equations (SOE)

The second method will try to determine the strength, the location and the orientation of the magnetic noise source. To achieve this a system of equations will be used. In the system of equations the strength and direction of the noise sources need to be defined.

5.2.1. Noise representation

The noise sources inside a satellite are caused by wires and circuit boards. In these elements the current flows within loops, these current loops can exist on a part of a circuit board or between two boards connected by a wire, as stated by Niel Et al [36]. Therefore the noise sources can be modeled as a current loop. The current loop can be simulated as a dipole with a magnetic dipole moment of a current loop assuming that R»r (R the distance from the current loop and r the radius of the loop). Using Boit-Savart law (Equation 5.1) an equation can be derived for the magnetic field of a dipole. The magnetic field of a dipole can be calculated using Equations 5.2 and 5.3 where the dipole moment m can be calculated with Equation 5.4. In the equations μ_0 is the magnetic constant and has a value of $4\pi \cdot 10^{-7}\ \frac{Tm}{A}$. R is the distance from the current loop in meters [m] and θ is the polar angle from the z-axis in radians [rad], where the z-axis is perpendicular to the current loop. I is the current through the loop in Ampere [A] and r is the radius of the loop in meters [m].

$$d\vec{\boldsymbol{B}} = \frac{\mu_0}{4\pi} \cdot \frac{Id\vec{\boldsymbol{l}} \times \hat{\boldsymbol{r}}}{r^2} \tag{5.1}$$

$$B_r = \frac{\mu_0}{4 \cdot \pi} m \frac{2cos(\theta)}{R^3} \tag{5.2}$$

$$B_\theta = \frac{\mu_0}{4 \cdot \pi} m \frac{sin(\theta)}{R^3} \tag{5.3}$$

$$m = I\pi r^2 \tag{5.4}$$

Modeling the noise sources as current loops simplify the system of equations by reducing the unknowns. In this situation small electronic elements that create a magnetic field themselves such as conductors are seen as part of the current loops. A circuit board consists of multiple current loops, the number of loops depend

on the size and complexity of the board. All these loops are small in size and the number of current loops will make the system too complex to simulate. Therefore every circuit board will be simulated as one noise source and thus as one current loop. Components like a antenna can still be simulated as a dipole with a magnetic dipole moment of a current loop at larger distances. For calculating the strength of the noise source calculating the dipole moment m will be enough because it only depends on the current I and loop size r which have no further effect on Equations 5.2 and 5.3. The relation is important to define the domain of possible values of m which will be discussed in Section 5.3.1

As can be noted Equations 5.2 and 5.3 are written in polar coordinates. Equation 5.5 to 5.8 can be used to convert from Cartesian coordinates to spherical coordinates. Here θ is the polar angle from the z-axis and has a range of $0 \leq \theta \leq \pi$. ϕ is the azimuth angle with a range of $0 \leq \phi \leq 2\pi$

$$R = \sqrt{x^2 + y^2 + z^2} \tag{5.5}$$

$$\theta = acos(\frac{z}{R}) \tag{5.6}$$

$$\phi = asin(\frac{y}{R_2}) \tag{5.7}$$

$$R_2 = \sqrt{x^2 + y^2} \tag{5.8}$$

Another factor that needs to be considered is the pointing angles of the noise sources. The pointing angles are defined as $\theta_{pointing}$ and $\phi_{pointing}$ with ranges of $0 \leq \theta_{pointing} \leq \frac{1}{2}\pi$ and $0 \leq \phi_{pointing} \leq 2\pi$. Notice that these ranges only describe half a sphere, the reason for this is the mirror effect of the magnetic field if a negative current is applied. To take this into account Equations 5.2 and 5.3 are modified to Equations 5.9 and 5.10.

$$B_r = \frac{\mu_0}{4 \cdot \pi} m \frac{2cos(\theta - \theta_{pointing})}{R^3} \tag{5.9}$$

$$B_\theta = \frac{\mu_0}{4 \cdot \pi} m \frac{sin(\theta - \theta_{pointing})}{R^3} \tag{5.10}$$

5.2.2. The SOE explained

The SOE will look as shown in Equation 5.11. In these equations B_{ms} are the measured magnetic fields, the number indicates the sensor number and the letters x,y and z indicate the direction. The Earth magnetic field is B_{me} which is subdivided in its directional components. B_{s1-n1_x} is the magnetic noise generated by noise source 1 (n1) on sensor 1 (s1) in the x direction. Again x, y and z indicate the direction of the force. The rest of the subscript indicate the effect of a particular noise source on a particular sensor.

$$\begin{aligned}
B_{ms1_x} &= B_{me_x} + B_{s1-n1_x} + B_{s1-n2_x} + B_{s1-n3_x} + ... \\
B_{ms1_y} &= B_{me_y} + B_{s1-n1_y} + B_{s1-n2_y} + B_{s1-n3_y} + ... \\
B_{ms1_z} &= B_{me_z} + B_{s1-n1_z} + B_{s1-n2_z} + B_{s1-n3_z} + ... \\
B_{ms2_x} &= B_{me_x} + B_{s2-n1_x} + B_{s2-n2_x} + B_{s2-n3_x} + ... \\
... &= ... \\
... &= ... \\
... &= ...
\end{aligned} \tag{5.11}$$

The values for B_{s1-n1_x} can be calculated with Equations 5.5 to 5.10. The locations of the sensors and the measured magnetic field should be known. The earth magnetic field has three unknowns namely $B_{me_x}, B_{me_y}, B_{me_z}$ and every noise sources has six unknowns namely $x_n, y_n, z_n, \theta_{pointing}, \phi_{pointing}$ and m. The measured magnetic field can be split in three directions as can be seen in Equation 5.11. To create a determined SOE the following condition needs to be true: $3 \cdot N_{sensors} \geq 6 \cdot N_{noisesources} + 3$. So $3\frac{1}{3}$ sensors are needed if one noise source is present and for every noise source added after the first $2\frac{1}{3}$ sensors need to be added. The number of sensors need to be rounded up to the nearest integer.

5.3. Optimization for the SOE

To find a solution for the system of equations an optimization method will be used. The constraints of the different variables need to be analyzed before choosing a optimization method.

5.3.1. Constraints

The first set of constraints are the boundary conditions (B.C.) which relate the physical constraints imposed by the satellite. The B.C. can be seen in Equation 5.12. The first three conditions are related to the size of the satellite and thus cannot be bigger than the satellite dimensions. The values of the pointing angles are discussed in the previous section. The current can go in both the negative and positive direction and can be as big as the biggest expected current. r_{max} is the maximum size of the expected loop.

$$\begin{aligned} 0 \leq x \leq x_{max} \\ 0 \leq y \leq y_{max} \\ 0 \leq z \leq z_{max} \\ -m_{max} \leq m \leq m_{max} \\ 0 \leq \theta_{pointing} \leq \frac{1}{2}\pi \\ 0 \leq \phi_{pointing} \leq 2\pi \end{aligned} \tag{5.12}$$

The specific current and loop size combination is not of importance to the simulation as mentioned above. They are however important to determine the boundaries of the dipole moment in Equation 5.12. Therefore they need boundary conditions of their own which are mentioned in Equation 5.13. The boundaries can be used in combination with Equation 5.4 to calculate the boundaries of the dipole moment.

$$\begin{aligned} -I_{max} \leq I \leq I_{max} \\ 0 \leq r \leq r_{max} \end{aligned} \tag{5.13}$$

The variable R in Equations 5.2 and 5.3 needs to be nonzero to prevent a division by zero. Therefore the constraint in Equation 5.14 will be used.

$$0 < |x + y + z| \tag{5.14}$$

5.3.2. Equation to optimize

To perform an optimization there needs to be a value to optimize for. Therefore Equation 5.11 will be rewritten to Equation 5.15. In this equation a vector F is introduced which is a vector of redundant values and should be zero to find a solution to the SOE.

$$\begin{aligned} F[0] &= -B_{ms1_x} + B_{me_x} + B_{s1-n1_x} + B_{s1-n2_x} + B_{s1-n3_x} + ... \\ F[1] &= -B_{ms1_y} + B_{me_y} + B_{s1-n1_y} + B_{s1-n2_y} + B_{s1-n3_y} + ... \\ F[2] &= -B_{ms1_z} + B_{me_z} + B_{s1-n1_z} + B_{s1-n2_z} + B_{s1-n3_z} + ... \\ F[3] &= -B_{ms2_x} + B_{me_x} + B_{s2-n1_x} + B_{s2-n2_x} + B_{s2-n3_x} + ... \\ ... &= ... \\ ... &= ... \\ ... &= ... \end{aligned} \tag{5.15}$$

5.3.3. Optimization method

There are several methods available that are used for optimization and depend on the programming languages used. The programming language used is Python which has a set of optimization methods in the Scypy package. In this case a SOE needs to be solved which exists of multiple non-linear equations. The size of the system is variable and will have occasions where there are more equations than variables and more often cases where there are more variables than equations. These properties lead to the use of the Root finding

functions which are specialized for these situations. The Levenberg-Marquardt of this function can compute answers with different size SOE. This method uses a combination of the Gauss-Newton algorithm and the method of gradient decent to minimize the residuals of a model, in this case the system of equations. A downside of this method is that it can find local minimums instead of a global minimum.

To minimize the chance of finding a local minimum the boundary conditions mentioned in Section 5.3.1 will be used. The python function does not have an input for constraints, but the constraints can still be added in the form of a weight function. To do this Equation 5.15 will be multiplied with a weight function as seen in Equation 5.16 where F is the residual vector presented in Equation 5.15. $G(x, y, z, ...)$ is the weight function and F_w is the weighed residuals vector.

$$F_w = G(x, y, z, ...) \cdot F \tag{5.16}$$

The weight function should be one within the constraints and become rapidly bigger outside these constraints. This is shown in Equation 5.17. The weigth function can only be one if all B.C. are zero within the constraints, to achieve this the B.C are written as shown in Equation 5.18. Here a is the correction for the middle of the B.C. and b is a multiplication factor to ensure a steep ascent outside the boundary conditions. The values used for b is the domain of the boundary condition. To minimize this function a zero result is generated by making sure there is a zero multiplication for every possible value between the boundary conditions. In the Python code this can be realized using a if statement.

$$G(x, y, z, ..) = 1 + BC_x + BC_y + ... \tag{5.17}$$

$$BC_1 = ((x - a) \cdot \frac{1}{b})^6 \cdot (x - x_{max}) \cdot (x - x_{bc}) \cdot ..... \tag{5.18}$$

5.4. SOE with multiple measurements

The SOE mentioned until now is for static situations only and thus for one measurement at the time. The SOE can be extended to be used for multiple measurements at one time. An advantage would be reducing the number of sensors needed to get a determined system of equations. As mentioned before the condition for getting a determined SOE is: $3 \cdot N_{sensors} \geq 6 \cdot N_{noisesources} + 3$. Ideally the location and the pointing angles stay the same over time, assuming there are no moving parts. The unknowns for every consecutive measurement are the dipole moment m and the Earth magnetic field in all directions. Therefore the condition for a determined equation becomes Equation 5.19. This also means that it should be possible to create a determined SOE if more than two sensors are used. The effectiveness needs to be tested with simulations.

$$N_{measurements} \cdot 3 \cdot N_{sensors} \geq (6 \cdot N_{noisesources} + 3) + (N_{measurements} - 1) \cdot (N_{noisesources} + 3) \tag{5.19}$$

6

Verification of the sensor data processing methods

Before using the methods presented in the previous Chapter they need to be verified. The methods to be verified are the averaging method and the system of equations method. A standard testing configuration will be presented in Section 6.1 which will be used in multiple verification methods. In Section 6.2 the averaging method will be verified. The SOE method will be verified in Section 6.3.

6.1. Standard testing configuration

First is to present a standard configuration for testing. In this case a 30x30x30 cm satellite is chosen with sensors at all corners of the satellite as represented in Table 6.1. All the sensors in this configuration are oriented in the same direction with the x,y and z axis parallel to the axis of the satellite. The placement of the noise sources are shown in Table 6.2. For the validation all sensors and noise sources or a subset of them will be used. The ambient magnetic field used is 1E-6, 1E-6 and 0.05E-6 in the x,y and z direction respectively. The presented values will change depending on the test, these changes will be mentioned.

Table 6.1: Sensor locations

Sensor number	X location [cm]	Y location [cm]	Z location[cm]
1	0	0	0
2	30	30	0
3	30	0	30
4	0	30	30
5	30	30	30
6	0	0	30
7	0	30	0
8	30	0	0

Table 6.2: Noise locations, pointing direction and dipole strength

Noise number	X location [cm]	Y location [cm]	Z location[cm]	m [Am^2]	θ [rad]	ϕ [rad]
1	10	10	10	2.36E-4	0	0
2	10	10	0	-1.96E-4	0	0

6.2. Verification of the averaging method

There are two ways to verify the averaging method. First one is to show the Earth magnetic field measured at each sensor and the average taken of all the sensors.

The error in Earth magnetic field measurements should be constant if the Earth magnetic field is the only variable that changes. Therefore a second verification method will be used where the Earth magnetic field will vary and the magnetic noise of the noise sources will be constant in all tests.

6.2.1. Verification method 1

Multiple configurations will be used to verify the averaging method. A two, four and eight sensor configuration will be used from the standard configuration presented in the previous section. Four different noise source configurations will be used for the verification. The first noise source configuration will be the standard noise configuration presented in the previous section and will be denoted further as configuration 1. The other configurations are presented in Table 6.3. The results can be found in Tables 6.4 to 6.7. These tables show the Earth magnetic field, the magnetic field measured at each sensor and the calculated average magnetic field when two, four or eight sensors are considered for the four different noise source configurations discussed above. The tables show that the averaging method works and is highly dependent on the measured magnetic fields at the sensors. A large error in one of the sensor measurements can cause a big difference in the averaging result, this effect decreases with more sensors.

Table 6.3: Noise locations, pointing direction and dipole strength

	Noise number	X location [cm]	Y location [cm]	Z location[cm]	m [Am^2]	θ [rad]	ϕ [rad]
Configuration 2	1	15	15	30	1.80E-4	0.10π	0.5π
	2	0	15	30	3.00E-4	0.25π	0.5π
Configuration 3	1	10	10	10	2.36E-4	0.10π	0.5π
	2	10	10	0	-1.96E-4	0.25π	0.25π
Configuration 4	1	10	10	10	1.80E-4	0.4π	π
	2	10	10	0	-1.96E-4	0.25π	0.25π

Table 6.4: The results of configuration 1 with the averaging method

Direction	Earth magnetic field	Sensor 1	Sensor 2	Sensor 3	Sensor 4	Sensor 5	Sensor 6	Sensor 7	Sensor 8	Average of 2	Average of 4	Average of 8
x	1000	1004.534	998.418	1000.682	999.659	1000.270	998.837	1000.802	998.397	1001.976	1001.073	1000.325
y	1000	1004.534	998.418	999.659	1000.682	1000.270	998.837	998.3997	1000.802	1001.976	1001.073	1000.325
z	50	56.936	50.285	49.943	49.943	49.835	50.821	50.953	50.953	53.611	51.777	51.209

Table 6.5: The results of configuration 2 with the averaging method

Direction	Earth magnetic field	Sensor 1	Sensor 2	Sensor 3	Sensor 4	Sensor 5	Sensor 6	Sensor 7	Sensor 8	Average of 2	Average of 4	Average of 8
x	1000	1001.094	999.656	998.284	1014.691	1001.716	985.309	998.906	1000.344	1000.375	1003.431	1000.000
y	1000	999.631	1000.319	997.743	1001.175	997.743	1001.175	999.631	1000.319	999.975	999.717	999.717
z	50	49.462	49.696	49.058	53.160	49.058	53.160	49.462	49.696	49.579	50.344	50.344

6.2.2. Verification method 2

For this verification method a varying Earth magnetic field will be used instead of the one presented in Section 6.1. The Earth magnetic field will be randomly varied and two noise source configurations will be analyzed. The noise source configuration used are configuration 1 and 4 as described in the previous section. Both noise configurations will be analyzed with a four and eight sensor configuration as mentioned above.

Figure 6.1 displays the calculated magnetic field error in the x, y and z direction and the Earth magnetic field that is used as input. The randomly generated Earth magnetic field displayed in Figure 6.1a is almost not readable because of big fluctuations of the magnetic field between each simulation. Therefore it is still good to show for reference because even if the input magnetic field is so erratic a constant magnetic field error is found with the averaging method as expected.

The results of both verification methods show that the averaging method performs as it should and therefore can be used for simulations and/or testing.

Table 6.6: The results of configuration 3 with the averaging method

Direction	Earth magnetic field	Sensor 1	Sensor 2	Sensor 3	Sensor 4	Sensor 5	Sensor 6	Sensor 7	Sensor 8	Average of 2	Average of 4	Average of 8
x	1000	1013.130	998.652	999.542	1001.069	1000.601	998.523	998.714	999.395	1005.891	1003.098	1001.203
y	1000	997.274	1000.048	998.830	1000.661	999.424	1000.964	997.276	1002.951	998.661	999.203	999.678
z	50	45.946	48.696	50.358	50.358	49.966	51.892	47.574	47.574	53.611	48.152	48.702

Table 6.7: The results of configuration 4 with the averaging method

Direction	Earth magnetic field	Sensor 1	Sensor 2	Sensor 3	Sensor 4	Sensor 5	Sensor 6	Sensor 7	Sensor 8	Average of 2	Average of 4	Average of 8
x	1000	1013.926	998.017	1000.711	999.720	1000.285	998.241	999.985	997.533	1005.971	1003.094	1001.052
y	1000	1003.522	999.317	999.517	1000.813	1000.260	998.755	995.868	1003.314	1001.420	1000.792	1000.171
z	50	46.786	50.160	50.282	50.282	50.192	50.244	49.921	49.921	48.473	49.377	49.723

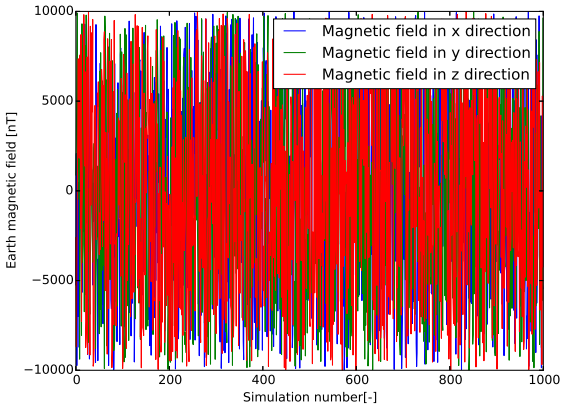

(a) The Earth magnetic field used as input

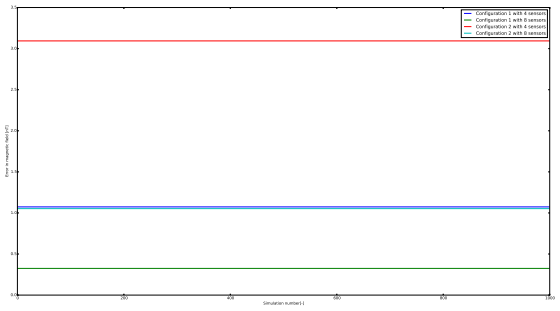

(b) The error in the calculated magnetic field in the x-direction

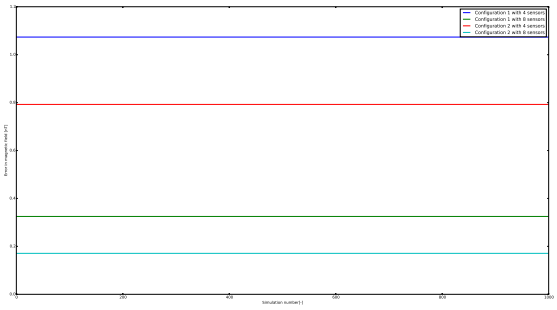

(c) The error in the calculated magnetic field in the y-direction

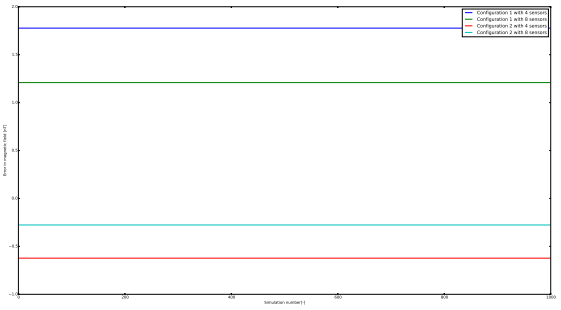

(d) The error in the calculated magnetic field in the z-direction

Figure 6.1: The result of multiple randomized Earth magnetic field conditions with the averaging method

6.3. Verify SOE method

The SOE method consists of three distinct cases which are the underdetermined, the determined and overdetermined systems. The SOE will have a different behavior for each of these cases. Before the SOE method can be verified some verification criteria need to be set in Section 6.3.1. Three tests will be used to analyze the performance of the SOE method. These tests are performed with a varying initial guess, a varying Earth magnetic field and varying noise sources which are performed in Sections 6.3.2, 6.3.4 and 6.3.5 respectively. An adjustment in the method will be made in Section 6.3.3 due to the results of Section 6.3.2

6.3.1. Verification criteria

The most important values for the SOE method are the calculated Earth magnetic field values therefore the error between the calculated and actual Earth magnetic field will be used to verify the SOE method. The allowable error can be derived from the accuracy requirements discussed in Section 2.3. The relevant requirements are NMAG-1a-INSTR6 and NMAG-1a-INSTR7 which say the total system should have a pointing accuracy of 50 nT for an attitude control instrument and 0.5 nT for a scientific instrument. The requirements are for the whole system and therefor only a fraction of the required accuracy can be allowed for a calculation method, in this case a tenth of the required accuracy will be used as verification value. An accuracy of 5 nT and 0.05nT is therefor used for verification. The verification value of 5 nT for the attitude control instrument is also smaller than the sensitivity of the selected sensor of Section 3.3 which has a sensitivity of 8 nT. Preferably the calculation method should have an accuracy which is better than the sensitivity of the sensor such that the total system accuracy is driven by sensor instead of the calculation method.

While the actual values of the noise sources, such as location, strength and pointing direction, are not important, they should all be within the boundary conditions as discussed in Section 5.3.1. The Boundary conditions for location are determined by the outer dimensions of the satellite. The maximum dipole moment can be calculated assuming the maximum current is 10 A and the maximum loop size 0.01 m.

6.3.2. Varying initial guess

The standard test case described in Section 6.1 will be used to test for a varying initial condition. The initial conditions used for the SOE method will be generated randomly (in this case the random library of Python is used with a seed number of 3). 5000 calculations will be performed so accurate graphs can be created. Figures 6.2, 6.3 and 6.4 show the results of the test for the underdetermined, determined and overdetermined systems respectively.

Figures 6.2a to 6.2c, 6.3a to 6.3c and 6.3a to 6.3c show the calculated noise characteristics (location, strength and pointing direction). All the values found for the noise characteristics adhere to the boundary conditions set in Section 5.3.1.

The determined SOE should only have one solution. As can be seen in a scatter plot in Figure 6.3d this is not the case. There are instances that the calculated result is far from the actual Earth magnetic field. To show the frequency of this occurrence an inverse cumulative density plot is made of the absolute magnetic field error in all directions in Figure 6.3e. The same is done for the two underdetermined and the overdetermined systems in Figures 6.2e, 6.2f and 6.4e. Except for the 2 sensor underdetermined system most of the results are within the $\leq$ 2.5 nT error range.

The percentage of results in the z-direction that are within the ranges of -2.5 to 2.5 nT and -0.25 to 0.25 nT can be seen in Table 6.8. The z-direction is analyzed because this direction has the biggest error. For the determined and overdetermined system a high percentage of the results comply to the verification criteria of 5 nT accuracy related to the attitude control instrument. The Table also indicates that in all cases the accuracy for the scientific instrument will not be achieved on a regular basis with this approach. Therefore it can be concluded that a scientific instrument cannot be made with the SOE method and thus will not be tested for from hereon. The underdetermined system with 2 sensors also has this problem with the criteria for attitude control. The underdetermined system with 4 sensors produce a higher number of results within the 5 nT criteria with about 50 % in the x and y direction and about 40 % in the z direction and so there is still a low consistency to stay within the 5 nT accuracy range.

Table 6.8: The percentage of results within the specified range in the z-direction

Range	Results in range underdetermined (2 sensor)[%]	Results in range underdetermined (4 sensor)[%]	Results in range determined[%]	Results in range overdetermined[%]
-2.5 to 2.5	6.94	61.56	81.79	94.08
-0.25 to 0.25	0.98	8.17	13.76	5.02

As mentioned before the determined system should have an unique result and thus a magnetic field error of 0 nT is to be expected. In most of the cases the optimization technique of the SOE method (as described in Section 5.3.3) finds a point where the sum of squares of the residuals of both the actual and predicted reduction are both zero or the relative error between two consecutive reiterations is 0. This indicate that multiple local minimums are introduced due to numeric errors in the calculations of the optimizer. The biggest deviations occur usually when multiple initial values for noise characteristics and Earth magnetic field are far from the actual values. This indicates a lower limit to the number of sensors needed to get a sufficient accuracy. This relationship will be further explored in Section 7.2

6.3.3. Adjustments to the method

In the previous section it is shown that initial conditions exist that produce a magnetic field error higher than the 5 nT criteria. The percentage of results within this criteria vary depending on ratio between sensors and noise sources as could be seen in Section 6.3.2. There are two adjustments to the SOE method that might be able to provide more consistent results.

The first adjustment uses multiple random initial guess calculations which are averaged. The results of the multiple calculations will be compared to the median of all results. Values that deviate too much from the median will be removed from the set of results. Figure 6.5 shows the flow chart of this filtering method. The effect of this filtering method is tested and displayed in Tables 6.9 to 6.11. Each directional component of the magnetic field is calculated separately and therefore also display separately. This is done so that the directional component with the largest error can be identified. The biggest error is consistently found in the z direction. Most likely this is because its Independence from the variable $\phi_{pointing}$ which is a value that can compensate an error in $\theta_{pointing}$ for the x and y direction.

The table shows that using multiple calculations is always beneficial to find a resulting Earth magnetic field that adheres to the 5 nT accuracy. The number of necessary calculations vary depending on the type (underdetermined, determined and overdetermined) of SOE. The determined and overdetermined SOE have only a small improvement in accuracy after 50 calculations are used in combination with the filtering method. At the same time the underdetermined SOE with 2 sensors needs more than 5000 calculations with filtering to get the accuracy necessary for a 5 nT accuracy in all directions but provides reasonable results in the x and y direction when 50 calculations are filtered. Therefore to limit the number of optimizations to be performed it was chosen to use 50 calculations with filtering for the verification in the next sections.

Table 6.9: The magnetic field error calculated using multiple calculations with the filtering in the x direction

Number of calculations	Error underdetermined (2 sensors) [nT]	Error underdetermined (4 sensors) [nT]	Error determined [nT]	Error range overdetermined [nT]
10	-155.1	0.1815	-0.1370	9.158E-2
50	-0.2100	-0.2288	2.056E-3	0.1024
100	0.5668	-0.2288	-9.145E-2	8.632E-2
200	0.5668	-0.2627	-5.761E-2	7.024E-2
500	2.039	-0.2632	-6.466E-2	7.388E-2
1000	2.545	-0.2236	-6.707E-2	7.423E-2
5000	0.8426	-0.2235	-7.375E-2	7.811E-2

Table 6.10: The magnetic field error calculated using multiple calculations with the filtering in the y direction

Number of calculations	Error underdetermined (2 sensors) [nT]	Error underdetermined (4 sensors) [nT]	Error determined [nT]	Error range overdetermined [nT]
10	221.5	-0.2770	-0.1736	0.2150
50	1.500	-0.2288	-7.649E-2	0.1000
100	2.713	-0.2288	-0.1019	8.160E-2
200	2.713	-0.2620	-7.291E-2	8.002E-2
500	0.8992	-0.2609	-9.149E-2	8.818E-2
1000	2.596	-0.2235	-0.1079	8.529E-2
5000	0.4771	-0.2232	-9.297E-2	8.017E-2

Table 6.11: The magnetic field error calculated using multiple calculations with the filtering in the z direction

Number of calculations	Error underdetermined (2 sensors) [nT]	Error underdetermined (4 sensors) [nT]	Error determined [nT]	Error range overdetermined [nT]
10	338.7	0.5399	0.4578	1.195
50	4.600	0.8595	0.6824	1.139
100	4.188	0.8595	0.6970	1.076
200	4.188	0.8835	0.6917	1.053
500	5.627	0.8824	0.7520	1.069
1000	6.077	0.8890	0.7352	1.066
5000	0.587	0.8893	0.7379	1.058

The second adjustment can only be used in a dynamic system. It uses the calculated Earth magnetic

field of the previous result as input for the new calculation. This is done in the form of a B.C. with the previous result ≤ 100 nT as the boundaries. This can only be done when the Earth magnetic field changes slowly over time which should happen during normal operations (not while tumbling for instance). According to the requirements for attitude control the accuracy of the system needs to be at least be 50 nT. A maximum difference between two consecutive calculated magnetic fields can be determined combining the minimum accuracy of 50 nT and the maximum change of 100 nT between measurements. This would lead to a difference of 200 nT, which is the sum of two times the minimum accuracy and the maximum expected change. By limiting the possible results, outliers should naturally occur less and the optimization has less options and thus an answer should be found faster. This will be tested during the simulations in Chapter 7

6.3.4. Varying earth magnetic field

The accuracy of SOE method is dependent on the initial condition as discussed in Section 6.3.2 and therefore a correction to the SOE was made in Section 6.3.3. The tests performed in this section will therefore use the adjustment suggested in Figure 6.5 while using 50 initial conditions. To get an accurate view of the effect of the Earth magnetic field as input, 200 calculations are performed all with a random generated magnetic field. The results can be seen in Figure 6.6. In case of a determined and an overdetermined system the error is smaller than 1.5 nT and thus below the 5 nT needed for attitude control. The underdetermined system is split in two different tests one for undetermined system (number of unknown variables » number of equations) with 2 sensors as performed above and a slightly underdetermined system (number of unknown variables > number of equations) with four sensors. All results of the slightly underdetermined (using 4 sensors) performs within the 5 nT criteria but the far undetermined system (using 2 sensors) is still widely varying with large errors.

6.3.5. Varying noise sources

The adjusted SOE method mentioned in Section 6.3.3 is again used for the calculations in this section. To get an accurate view of the effect of different noise sources as input, 200 calculations will be performed all with random generated noise sources. The error with respect to the actual magnetic field in the z-direction can be seen in Figure 6.7. A comparison of the z-direction is chosen because here are the most variations. As can be seen most of the results are within the 5 nT range in agreement with the verification criteria set for the attitude control, but the diversity is bigger than previous sections. Table 6.12 shows the percentage of results within three different magnetic field error ranges in the z-direction. There are two situations where these deviations are noticed. The first is related to the distance between the sensor and the noise source. If the noise source is too close to one of the sensors it causes the sensor to measure a large magnetic field in comparison to the other sensors. The second situation occurs when one of the noise sources is much bigger compared to the others and the effect of the biggest noise source is seen by most of the sensors. For example a five sensor configuration is used and the Earth magnetic field in the z-direction should be 50 nT but due to the effects of the noise sources the sensors measure around 38 nT (± 3 nT) on 3 or 4 of the 5 sensors then the solution tends to be within the 38 nT region. This leads to the conclusion that the design of the configuration is an important factor. The effect of configuration will further be studied in Section 7.3.

Table 6.12: Percentage of calculation error in mentioned ranges in the z direction

	<-2.5 nT	-2.5 to 2.5	>2.5 nT
underdetermined 2 sensors	8	81	11
underdetermined 3 sensors	7	77	17
underdetermined 4 sensors	7.5	86	6.5
determined	8.5	81.5	10
overdetermined 8 sensors	8	81	11

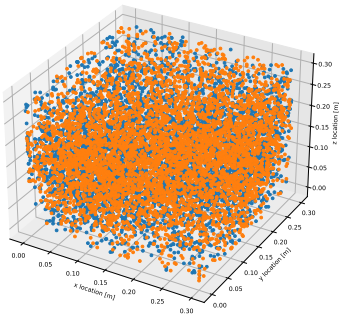

(a) The calculated noise locations using 2 sensors

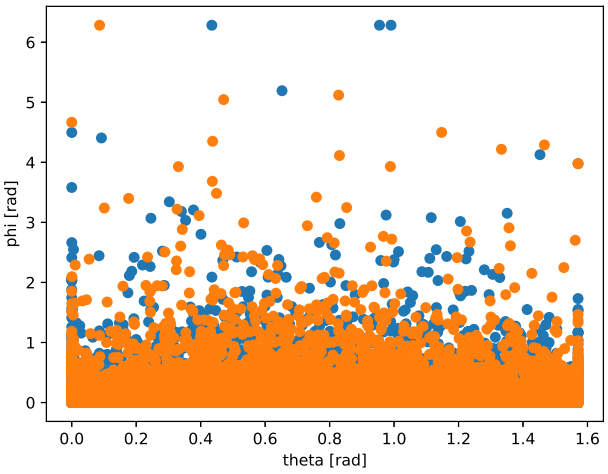

(b) The calculated noise pointing direction using 2 sensors

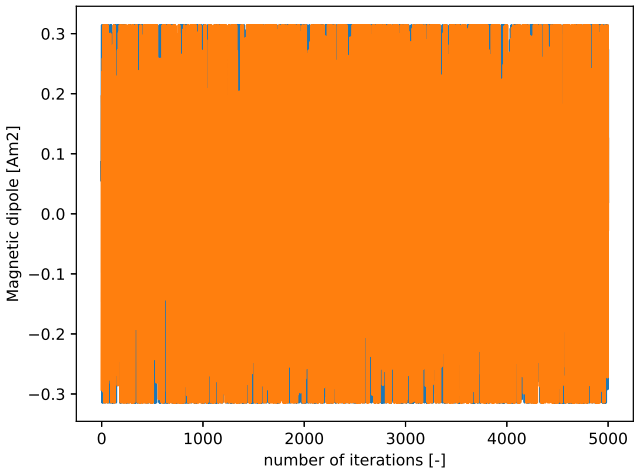

(c) The calculated noise dipole moments using 2 sensors

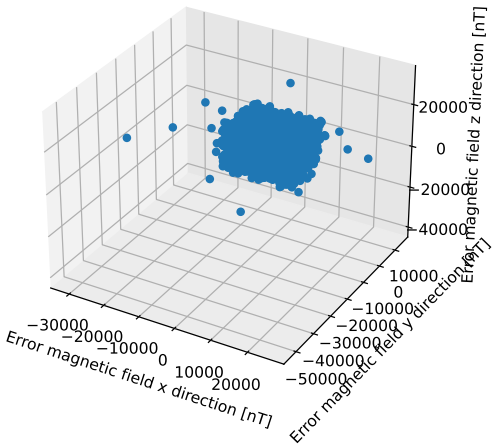

(d) The calculated earth magnetic field using 2 sensors

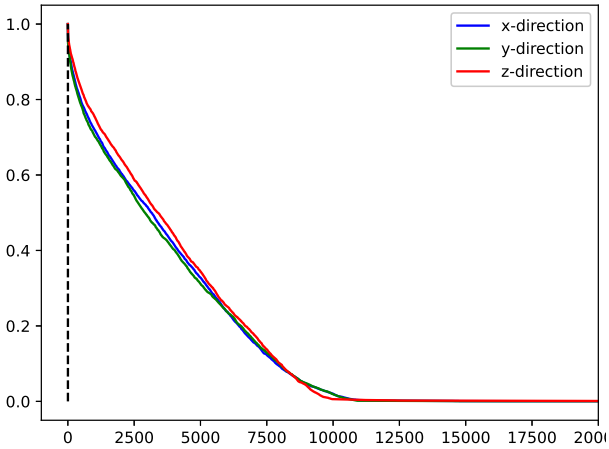

(e) A cumulative density plot of the absolute Magnetic field error in all directions direction using 2 sensors

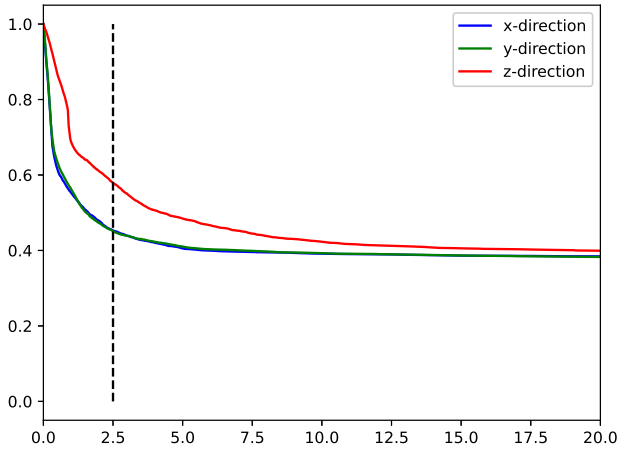

(f) A cumulative density plot of the absolute Magnetic field error in all directions direction using 4 sensors

Figure 6.2: The results of multiple randomized initial conditions for solving the system of equations for an under-determined system

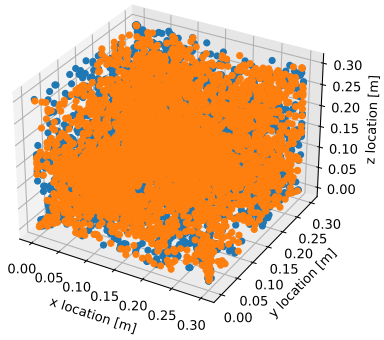

(a) The calculated noise locations

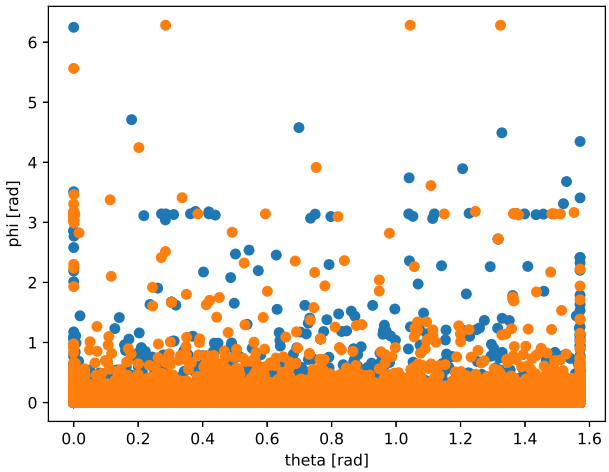

(b) The calculated noise pointing direction

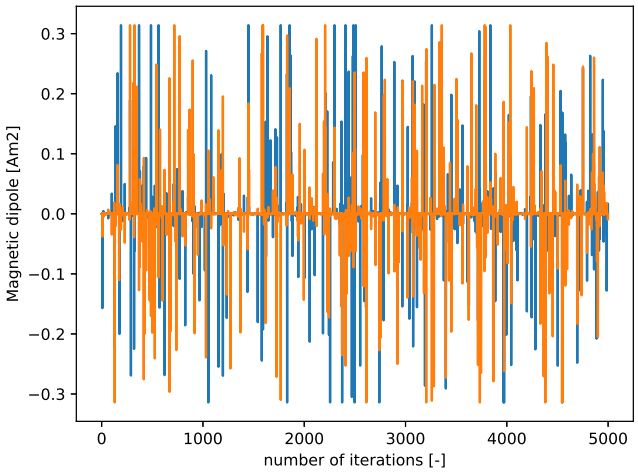

(c) The calculated noise dipole moments

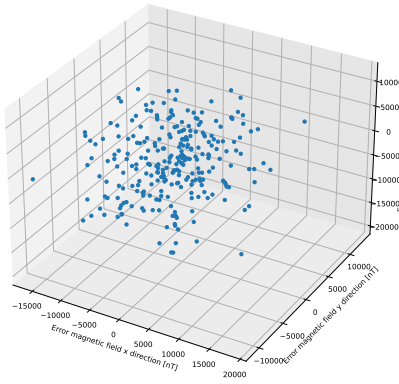

(d) The calculated earth magnetic field

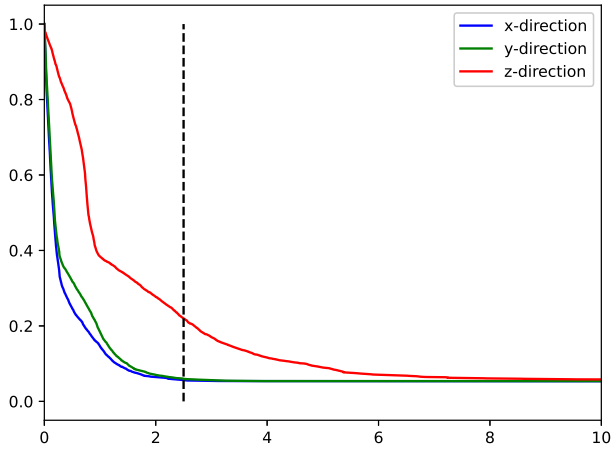

(e) A cumulative density plot of the absolute Magnetic field error in all directions direction

Figure 6.3: The results of multiple randomized initial conditions for solving the system of equations for a determined system

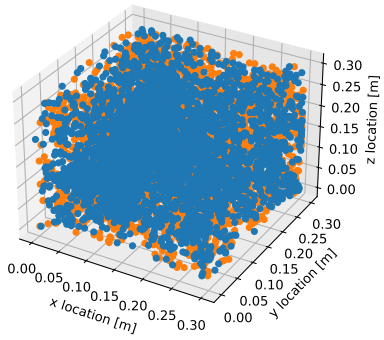

(a) The calculated noise locations

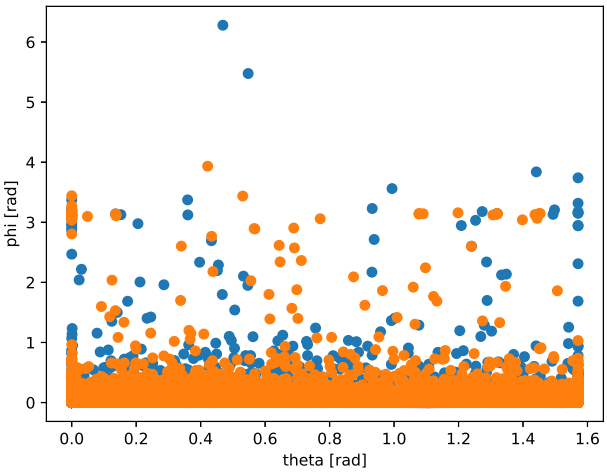

(b) The calculated noise pointing direction

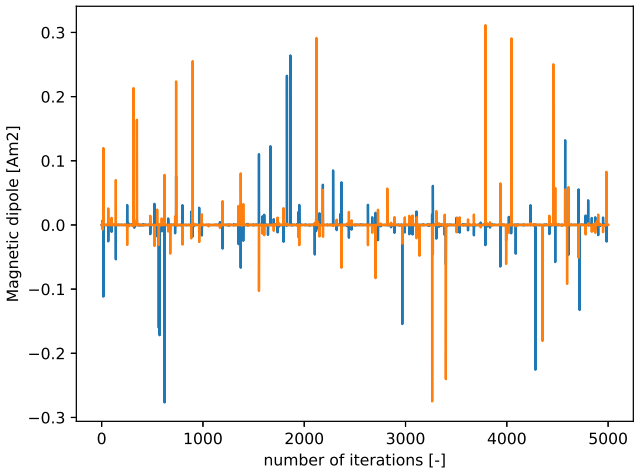

(c) The calculated noise dipole moments

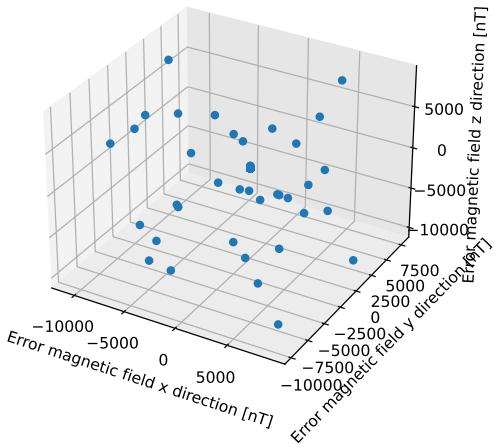

(d) The calculated earth magnetic field

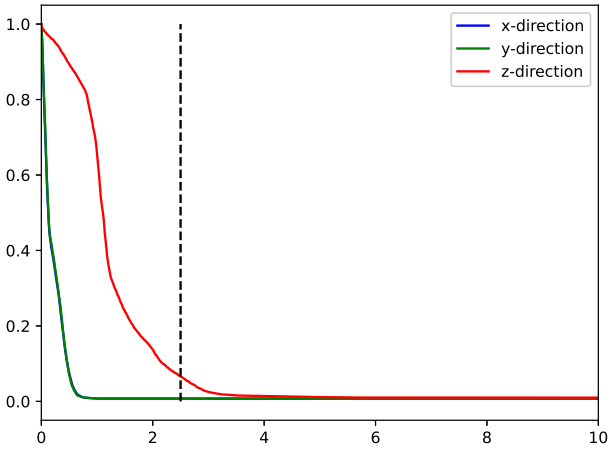

(e) A cumulative density plot of the absolute Magnetic field error in all directions direction

Figure 6.4: The results of multiple randomized initial conditions for solving the system of equations for an overdetermined system

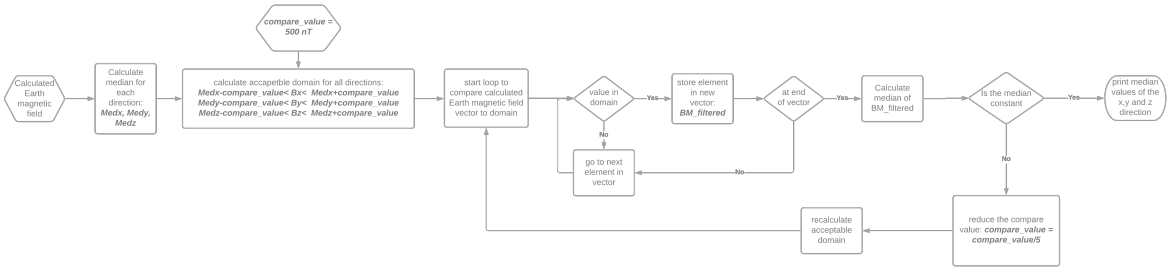

Figure 6.5: Flowchart of the filtering adjustment

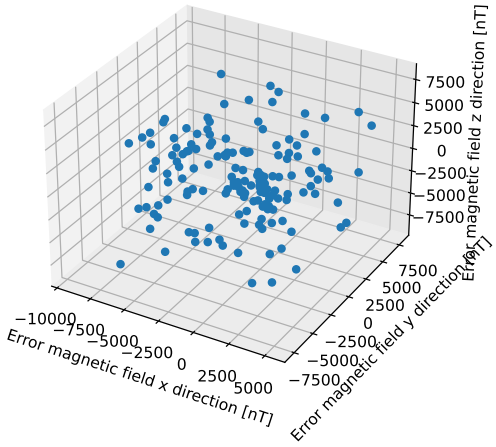

(a) Underdetermined system (2 sensors)

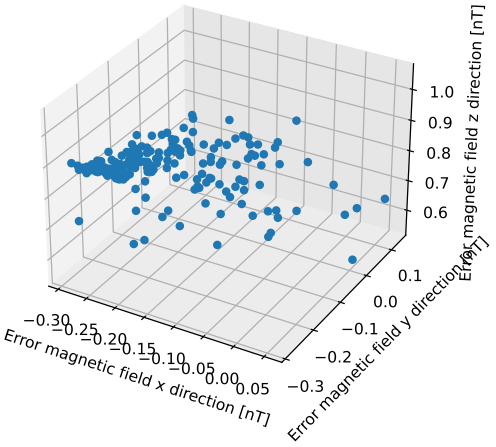

(b) Underdetermined system (4 sensors)

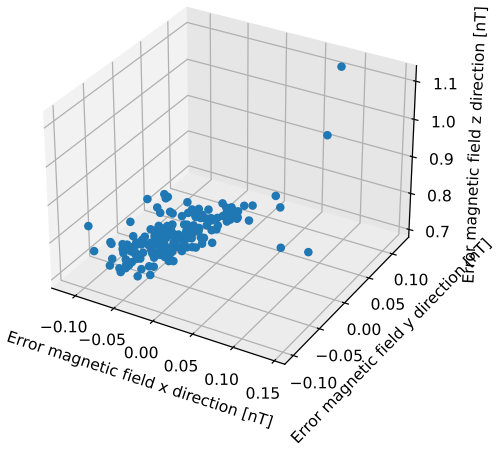

(c) Determined system

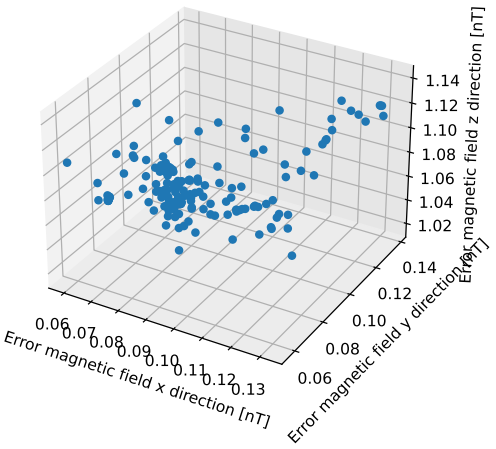

(d) Overdetermined system

Figure 6.6: The errors in calculated magnetic field due to multiple randomized Earth magnetic fields for different systems

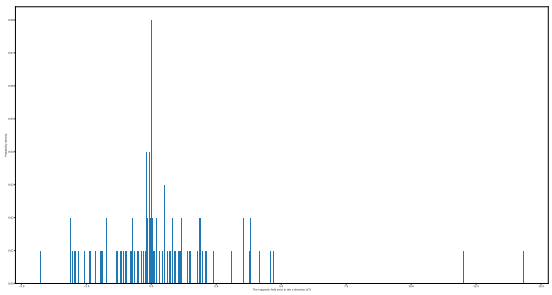

(a) Underdetermined system (2 sensors)

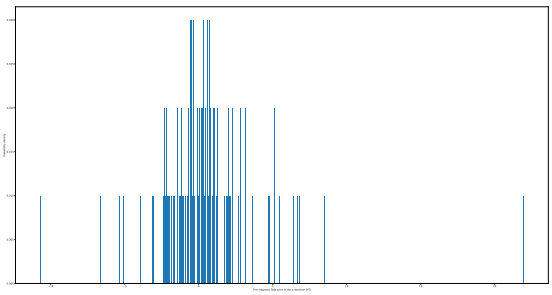

(b) Underdetermined system (3 sensors)

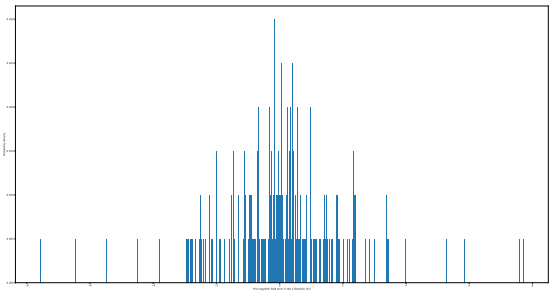

(c) Underdetermined system (4 sensors)

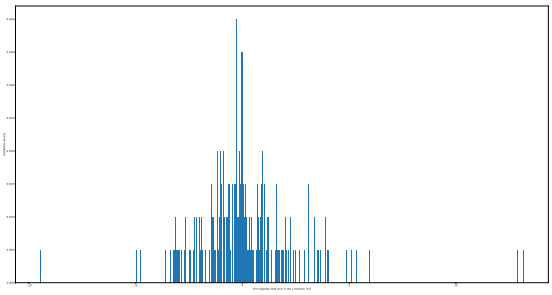

(d) Determined system

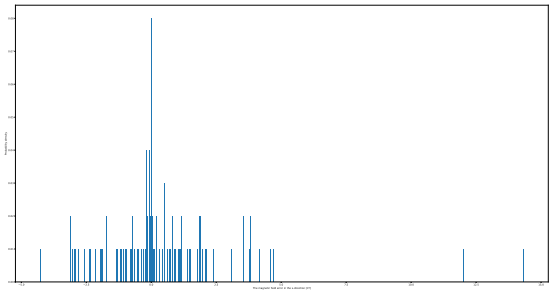

(e) Overdetermined system

Figure 6.7: The errors in calculated magnetic field due to multiple randomized noise sources

7

Simulation

Two data processing methods were discussed in Chapter 5 and verified in Chapter 6. In this Chapter these methods will be compared on effectiveness. The comparison will be done through simulation. The effectiveness of the models will be determined by accuracy and the computational time. Here the accuracy will be the main criteria for comparison. The simulations will be split in three sets to individually analyze the effect of certain characteristics which will be described below. Two of these simulation sets relate to the sub-questions presented in Section 2.2.

The first simulation set studies the effect of the number of sensors on the effectiveness of the system. A varying number of sensors is used during the verification of the SOE method but only to show the difference between the under-, over- and determined systems. This verification lacks the comparison between processing tools and does not investigate the effectiveness of increasing the number of sensors. In the first set of simulations the number of sensors will vary from one to eight.

The second simulation set studies the effect of sensor location on the effectiveness of the system. The simulation will exclude configurations where the distance of a noise source to a sensor is less than 3 cm. These configurations are excluded because noise sources too close to a sensor induces a large magnetic noise.

The third simulation set studies the system effectiveness due to difference between number of noise sources in set-up and assumed in calculation. In a satellite there can be numerous systems/system parts that can generate a magnetic field. As mentioned before a small chip creates multiple small magnetic fields. Therefore the number of actual noise sources in a satellite will most of the time be different from the number of sources assumed for calculations. In this case a set number of noise sources will be generated and the number of assumed noise sources will vary.

All the changing variables in the simulation sets are not completely independent. Therefore a conclusion will be drawn at the end of the chapter such that all simulation sets can be analyzed taking into account all the variables even if they are not completely independent.

The tools that will be tested are the averaging method and the SOE method. The SOE using multiple measurements (SEOMM) as described in Section 5.4 will not be used for simulations because the increase in used equations and unknown variables increases the computational time exponentially. One calculation can take up to 30 minutes.

7.1. General simulation set-up

The simulation can be divided into multiple parts. The first parts are directly related to the inputs. These are the Earth magnetic field, the sensor configuration and the noise source configuration. The other parts are the generation of measurement noise and a filtering method to reduce the effect of the noise. All these parts will be discussed in the sections below. Most of the information presented in this section will be used for each case. Differences or changes to the general set-up will be discussed per simulation set.

A satellite of 30 cm cube will be used for the simulations and all sensors and noise sources are within this space. A nadir pointing satellite with no wobble is assumed during the simulations. The main reason for this assumption is that the physical test will be performed with a place fixed nadir pointing satellite. Therefore the simulations have a better relation with the physical tests.

7.1.1. Earth magnetic field

The Earth magnetic field will be simulated using Equation 7.1. The values are derived for an orbit altitude of 300 km. Here t is the time in seconds. Ten seconds will be simulated with a time set of 0.1 s so that the requirement NMAG-1a-INSTR4 of a measuring frequency of 10 Hz can be met.

$$\begin{aligned} B_{mex} &= 23500 \cdot sin(t \cdot \frac{\pi}{2700}) \\ B_{mey} &= -12000 \cdot sin(t \cdot \frac{\pi}{2700}) \\ B_{mez} &= 50000 \cdot cos(2t \cdot \frac{\pi}{2700}) \end{aligned} \tag{7.1}$$

7.1.2. Sensor model

The sensor locations and the effect of the noise sources will be discussed for each simulation set separately. Other than these variables there are other sources that affect the measured signal. Two of these sources come from the sensor itself and are the measurement noise and the quantification error. These are resolved in the same order as presented below.

During measuring there is a chance that the sensors itself produce noise called measurement noise. This will be simulated using a normal distribution. The mean of the normal distribution will be the magnetic field measured at the sensor. For the simulations of the measurement noise a variance of 10 nT will be assumed. The measurement noise is applied to each direction separately because the sensor measures them separately.

The quantification error can be related to the sensitivity of the sensor if an A/D converter is included with the sensor. In this case a sensitivity of 8 nT is used which corresponds with the LSM303D sensor that was chosen in Section 3.3. The sensitivity will be simulated by rounding the measured magnetic field including the measurement noise to the nearest multiplication of 8 nT.

7.1.3. Filtering method

A one dimensional Kallman filter is used for filtering the computed Earth magnetic field. The filter is applied to the x, y and z directions separately. The Kallman equations are shown in Equation 7.2. As can be seen the rate of change is included in the used filter. In these equations K is the Kallman gain, z is the measured value, the time step is indicated by dt. The predicted values are indicated by x, P is the extrapolated estimated uncertainty, r is the measurement uncertainty and q is the process uncertainty.

$$\begin{aligned} x_{n+1,n} &= x_{n,n} + \dot{x}_{n,n} * dt \\ \dot{x}_{n+1,n} &= \cdot x_{n,n} \\ K_n &= \frac{P_{n,n-1}}{P_{n,n-1} + r_n} \\ \dot{K}_n &= \frac{\dot{P}_{n,n-1}}{\dot{P}_{n,n-1} + \dot{r}_n} \\ x_{n,n} &= x_{n,n-1} + K_n \cdot (z_n - x_{n,n-1}) \\ \dot{x}_{n,n} &= \dot{x}_{n,n-1} + \dot{K}_n \cdot (\frac{z_n - x_{n,n-1}}{dt}) \\ P_{n,n} &= (1 - K_n) \cdot P_{n,n-1} \\ \dot{P}_{n,n} &= (1 - \dot{K}_n) \cdot \dot{P}_{n,n-1} \\ P_{n+1,n} &= P_{n,n} + dt^2 \cdot \dot{P}_{n,n} + q_n \\ \dot{P}_{n+1,n} &= \dot{P}_{n,n} + \dot{q}_n \end{aligned} \tag{7.2}$$

The filter needs estimated values for x, p and their derivatives for the first iteration. The measurement uncertainty (r) and process uncertainty (q) are constant and dependent on the sensors and the model. Therefore these values will be different for the Averaging and SOE method and can be seen in Table 7.1. These values are based on estimates and perfected during multiple iterations were the variables were changed. For both methods the first estimation is based on the first average measured.

Table 7.1: Values uses for Kallman filter

Variable	r_n	$\dot{r}_n$	q_n	$\dot{q}_n$	$P_{estimate}$	$\dot{P}_{estimate}$
Averaging	200^2	10^2	0.01	1	2.5^2	10^2
SOE	25^2	100^2	0.01	1	10^2	20^2

7.2. The system effectiveness due to number of sensors

This case studies the effect of the number of sensors on the accuracy and computational time. The number of sensors used will vary from one to eight sensors. The minimum of one sensor is chosen because most missions use one or two sensors as discussed in Section 2.1. The maximum of eight sensors because this is the number of sides or corners a boxed shape satellite has. The results will compare the error between the total calculated magnetic field and the total Earth magnetic field. The computational time of all configurations will be shown separately.

The general simulation set-up described in Section 7.1 will be used for all the simulations. To complete the simulation set-up the sensor locations and noise configurations will be discussed in the following sections.

7.2.1. Sensor configuration

The sensors are located at each corner of the satellite. Table 7.2 shows the location of each sensor with their sensor number. The sensor locations will stay constant but the number of sensors used will differ each simulation. So if two sensors are tested the first sensor would have the coordinates (0,0,0) and the second sensor would have the coordinates (30,30,0) in cm.

Table 7.2: Sensor configuration 1

Sensor number	X location [cm]	Y location [cm]	Z location[cm]
1	0	0	0
2	30	30	0
3	30	0	30
4	0	30	30
5	30	30	30
6	0	0	30
7	0	30	0
8	30	0	0

Simulating the one to eight sensors separately will be one set of simulations. The same values for noise source configuration, Earth magnetic field and measurement noise will be used for each set. Three sets of simulations will be performed. The time interval of the simulations will be 10 seconds with a measurement frequency of 10 Hz starting at t=0 s. The noise configurations used can be found in Appendix B.

7.2.2. Noise source configuration

Five noise sources will be simulated. The specifications of each noise source (location, pointing direction and dipole strength) will be randomly generated. Two of the noise sources will provide a constant noise and three noise sources will have a dynamic component.

The varying dipoles are split in three kinds which are presented by Equations 7.3 to 7.5. Equation 7.3 represent a combination of noise sources that have an AC characteristic. Equation 7.4 represents a combination of noise sources that have a constant current usage and a part that switches on and off during operation. Equation 7.5 simulates the power generation system in the satellite. Here f is the angular frequency of the dipole change, A is the amplitude of the dipole change, $m_{constant}$ is the random generated value from above. S_{on} is a variable that represents the on state of a system and will randomly be a 1 or 0. Table 7.3 displays the minimum and maximum value for each variable that will be randomized. The distance from a sensor should always be at least 3 cm, this complies to the physical parameters of the sensor which is 1 x 3 cm and the assumption of R»r made in Section 5.2.1.

$$m_{vary} = m_{constant} + A_1 \cdot sin(t \cdot f) \tag{7.3}$$

$$m_{vary} = m_{constant} + A_2 \cdot S_{on} \tag{7.4}$$

$$m_{vary} = |m_{constant} \cdot sin(t \cdot f)| \tag{7.5}$$

Table 7.3: Range of values for noise configuration

Variable	Max	Min	Unit	Type of distribution
x	0	0.3	m	uniform
y	0	0.3	m	uniform
z	0	0.3	m	uniform
$\cos(\theta)$	0	1	-	uniform
ϕ	0	2π	radians	uniform
$m_{constant}$	- 0.157	0.157	$\frac{N \cdot m}{T}$	uniform
f	1	100	$\frac{radians}{s}$	uniform
A	$-\pi * 10^{-4}$	$\pi * 10^{-4}$	$\frac{N \cdot m}{T}$	uniform

7.2.3. Simulation result

The results of the simulations can be found in Table 7.4 and Figure 7.1. To perform the simulations an HP ZBook 15 laptop was used with an Intel core i7-4700MO CPU and 8GB of memory.

Table 7.4: Average computation time of simulation set 1 in seconds

Method	1 sensor	2 sensors	3 sensors	4 sensors	5 sensors	6 sensors	7 sensors	8 sensors
Average	-	2.28E-5	3.67E-5	2.50E-5	2.91E-5	3.12E-5	3.00E-5	6.78E-5
SOE	23.61	39.57	56.30	69.57	84.78	95.37	107.59	123.18

7.3. The system effectiveness due to sensor location

This case studies the effect of sensor location on the accuracy and computational time. The standard corner location will be compared to sets of random sensor locations to see if an optimum location for the sensors exists. The results will compare the error between the total calculated magnetic field and total Earth magnetic field.

The same set of noise configurations as described in the previous section will be used as well as the one and eight sensor configuration from Table 7.2. This sensor configuration will be the first of four configurations. Another sensor configuration that will be used is all sensors in one plane which is shown in Table 7.5. The other sensor configurations will be randomly generated after the noise source characteristics have been decided. A uniform distribution will be used to determine the x,y and z coordinates of each sensor with values between 0 and 0.3 m so that the sensors are within the satellite. The sensors will again be at least 3 cm from the noise sources and the sensors cannot be at the same location.

Table 7.5: Sensor configuration 4

Sensor number	X location [cm]	Y location [cm]	Z location[cm]
1	0	0	0
2	15	0	0
3	30	0	0
4	30	15	0
5	30	30	0
6	15	30	0
7	0	30	0
8	0	15	0

7.3.1. Simulation result

The results of the simulations can be found in Figure 7.2.

7.4. Simulate with two and three noise sources

In the previous sections multiple simulations show that the absolute error of the SOE method is generally more than 50 nT. This doesn't comply to the requirements for the sensor system. This is possibly due to the use of an undetermined SOE. A simulation will be performed with 2 and 3 noise sources to analyze the effect of a determined SOE on a satellite with sensor noise.

The eight sensors will be placed in each corner as described in Section 7.2.1 and the noise sources will be generated as described in Table 7.3. One noise source is simulated as power generating as described in

Equation 7.5 and one as a noise source that switches between an on and off state as shown in Equation 7.4. The third noise source will be constant if used. The results can be found in Figure 7.3. This figure shows that a determined or even an overdetermined system is not enough to calculate the earth magnetic field within the 50 nT range necessary. Only a very overdetermined system, like the two noise source and eight sensor configuration presented, is able to calculate the Earth magnetic field with an accuracy requirement of 50 nT. The SOE method with an overdetermined system is still possible to produce a more accurate result than averaging.

7.5. The system effectiveness due to difference between number of noise sources in set-up and assumed in calculation

In reality there are multiple noise sources in a satellite. To simulate this effect 100 different small noise sources will be simulated and only a couple will be determined for the SOE method. As shown in Chapter 6 and the previous section, the SOE works the best when the system is (over-) determined. Therefor the SOE method will be used twice, once assuming that two sources are present and one time when three noise sources are present.

7.5.1. Specific set-up

The sensor configuration that will be used is the same as described in Section 7.2.1, which has eight sensors each in a corner of the satellite. The noise sources will be split in different groups. The first group represent the power generation which uses Equation 7.5 and the noise characteristics will be generated according to Table 7.3. The noise sources in the other groups will use the values of Table 7.6 to generate the noise characteristics which has a smaller value of dipole moment. The second group exist of 40 noise sources that switch between an on and off state as shown in Equation 7.4. The third group consist of 10 noise sources with an AC characteristic as shown in Equation 7.3. The fourth group consist of 49 noise sources which generate a constant magnetic noise. The sensors will again be at least 3 cm from the noise sources.

Table 7.6: Range of values for noise configuration simulation set 3

Variable	Max	Min	Unit	Type of distribution
x	0	0.3	m	uniform
y	0	0.3	m	uniform
z	0	0.3	m	uniform
$\cos(\theta)$	0	1	-	uniform
ϕ	0	2π	radians	uniform
$m_{constant}$	- 0.00157	0.00157	$\frac{N \cdot m}{T}$	uniform
f	1	100	$\frac{radians}{s}$	uniform
A	$-\pi * 10^{-4}$	$\pi * 10^{-4}$	$\frac{N^s m}{T}$	uniform

7.5.2. Simulation result

The results of the simulations can be found in Figure 7.4.

7.6. Simulation conclusion

Multiple observations can be made from the simulation results presented in Figure 7.1 to 7.4 and Table 7.4. The first noticeable observation is related to the computation time. The averaging method slightly differs with increasing number of sensors with a longest average time of 6.78E-5 seconds. This is much lower than the 10 Hz measuring frequency which can be assumed as the total system frequency because the computational time is negligible compared to the measuring frequency of the sensor. The computation time of the SOE method varies largely with increasing sensors with the highest observed average of 123.18 seconds using 8 sensors and 6 noise sources and lowest 23.61 seconds using 1 sensor and 6 noise sources. Even the lowest possible computational time will be the leading time increment of the magnetic field instrument, which doesn't comply to the requirement NMAG-1a-INSTR4 of measurement frequency of 10 Hz. The computation time will differ depending on the processing power of a system. For research purposes more powerful systems could be used and even parallel processing becomes an option. For Attitude control the calculations need to be performed in real time on the satellite. A small satellite like a cubesat doesn't have the power for

such a processor at the time of writing this report and thus the requirement NMAG-1a-INSTR4 might be met in the future.

The results of Section 7.2 shows that increasing the number of sensors will not always produce a better result. The accuracy of both methods depends more on the configuration of the noise sources with respect to the sensor configuration and thus a higher accuracy can be achieved with a small number of sensors or even one if they are well placed. This is Further proven in Section 7.3 where multiple sensor locations were used. If multiple sensors are used it is best to place them at opposite sides of the satellite which is completely done in sensor configuration 1 and partly done in sensor configuration 4 where all sensor are placed in the same plane.

An accurate Earth magnetic field can be calculated if and only if a very overdetermined system can be generated as shown in Section 7.4. This is never realistic because eight sensors are already needed to accurately calculate the Earth magnetic field for two noise sources.

In most situations the averaging method produces better or equal results than the SOE method. Taking this into account and the extra computational time mentioned above, it can be concluded that the SOE method in its current form is not useful and averaging method is preferred.

The effectiveness of multiple sensors with the averaging method depends mostly on the combination of noise and sensor configuration. The results shown in Figure 7.3 indicates that a sensor configuration with sensors in each corner of the satellite is the most effective in multiple situations but not in all. The ideal number of sensors depends mostly on the noise source configuration and thus needs to be analyzed on a case by case basis. For the test set-up it will be recommended to increase the minimum distance between a noise source and sensor to 5 cm so that the effect of the noise on the sensor is reduced. Also the placement of the biggest noise source should be as much in the middle as possible to maximize the distance from each sensor.

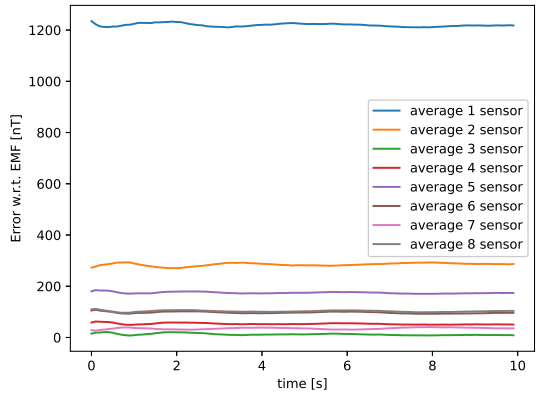

(a) configuration 1: averaging

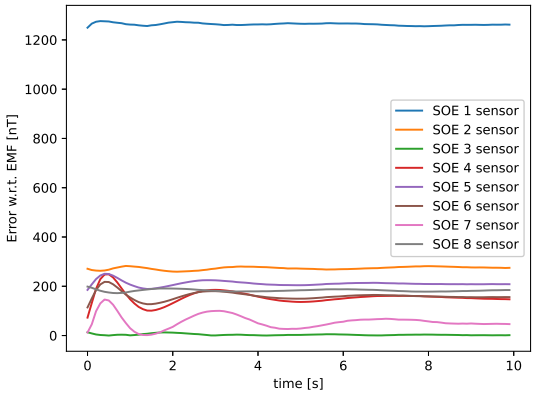

(b) configuration 1: SOE

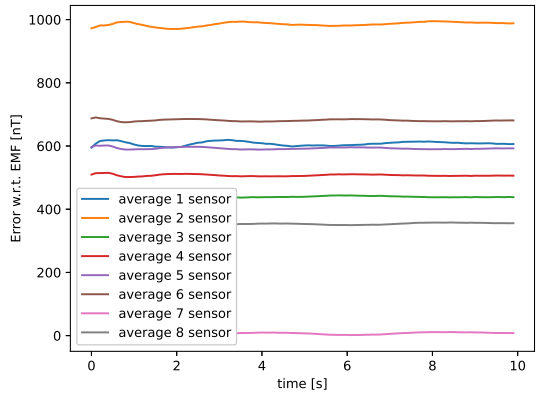

(c) configuration 2: averaging

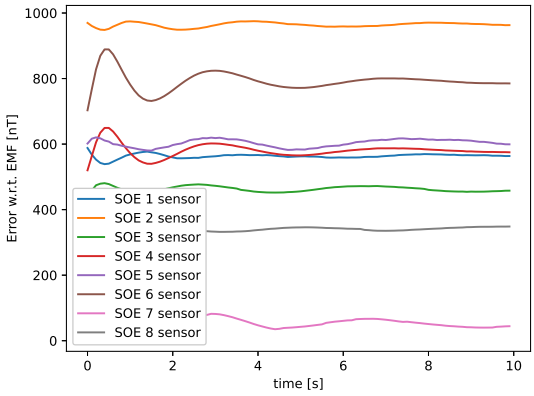

(d) configuration 2: configuration 2: SOE

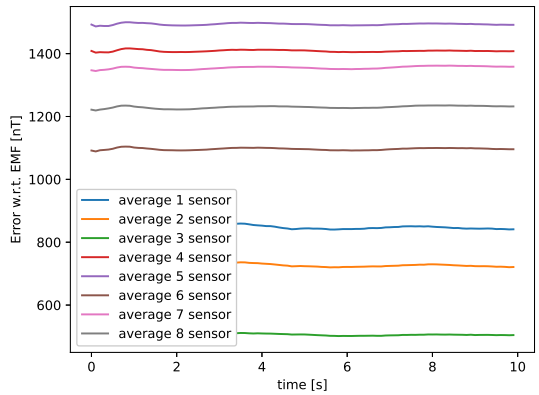

(e) configuration 3: averaging

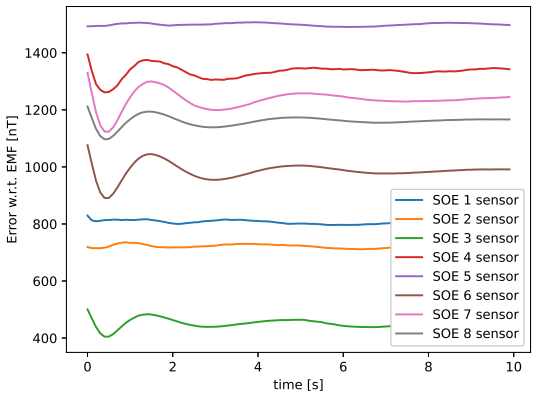

(f) configuration 3: SOE

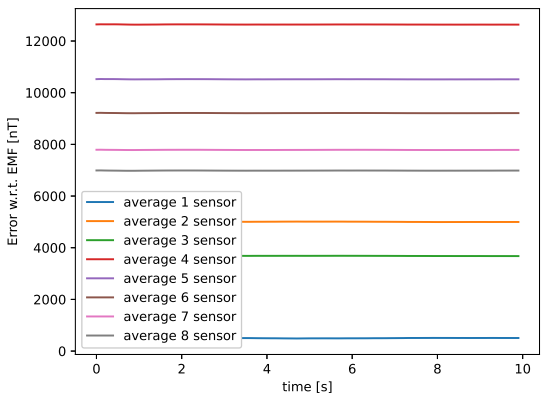

(g) configuration 4: averaging

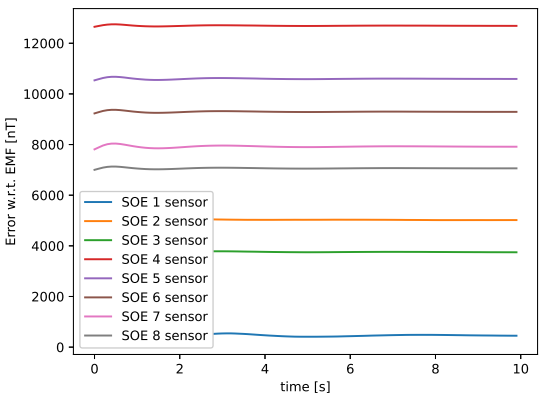

(h) configuration 4: SOE

Figure 7.1: Comparing the absolute magnetic field error of a changing number of sensors of simulation set 1

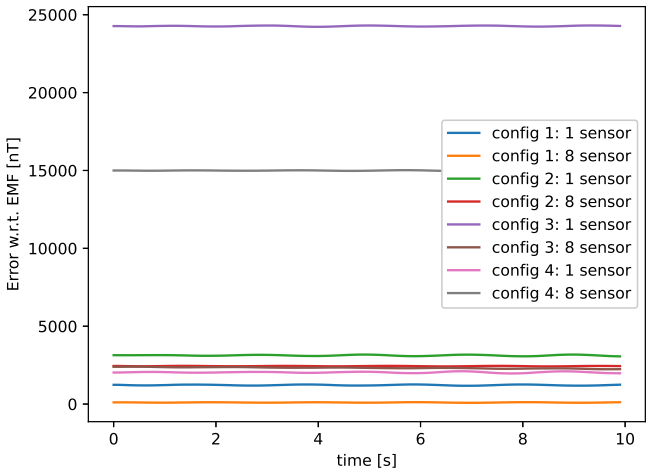

(a) configuration 1: averaging

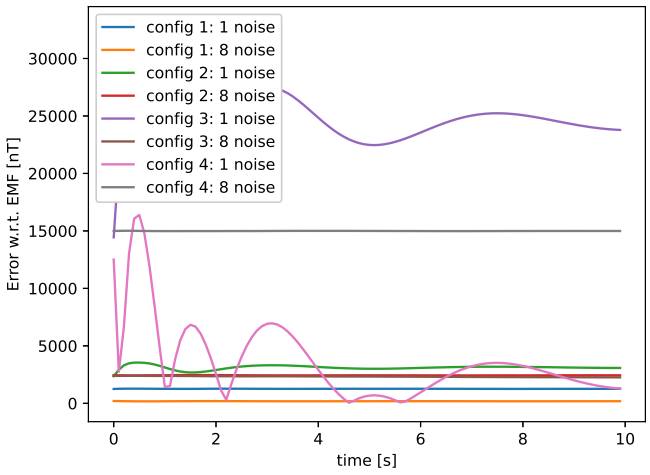

(b) configuration 1: SOE

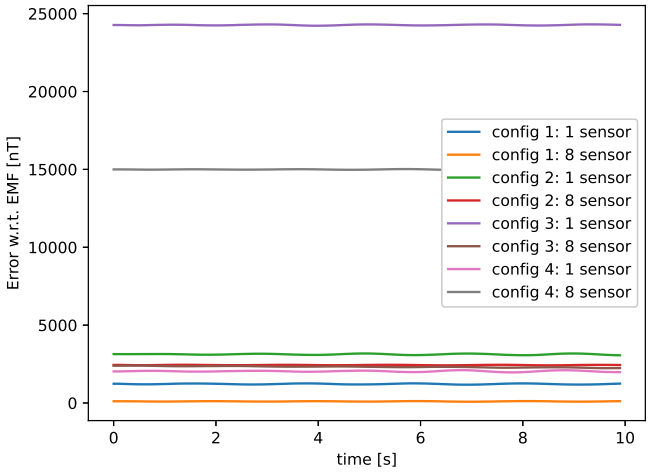

(c) configuration 2: averaging

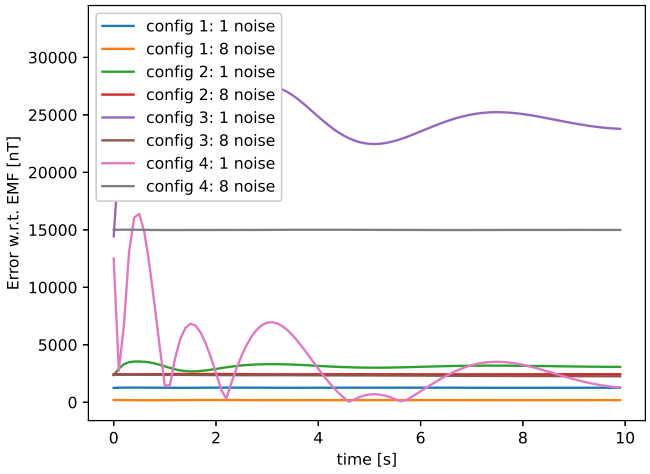

(d) configuration 2: configuration 2: SOE

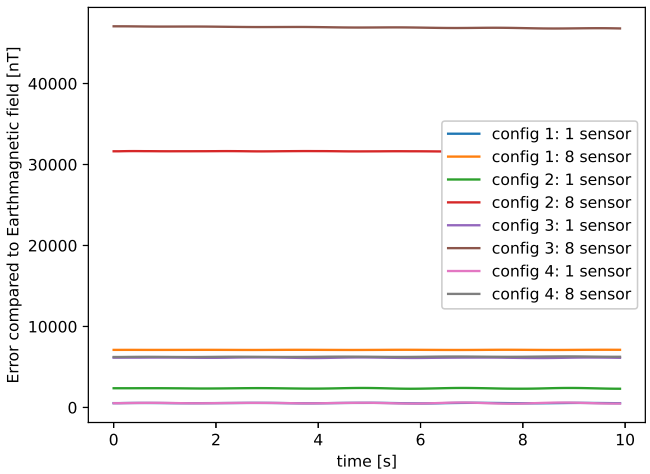

(e) configuration 4: averaging

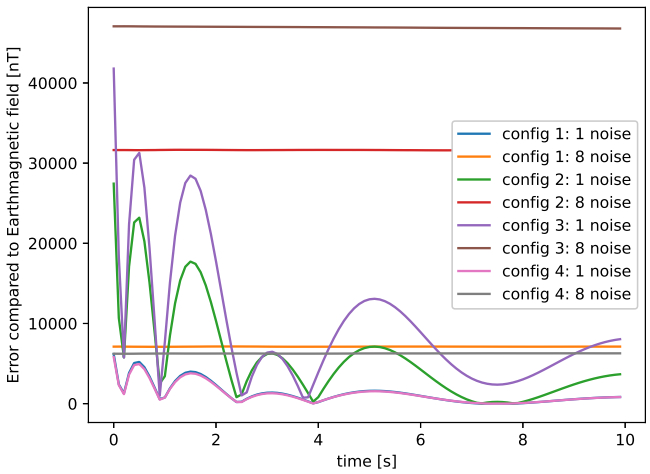

(f) configuration 4: SOE

Figure 7.2: Comparing the absolute magnetic field error of a changing sensors configuration of simulation set 2

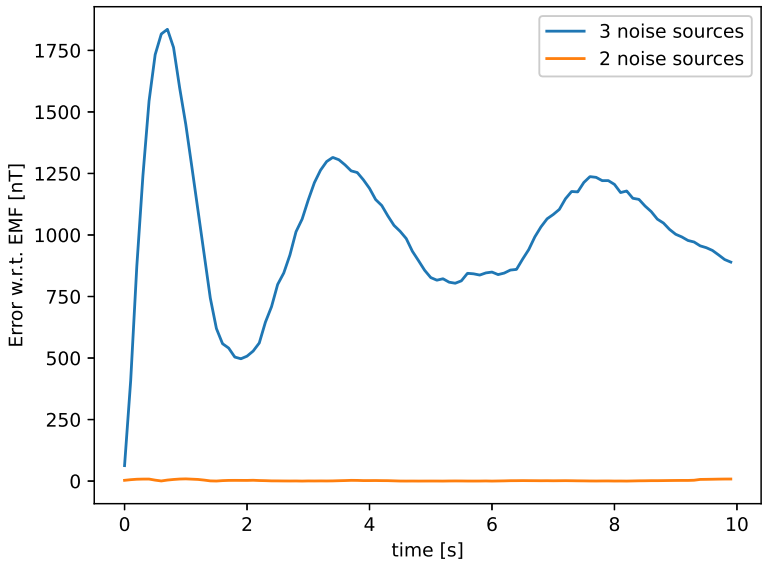

Figure 7.3: Comparing the absolute magnetic field error between two and three noise sources

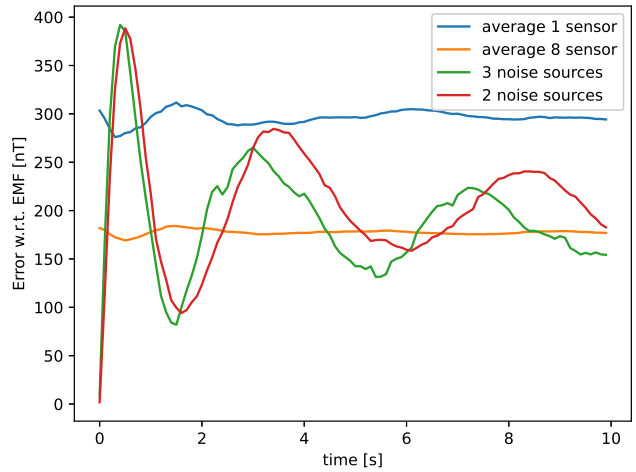

(a) configuration 1

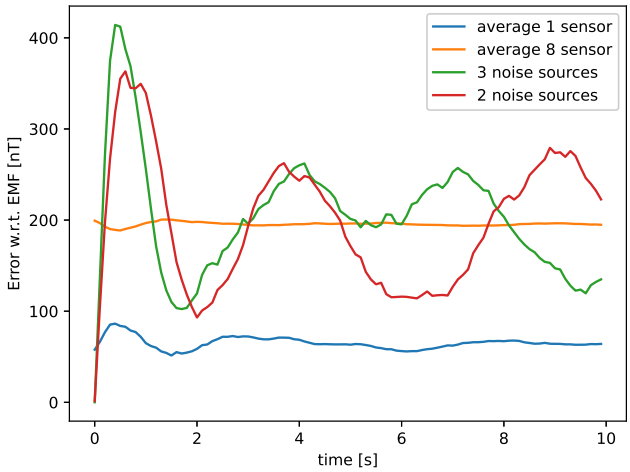

(b) configuration 2

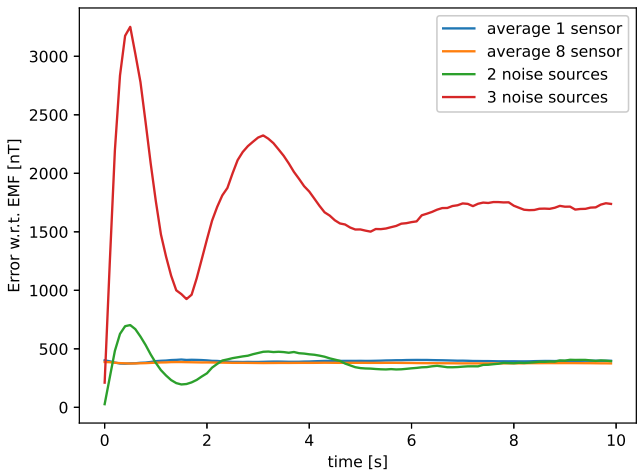

(c) configuration 3

Figure 7.4: Comparing the absolute magnetic field error of multiple noise sources simulated by a limited number of simulation set 3

8

Calibration

The previous chapters mentioned the selection of sensor parts and the methods to process the measured data. The next step is to test if the individual components of the magnetic field instrument work properly. This is done in the Section 8.1 for every component except for the sensors. The sensors are treated separately in Section 8.2 where they are tested and some calibration techniques are discussed. Finally this chapter is concluded with the calibration of the sensors.

8.1. Testing the components

Most of the components mentioned in Section 4.1 can easily be tested by connecting the component as described by their manufacturer in combination with a test program connected to a controller. These components are the Arduino mega2560, the SD writer/reader and the multiplexer. The Arduino mega2560 was tested using basic scripts such as "Blink" which are provided in the Arduino IDE environment. The Arduino is the brain of the system as the controller and thus will be continuously tested by testing the other components. The SD writer/reader needs a SD-card with a Fat16 or Fat32 file-system to work. To test this component the Arduino was tasked to create an empty file and then write to that file. The multiplexer could be tested by connecting it to the Arduino and two sensors and run a script which switches the communication between the sensors.

Testing the power converter can be done using a power source at the input of the chip and connecting a resistance at the output. As a step down converter, the output voltage should be lower than the input voltage and can be measured using a multi-meter. The voltage drop can be regulated physically with a screw. To prevent a high voltage to the system it is recommended to start with the highest voltage drop and slowly reduce the drop until approximately 5 V is reached. To prevent the chance that the total resistance at the output of the step-down converter effects the output voltage of the converter, this should be done every time parts are added or removed from the system so a failure will be prevented.

8.2. Calibration methods

Testing the basic functions of the LSM303D sensors is simple. Just connect it to the Arduino as specified by the manufacturer and do a test run. The effectiveness of the sensor however needs to be studied. The sensors will be programmed to the highest sensitivity setting for measuring magnetic fields while disabling the accelerometer part of the sensor so that the frequency of measurement could be increased. This also removes unnecessary data and power usage. The changes are all explained in the data sheet. The manufacturer states that bias calibration might be needed if these settings are changed. To determine the necessity of calibration several tests are performed. The first test is done by performing measurements of all the sensors in the same location and see the differences between the sensors. Figure 8.1 shows the measured magnetic field strength and the pointing angles for seven sensors. The figure also includes the Earth magnetic field that was present at the time of testing. The Figure shows that there is a ± 8000 nT difference between the maximum and minimum measured Earth magnetic field of the sensors. The sensors responsible for these upper and lower limits differ in each direction. A difference can be found in the directional angles as shown in Figures 8.1d and 8.1e because the bias of the sensor is different in each direction (x,y and z). The Figures also indicate the presence of a noise source which can be recognised by the difference between the measured magnetic fields and Earth

magnetic field. This difference is most noticeable in the z-direction. The noise source in the calibration set-up consists of the Arduino nano, the SD-card reader/writer and 9 V power source. Lastly a variation of 200 nT can be seen in each sensor measurements which is caused by a combination of the sensor, equipment and ambient magnetic field. All the figures indicate that the sensors need to be calibrated for the bias of the sensors itself and the noise caused by the other components. The elimination of the noise is important because the configuration of component differ between calibration set-up and final Assembly.

8.2.1. Calibration using provided code

The manufacturer provides a code for calibration which determines the minimum and maximum values in the x, y and z direction of a measurement. For the measurement the sensor needs to be rotated around its axis in all directions. This does not calibrate the sensors by itself, it just shows the maximum variation in all directions. The max and min values are only useful if a constant magnetic field was used which isn't checked by the program. The values can be used to find a constant correction values for the x, y and z direction and doesn't take rotational correction in consideration. The rotational correction is needed to compensate for a misalignment of the sensor. This happens for instance if the sensor is not parallel to the mounted surface. The calibration method provided by the manufacturer cannot be used to calibrate the sensors for the intended use of the sensors.

8.2.2. Calibration using Magcal

Magcal is a Matlab program which use Equation 8.1 to calibrate the sensor. In this equation $\boldsymbol{C}$ is the calibrated magnetic field vector. The measured magnetic field is indicated by D, which is a n by 3 matrix where n is the number of measurements. b is a correction vector and $\boldsymbol{A}$ is the correction matrix. The input for this method is the measured magnetic field, which is obtained by slowly rotating the sensor around each axis while measuring. The other input is the total ambient magnetic field which should be measured. This method helps in calibrating the directional measurement of the magnetic field but doesn't correct for the absolute value.

$$\boldsymbol{C} = (D - b) \cdot \boldsymbol{A} \tag{8.1}$$

8.2.3. Multi-position static tests

Another method that can be used for calibrating a magnetometer is called multi-position static tests (MST) which in commonly used for the inertial senor calibration of a inertial navigation system as stated by Hudak Et al. [4]. In this article, this method is used to calibrate their sensor. The goal of these tests is to approximate static conversion characteristics of 3-axis magnetometer based on analysis of measurement results obtained by rotating the sensor on a turning platform in the vertical plane around the x, y, z-axis. Part of the set-up can be seen in Figure 8.2.

Mathematically the relationship between the measured signal and calibrated signal can be written as seen in Equation 8.2.

$$\begin{bmatrix} \boldsymbol{B}_x \\ \boldsymbol{B}_y \\ \boldsymbol{B}_z \end{bmatrix} = \begin{bmatrix} \boldsymbol{M}_{xx} & \boldsymbol{M}_{xy} & \boldsymbol{M}_{xz} \\ \boldsymbol{M}_{yx} & \boldsymbol{M}_{yy} & \boldsymbol{M}_{yz} \\ \boldsymbol{M}_{zx} & \boldsymbol{M}_{zy} & \boldsymbol{M}_{zz} \end{bmatrix} \begin{bmatrix} b_x \\ b_y \\ b_z \end{bmatrix} + \begin{bmatrix} b_{x0} \\ b_{y0} \\ b_{z0} \end{bmatrix} \text{ [4]} \tag{8.2}$$

The uncalibrated output signals of the sensor are denoted by b_x, b_y, b_z. $\boldsymbol{M}_{xx}$, $\boldsymbol{M}_{yy}$, $\boldsymbol{M}_{zz}$ are the multiplicative (sensitivity) constants. The additive constants are b_{x0}, b_{y0}, b_{z0}. $\boldsymbol{M}_{xy}$, $\boldsymbol{M}_{xz}$, $\boldsymbol{M}_{yx}$, $\boldsymbol{M}_{yz}$, $\boldsymbol{M}_{zx}$, $\boldsymbol{M}_{zy}$ are orthogonality constants and $\boldsymbol{B}_x$, $\boldsymbol{B}_y$, $\boldsymbol{B}_z$ are the calibrated orthogonal outputs.

As mentioned during the calibration, the sensor will be mounted on a turntable and will slowly move around one axis at a time to perform measurements. In the tests performed by Hudak Et al. [4] they make steps of 1° over a range of 450°. For each degree and channel they gathered 100 samples. The range used covers 1.25 circles and thus generates more data for some angles. In a perfect world these points should be the same when a constant signal is generated. In reality there will not be a constant signal because there are other signals present such as the Earth magnetic field and magnetic fields generated by other devices. The 0.25 extra turn can thus be used to filter out some of the dynamic noise.

8.3. Modified multi-position static tests

The MST method is good but not complete. The sensor consists of multiple parts that measure the magnetic field strength of each direction separately and because of the possible misalignments there should be a constant error which should be taken into account with the correction matrix. Therefore Equation 8.3 is used to calculate the corrections. Here the vector C is a bias correction.

$$\begin{bmatrix} \boldsymbol{B}_x \\ \boldsymbol{B}_y \\ \boldsymbol{B}_z \end{bmatrix} = \begin{bmatrix} \boldsymbol{M}_{xx} & \boldsymbol{M}_{xy} & \boldsymbol{M}_{xz} \\ \boldsymbol{M}_{yx} & \boldsymbol{M}_{yy} & \boldsymbol{M}_{yz} \\ \boldsymbol{M}_{zx} & \boldsymbol{M}_{zy} & \boldsymbol{M}_{zz} \end{bmatrix} \left(\begin{bmatrix} b_x \\ b_y \\ b_z \end{bmatrix} + \begin{bmatrix} c_x \\ c_y \\ c_z \end{bmatrix} \right) + \begin{bmatrix} b_{x0} \\ b_{y0} \\ b_{z0} \end{bmatrix} \tag{8.3}$$

The measurements of the sensors are done using a rotational device which is shown in Figure 8.3 and fixed location measurements where the sensor is placed in four locations around the rest of the components. The locations are East, North, West and South of the sensor. For the fixed location measurements the x direction of the sensor is placed in the North direction. All measurements are performed in a location where only the earth magnetic field is present. The earth magnetic field can be determined using sources such as NOAA (National Oceanic and Atmospheric Administration) [37], the only inputs needed are the location on Earth, the elevation with respect to sea level and the date.

8.4. Location of the calibration

As mentioned in Section 8.2 the variation in the measurement is dependent on the sensor, the equipment and the ambient magnetic field. The sensor and equipment are part of the calibration system and therefore their effect cannot be changed. However the ambient magnetic field can be controlled which depends on the location. The best location would be a room with a zero magnetic field and a known magnetic field source. Unfortunately the amount of such rooms is limited and it was not possible to gain access to such a room at the time of writing this thesis. Therefore a location was found with a known magnetic field.

The Earth magnetic field can be used as reference magnetic field and can be determined from the database of NOAA (National Oceanic and Atmospheric Administration) [37]. Multiple locations were considered for the calibration of which two will be presented in this report. The locations considered are an apartment and the Biesbosch, all in Dordrecht, the Netherlands. The location in the Biesbosch can be found in Figure 8.4. The apartment is considered because there is no weather dependency, tests can be performed at each point of the day and all equipment is within arms reach. The Biesbosch has locations that are away from human build structures such as buildings and powerlines and should be relatively magnetically clean. The closest building is 700 m away from the chosen location. At each of these locations tests were performed to determine the best test location.

The results can be found in Figure 8.5. The apartment is not the most suitable location of the two which can be expected with all the electronics in the building acting as noise sources, most of these sources cannot be controlled. The downside of the Biesbosch is the movement of other humans with technology, fortunately there is minimal movement in the selected area and the problem can be mitigated. Therefore the calibration and the tests will be performed in the Biesbosch.

8.5. Calibration of the sensors

The results of the calibration can be found in Figure 8.6. The presented calibrated measurements use the original measurements which are presented in Figure 8.1. The calibrated measurements are closer to each other and closer to the actual Earth magnetic field. In this case the calibrated measurements can differ from the Earth magnetic field because everything except the sensor is considered a noise source and should be visible in the results.

There are some sensors that have an offset compared to the other sensors in a certain direction. This is mostly present in the y-direction for sensor five and six. This can be caused by an unexpected error during test with the rotational device.

Some of the measurements have a sudden large spike which is most probably caused by a communication error between the sensor and the Arduino because of the randomness of occurrence. A drift can be noticed in the first and last seconds of the measurement, this drift is caused by the observer leaving and entering the test area to switch the measuring equipment on or off. The drift is most prominent in the z-direction.

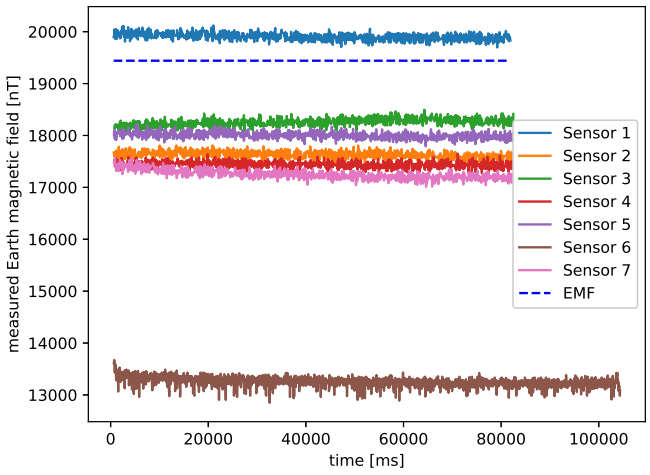

(a) All sensors in x direction

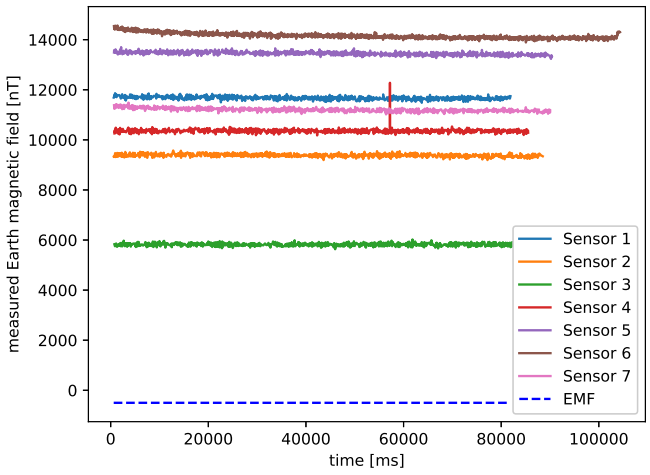

(b) All sensors in y direction

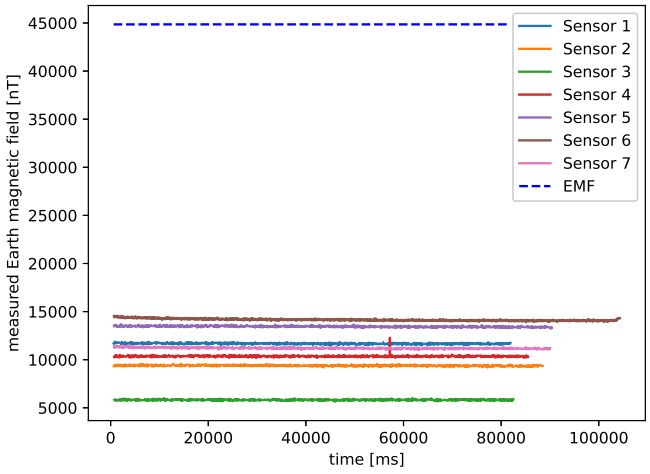

(c) All sensors in z direction

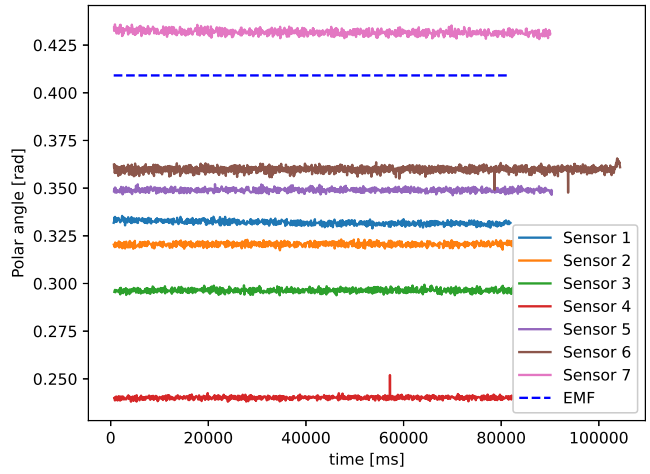

(d) Polar angles

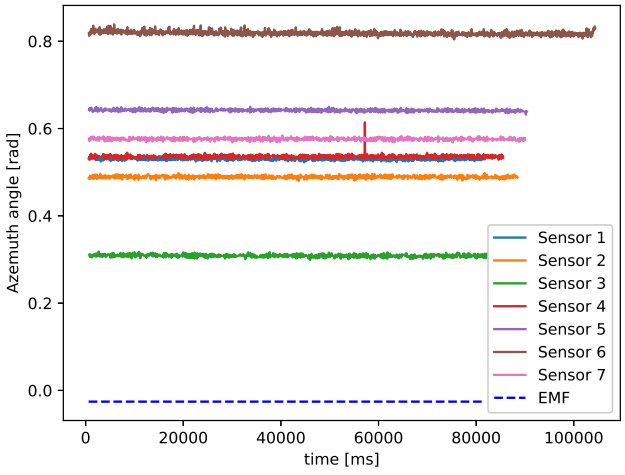

(e) Azimuth angles

Figure 8.1: Measured magnetic field and angles

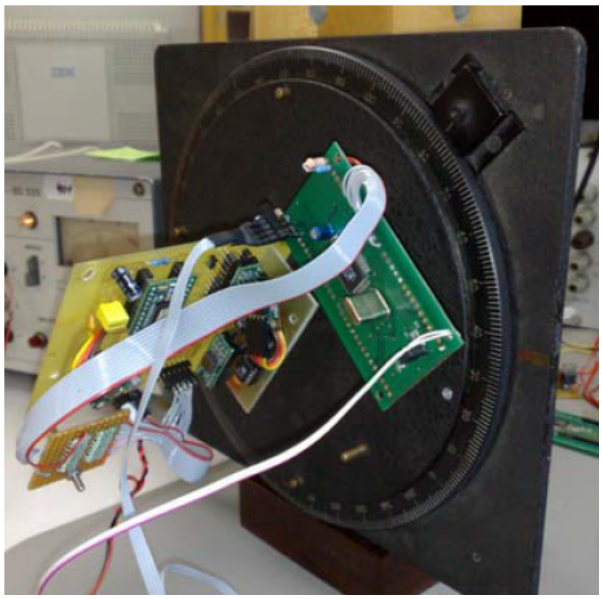

Figure 8.2: test set-up for calibration of a magnetometer [4]

Figure 8.3: Rotation device

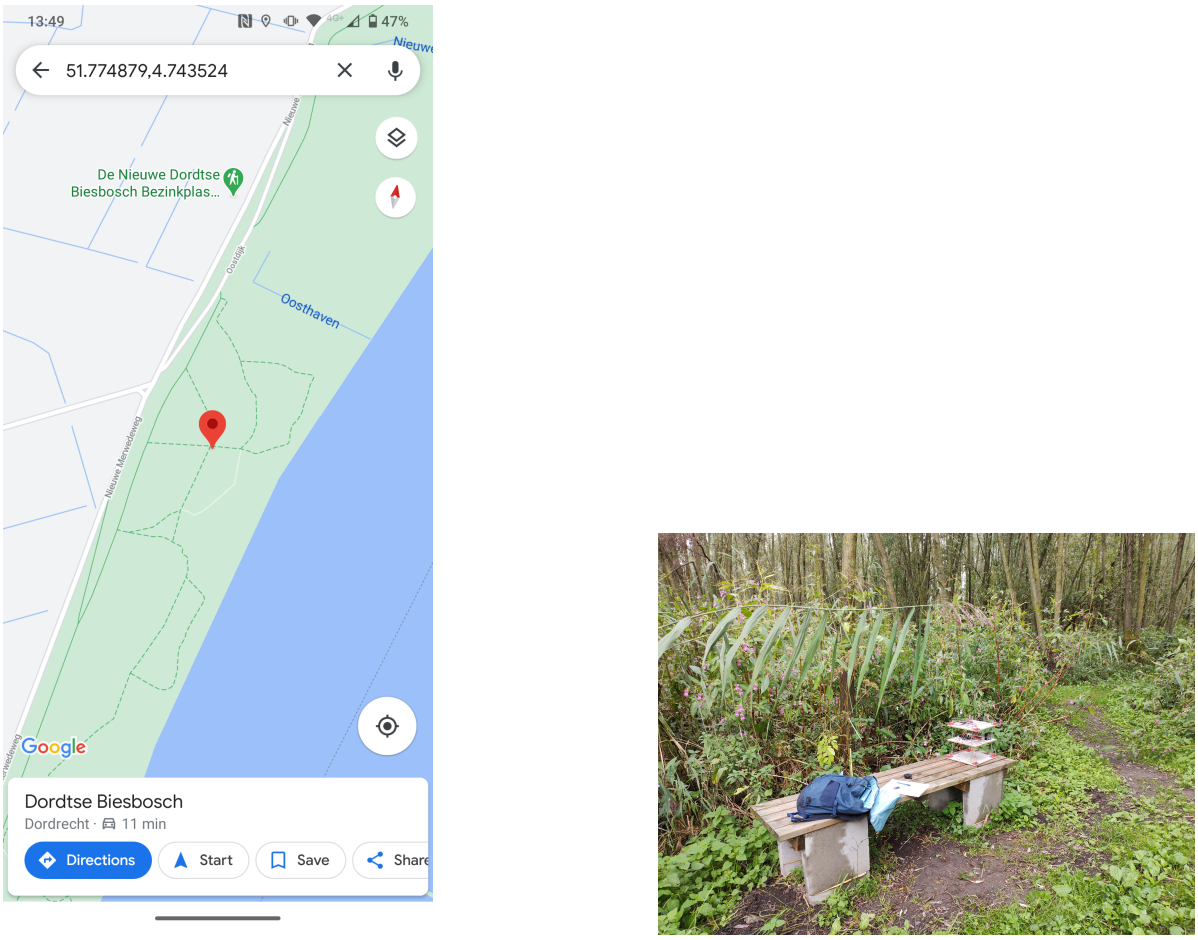

Figure 8.4: Test location

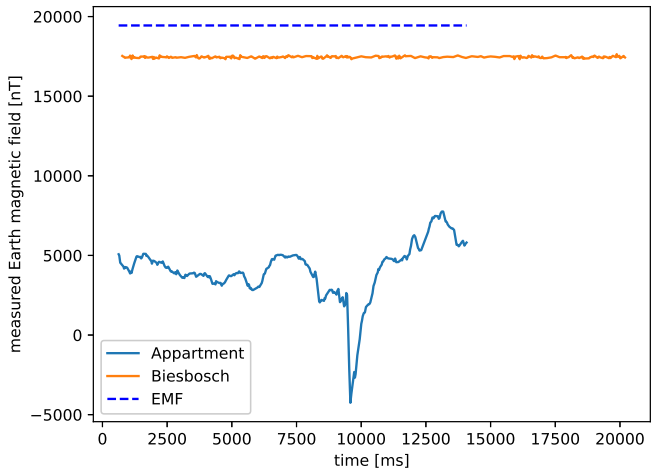

(a) All sensors in x direction

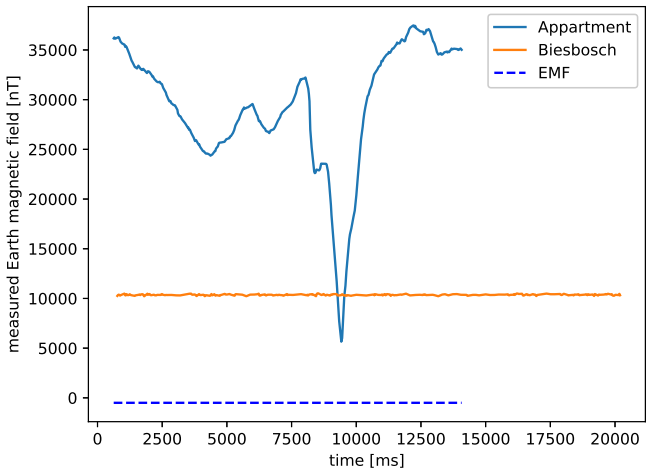

(b) All sensors in y direction

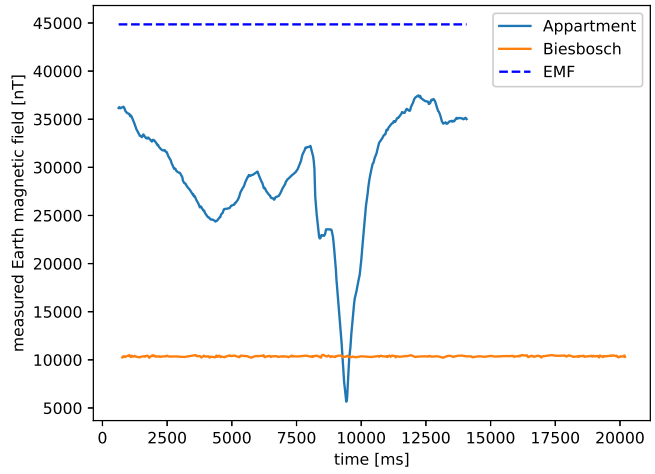

(c) All sensors in z direction

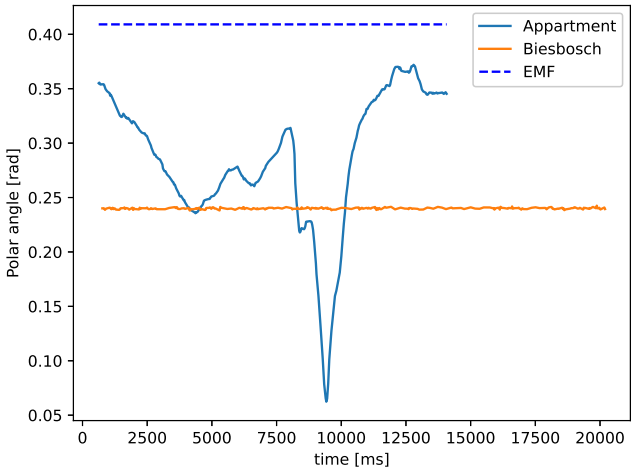

(d) Polar angles

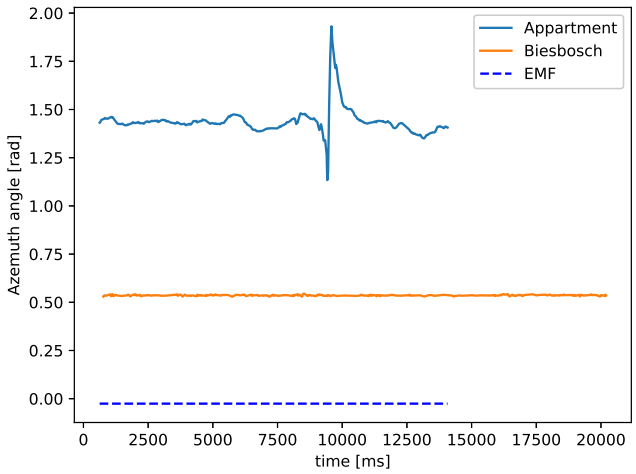

(e) Azimuth angles

Figure 8.5: Measured magnetic field and angles

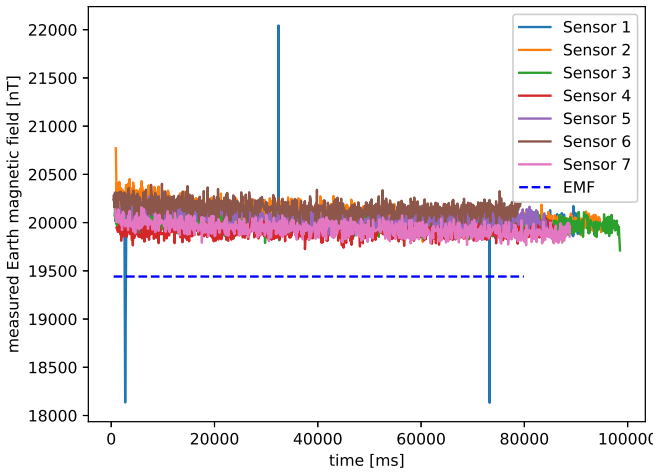

(a) All sensors in x direction

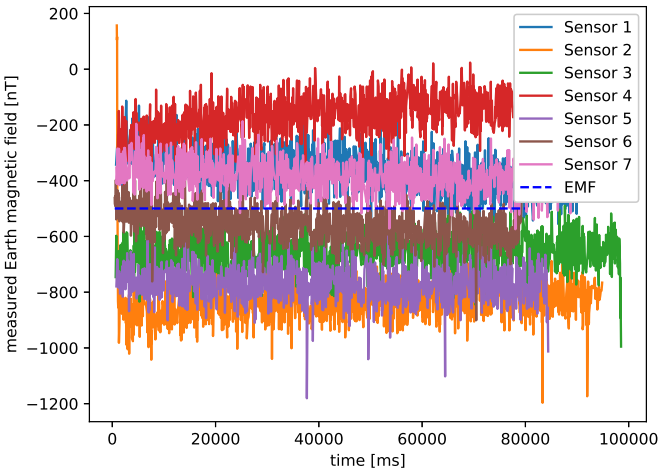

(b) All sensors in y direction

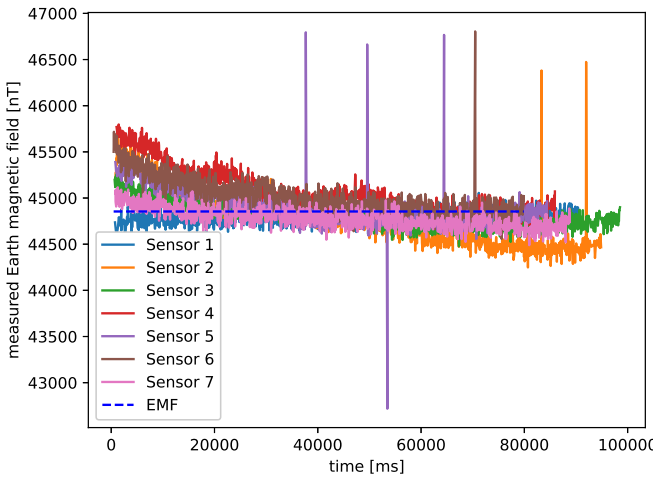

(c) All sensors in z direction

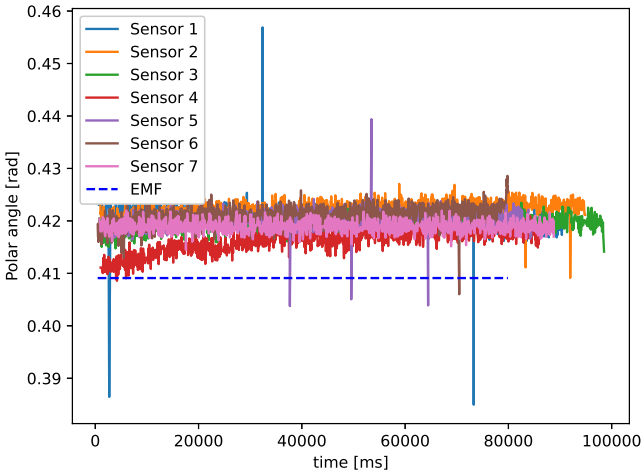

(d) Polar angles

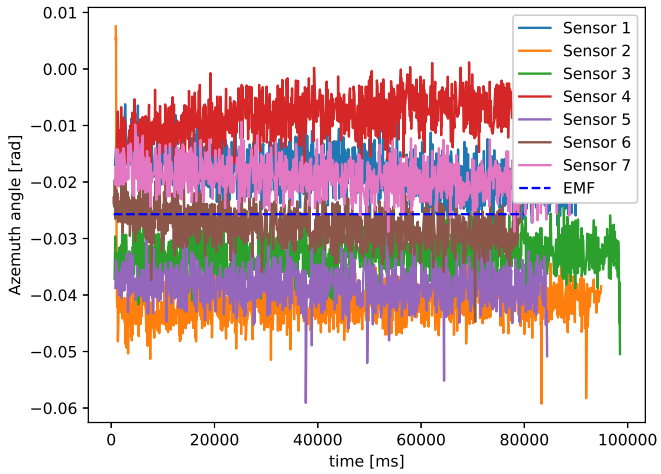

(e) Azimuth angles

Figure 8.6: Corrected measured magnetic field and angles

9

Test set-up

To test the selected sensors discussed in Chapter 3 and the control technique discussed in Section 5 a test set-up needs to be designed. The design of the set-up can be split in four separate parts: the platform, the noise sources, the testing location and finally the situations that will be tested. Each of them will be discussed in their own section in the same sequence.

9.1. Platform

A good test set-up should be able to represent a realistic situation and be adaptable to test different situations. For the simulations a satellite of 30 cm cube is used, so a platform is created which has the same dimensions. A technical drawing of the complete test set-up can be found in Figure 9.1 and a picture of the final design can be seen in Figure 9.2a. The platform consists of multiple layers connected by four pillars. Each layer is a 30 by 30 cm wooden plate and can hold multiple devices. In the middle of each plate there is a 10 mm hole to guide all wires present. In this way multiple configurations can easily be tested. Wood was chosen for the plate because of its low magnetic permeability of $1.257E-6$ [H/M]. In comparison a vacuum has a magnetic permeability of $4\pi E-7$ [H/m] and pure iron $6.3E-3$ [H/m]. The four pillars are made of galvanised steel threaded rods which are great for adjusting the height of the plates of the test set-up. A downside of these rods is the magnetic permeability which has a value around $1.26E-4$ [H/m]. A precise value cannot be determined because the exact composition of the steel is unknown. Thus the pillars will act as magnetic noise sources in response to the other active magnetic noise sources (magnetic field generated by electrical current). For the tests, multiple magnetic noise sources are required of different magnetic strengths and sizes. Therefore the pillars can be seen as separate noise sources. For a satellite design itself it would be better to replace the pillars with aluminium.

The Following components are present in the basic set-up (sensors system only):

- 8x Lsm303d sensor
- 8x small breadboards
- 1x big breadboard
- 1x Arduino mega 2560
- 1x 12V battery
- 1x TCA9548A multiplexer
- 1x MP1584 Power converter
- 1x Adafruit MicroSD card breakout board+
- Multiple wires

The sensors are each placed on a small breadboard and placed on each corner of the test set-up as close to the edge as possible. The rest of the equipment is placed on the middle section except for the wires which of course run from component to component. The wires are twisted when possible and kept short to reduce magnetic noise. The power converter, the multiplexer and SD-card reader/writer are all placed on the big breadboard to keep the wires as short as possible.

9.2. Noise sources

There are multiple noise sources present in a satellite of which some are semi-constant, such as direct loop currents, and some are time varying, such as alternating currents (high frequency, constant amplitude) or time varying (low frequency, varying amplitude) as can be seen in the research by Ke et al. [1]. Other semi-constant noise sources are for instance other components or instruments which generate a different constant noise depending on its operating state. An example of this is a component that has an on and off state and thus two different noise levels. An example of a time varying noise source is a solar cell of which the noise varies depending on the intensity of the sunlight on the cell. The noise sources are simulated using five current loops which are all connected in series with a resistor and the power supply. The current loops are numbered to identify specific windings, the numbering goes from top to down and from front to back according to the technical drawing which can be found in Figure 9.1. The complete set-up is displayed in Figure 9.2.

The Following components are used to create the noise source system:

- 1x Arduino nano
- 1x 9V battery
- Multiple wires (both connections and windings)
- 3 x 100 μF capacitor
- 3 x Transistor TO-92 NPN 40V PN2222A
- 2 x Schottky Diode 1N5819

The characteristics of each noise source can be found in Table 9.2 which includes the size, resistance, voltage of each winding and indicates which are varying and constant. All windings are connected to 1 small breadboard except for Winding 5 which is directly connected to the 12 V power supply. Winding 1 and 2 are connected to a varying current. The varying current is created with use of a one leg converter (as displayed in Figure 9.3) and an Arduino nano to provide a PWM signal. The frequency of the PWM signal is set to 122.5 Hz and the duty cycle changed every 500 ms.

Table 9.1: Noise sources

Name	Winding inner diameter [mm]	Number of winding [-]	Resistance [Ohm]	Voltage [V]	Source	Magnetic dipole [Am^2]
Winding 1	38	2.5	2200	0-4.2	varying	0 - 2.165E-5
Winding 2	40	2.5	100	0-4.2	varying	0 - 5.278E-4
Winding 3	40	3.5	10	9	dc	1.583E-2
Winding 4	40	1.0	4700	9	dc	9.62E-6
Winding 5	95	1.5	220	12	dc	2.320E-3

9.3. Test cases

The goal of the testing is to compare the results of the averaging method which uses data of multiple sensor and the measurements of a single sensor. To test the sensor system four test cases will be analyzed .

The first case will test only the sensor system and no additional noise sources. This is done to test the effectiveness of the single sensor calibration performed in Chapter 8 is holding up. The complete sensor system is more complex because of more components and different parts and thus introducing more impedances. Which can lead to an error in the measurements. If needed the sensor system can be calibrated again with the results of this test. The first case will consist of three test and for each test x-direction of the sensors will be pointed in a different direction, which are North, West and South. Each test will run for two minutes.

The second case test the sensor system in combination with the noise sources as discussed above. The test starts with the noise sources off and will be turned on during the test. Each test will be 2.5 minutes and

the noise sources will be switched on after 60 seconds. This case will be tested twice, once with the x-direction of the sensors pointing to the North and once with the x-direction of the sensors pointing south.

The third case will be performed the same as the second case with a change in the noise sources and the x-direction of the sensors will be pointed North initially. The new configuration can be found in Table 9.2. Over time the complete test set-up will be rotated around the z-axis.

Table 9.2: Noise sources 2

Name	Winding inner diameter [mm]	Number of windings [-]	Resistance [Ohm]	Voltage [V]	Source	Magnetic dipole [Am^2]
Winding 1	38	2.5	2200	9	dc	4.640E-5
Winding 2	40	2.5	100	9	dc	1.131E-3
Winding 3	40	3.5	10	0-4.2	varying	0 - 7.389E-3
Winding 4	40	1.0	4700	0-4.2	varying	0 - 4.492E-6
Winding 5	95	1.5	220	12	dc	2.320E-3

The fourth case involves the same set-up as the third case but this time all noise sources will be turned on from the beginning. While the system is running a sixth noise source will be introduced between sensor 1 and sensor 2. The new noise source will be a Motorola one hyper which is only running a stopwatch. This noise source will be placed at this location after 40 seconds from startup and will be relocated between sensor 5 and 6 at 70 seconds from start-up.

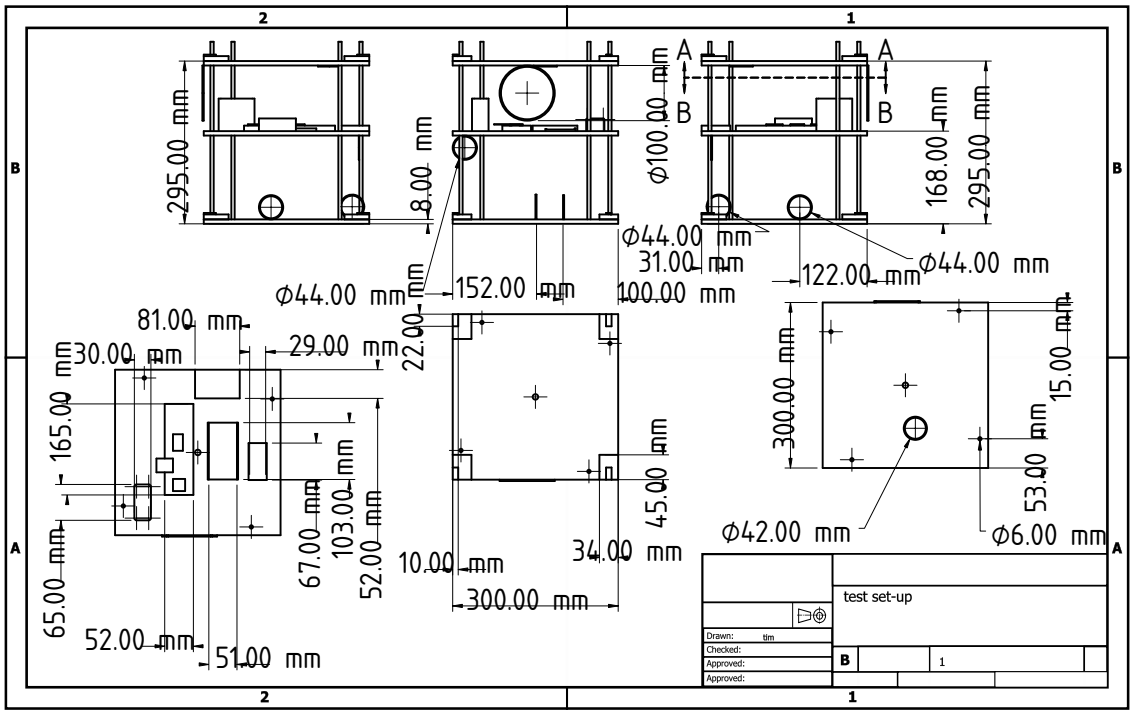

Figure 9.1: Test setup

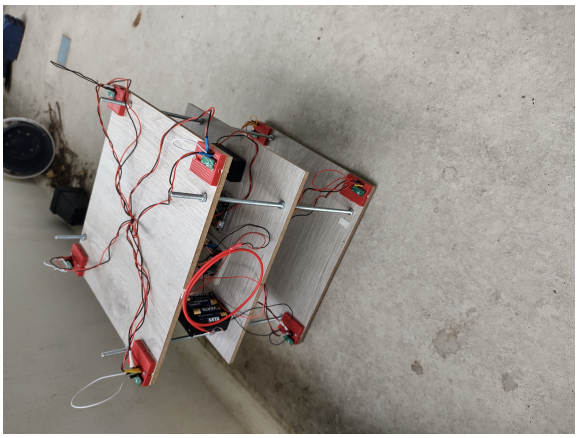

(a) Isometric view

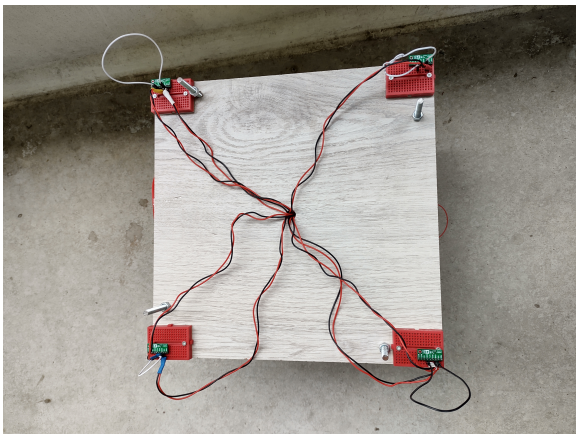

(b) Top view

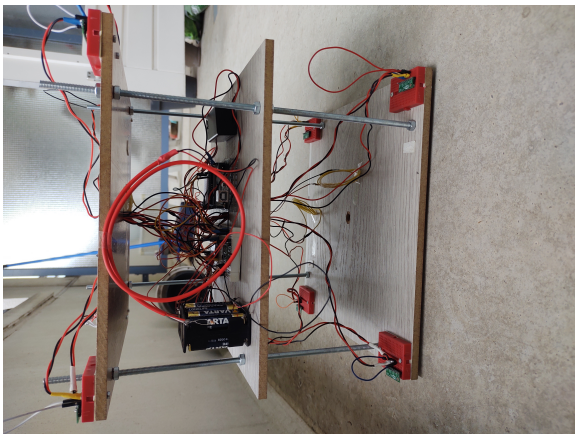

(c) Front view

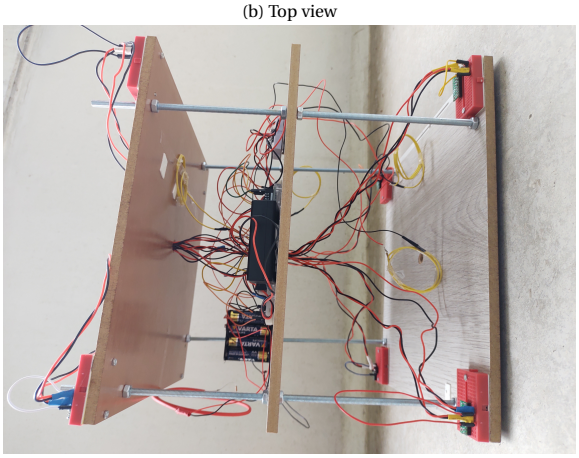

(d) Right side view

Figure 9.2: Test set-up

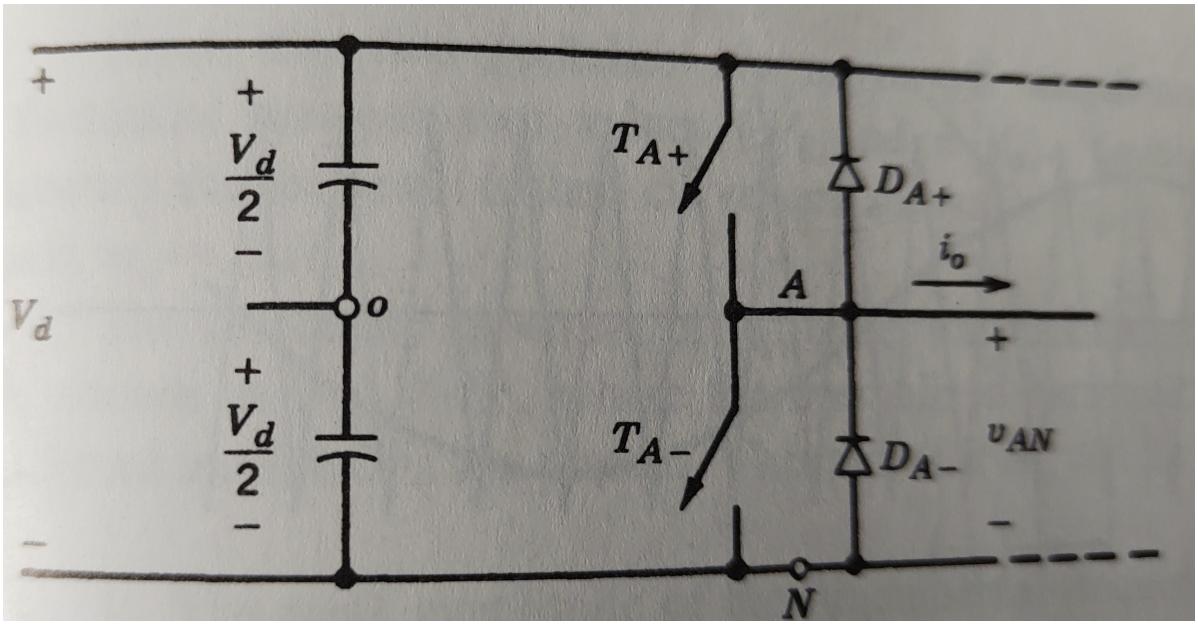

Figure 9.3: One-leg switch-mode inverter as seen in Power electronics by Mohan etal.[5]

10

Test results

The results of the tests performed with the specification from Chapter 9 will be discussed in this Chapter. The tests were performed on 3 May 2021. The values for the Earth magnetic field on the test location on this day are mentioned in Table 10.1.

Four cases were tested as described in Chapter 9. The tests of each case are presented in their own sections, which are Section 10.1 to 10.4. Each of these sections show the measurements per sensor, the results of the averaging method using different combinations of sensors or a combination of the two.

The averaging method is used with eight sensors, six sensors, four sensors and two sensors combinations. Multiple combination of sensors are analysed so that best solution can be found. The sensors used for each combination can be found in Table 10.2. Multiple combinations of two or four sensors are used. The difference between these sets is indicated by the letters a to d.

All the results will be discussed at the same time in Section 10.5.

Table 10.1: Earth magnetic field at 3 may 2021 in the Biesbosch

Direction	Strength	Unit
North	19440.8	nT
East	-499.7	nT
Nadir	44854.3	nT

Table 10.2: The sensors used for each instance of the averaging method. The sensors denoted with a x are used.

Name	Sensor							
	1	2	3	4	5	6	7	8
8 sensors	x	x	x	x	x	x	x	x
6 sensors		x	x	x	x	x		x
4 sensors a			x	x		x		x
4 sensors b	x		x		x			x
2 sensors a			x		x			
2 sensors b		x						x
2 sensors c		x				x		
2 sensors d		x	x					

10.1. Case 1: Testing complete sensor system

The results of testing the complete sensor system as discussed in Chapter 9 can be found in Figure 10.1. There is a range of more than 100000 nT between the minimum and maximum measured magnetic field. To put this into perspective in the x-direction the EMF should be 19440.8 nT so the range of measured values is 514 % bigger than the value that should be measured. This indicates that a new bias is introduced in the sensor by the complete system set-up and thus a re-calibration needs to be performed. The results of all three tests (x-direction pointing North, x-direction pointing West and x-direction pointing South) will be used. Figure 10.1 shows only the x-direction pointing North and the other directions can be found in Appendix C.

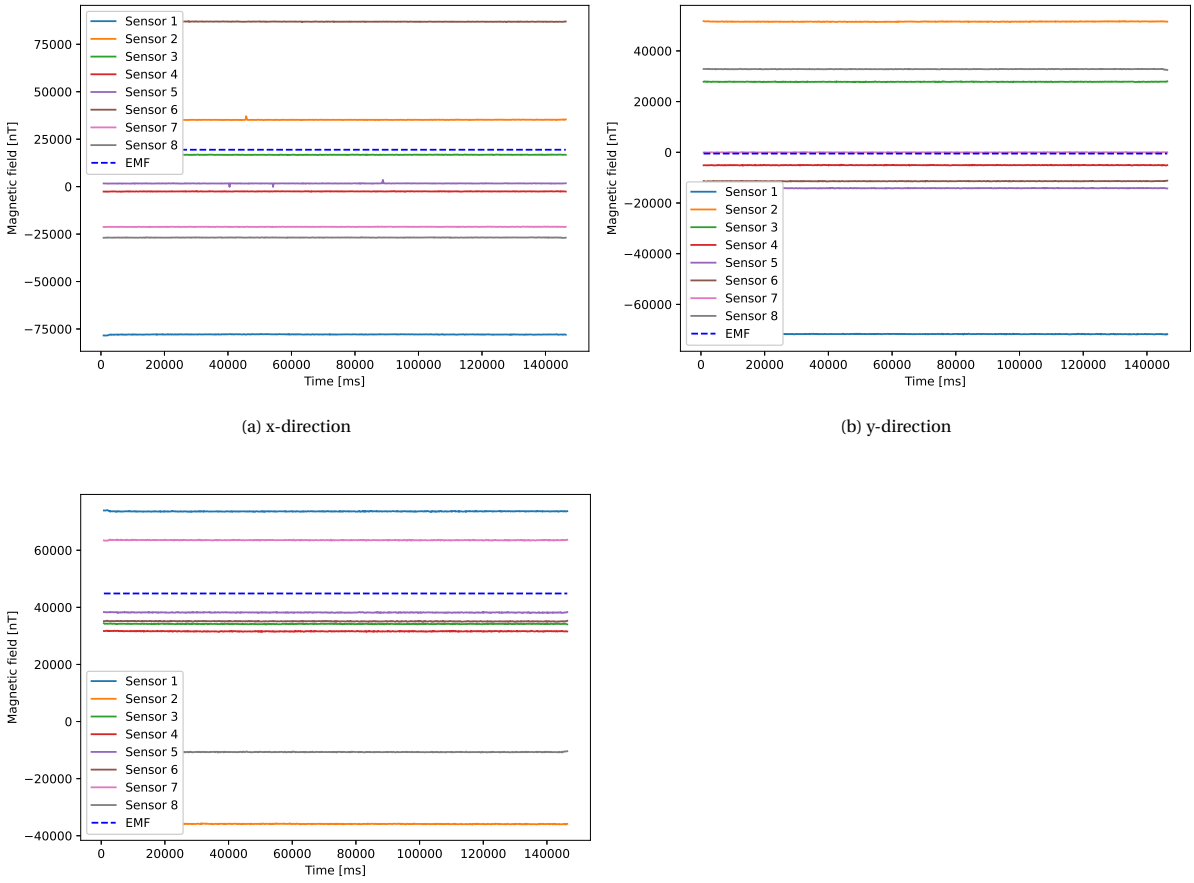

(a) x-direction

(b) y-direction

(c) z-direction

Figure 10.1: The measurements of each sensor in each direction while testing the complete sensor system. The x-direction of the sensors are facing North

The same measurements as displayed in Figure 10.1 after calibration can be found in Figure 10.2. There is still a difference between the sensor measurements and the EMF but is reduced significantly. The maximum error in the x-direction is now 24 % of the EMF. These errors can be explained by the noise generated by the system component in combination with the four iron rods.

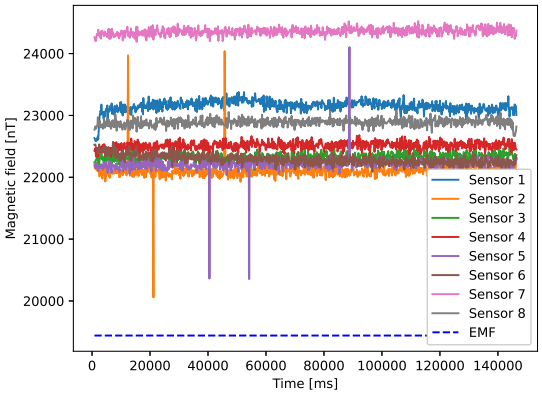

(a) x-direction

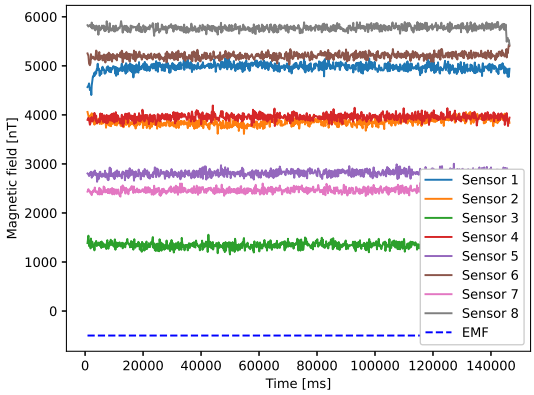

(b) y-direction

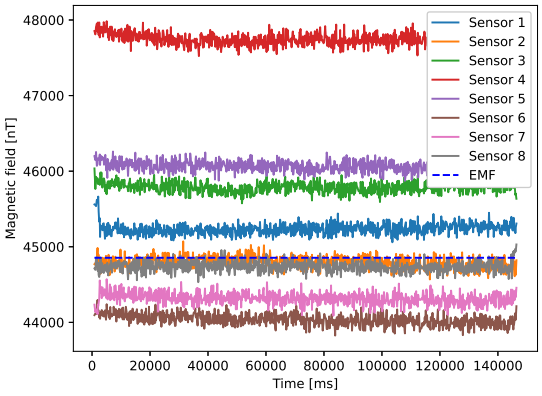

(c) z-direction

Figure 10.2: The measurements of each sensor in each direction while testing the complete sensor system after calibration. The x-direction of the sensors facing North

10.2. Case 2: Testing system including noise sources

Case 2 tests the complete sensor system without noise sources at the start. After 60 seconds the noise sources are turned on to observe the difference. The results of the single sensor measurements can be found in Figure 10.3 and the results of the averaging method can be found in Figure 10.4. At 60 seconds it is clear that the noise sources are switched on which is done in two steps. Winding 5 is turned on first, then all other windings are turned on simultaneously. The different windings and their specification can be found in Chapter 9. The charging of the capacitors can be noticed starting around 65 seconds. The differences in noise level are noticeable in all directions. For some unknown reason a drift is noticeable in the x and y-direction of sensor 1, this was not expected because the set-up without noise sources is the same as case 1 and case 1 doesn't display this characteristic.

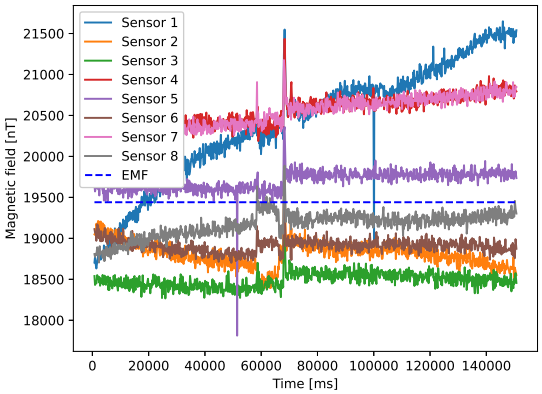

(a) x-direction

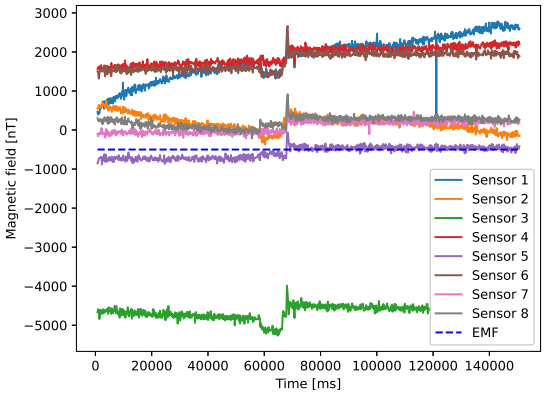

(b) y-direction

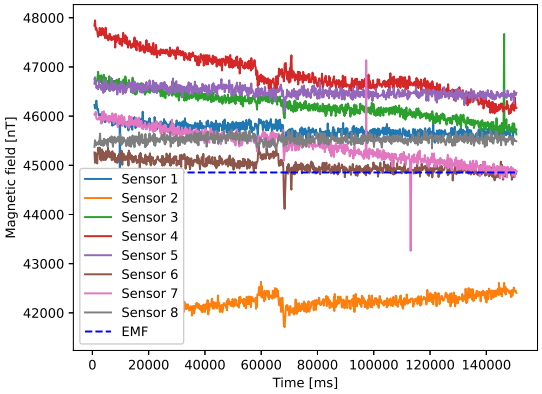

(c) z-direction

Figure 10.3: The measurements of each sensor in each direction while testing the complete sensor system while turning on the noise sources after the test began. The x-direction of the sensors facing North

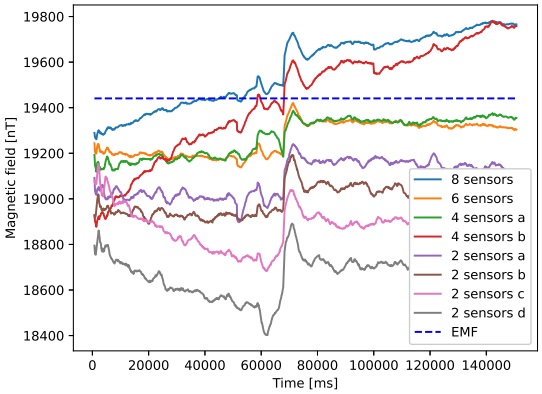

(a) x-direction

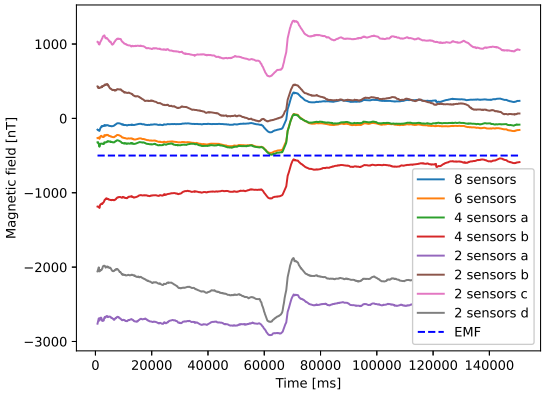

(b) y-direction

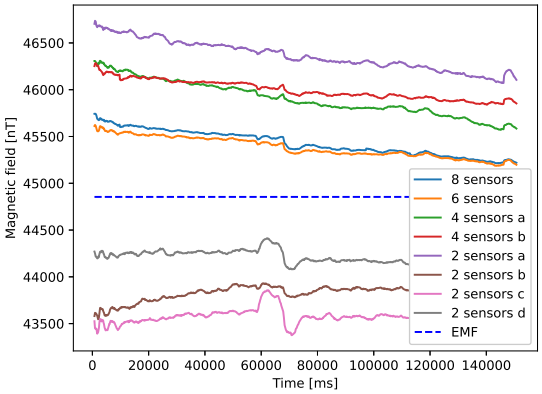

(c) y-direction

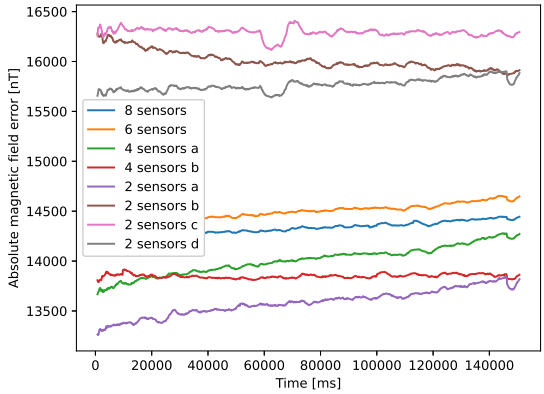

(d) Total absolute error in magnetic field

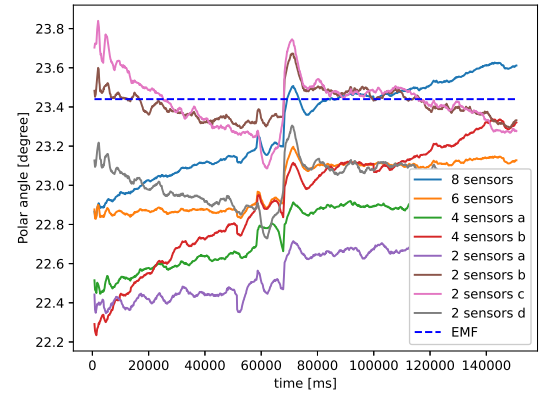

(e) Polar angle

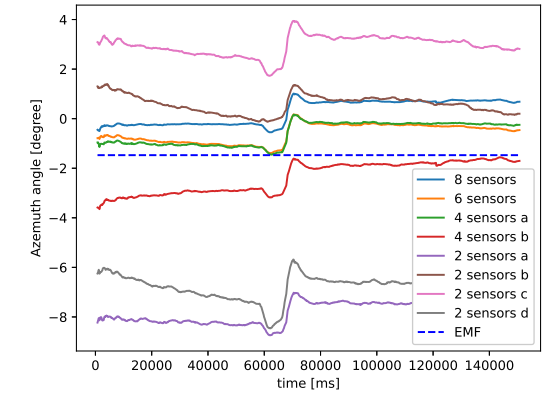

(f) Azimuth angle

Figure 10.4: The average of the measurements of test 2 in each direction while testing the complete sensor system while turning on the noise sources after the test began. The x-direction of the sensors facing North

10.3. Case 3: Rotating around z-axis

The complete set-up is turned around its z-axis in case 3. This includes that the noise sources on the satellite are powered on. The results can be found in Figure 10.5 which shows the angular measurements of two single sensor measurements and three different combinations using the averaging method. The figure also includes scatter plots to visualize the pointing direction of the pointing angles. For these scatter graphs a radius of 1 is assumed. The scatter plot for the azimuth angles shows a complete circle indicating that the sensors of the satellite measured the turning around the z-axis. Although the measurements cannot be compared to a reference magnetic field, a full rotation around the axis can be noticed. The small change in polar angles indicate that the test set-up was not completely level during the test.

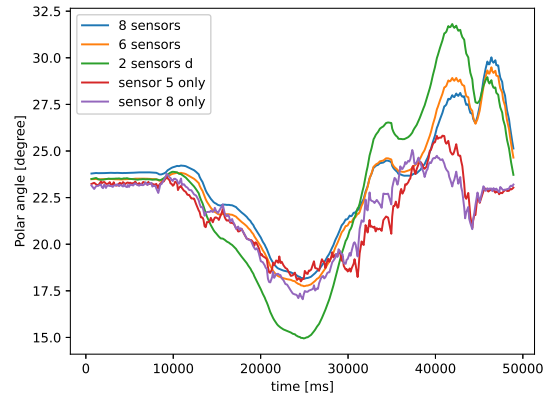

(a) Polar angle

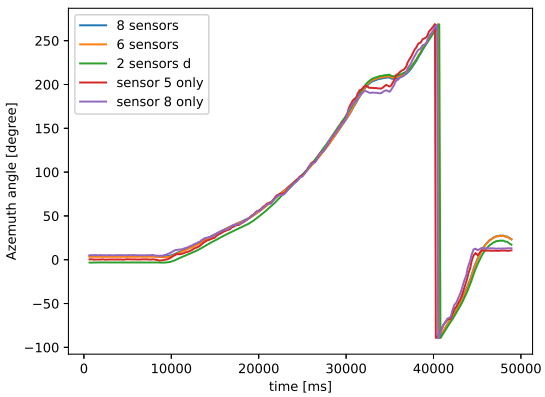

(b) Azimuth angle

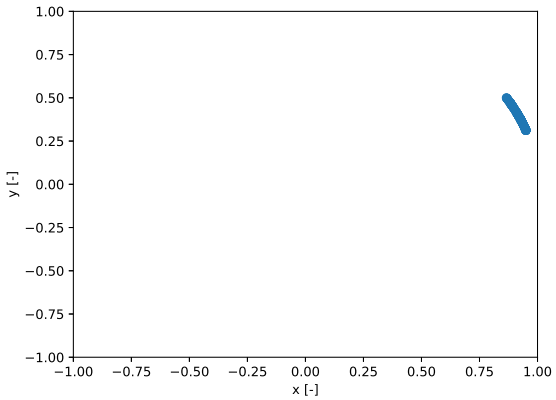

(c) Scatter graph to visualize the pointing direction of the polar angle for the 8 sensors averaging methods

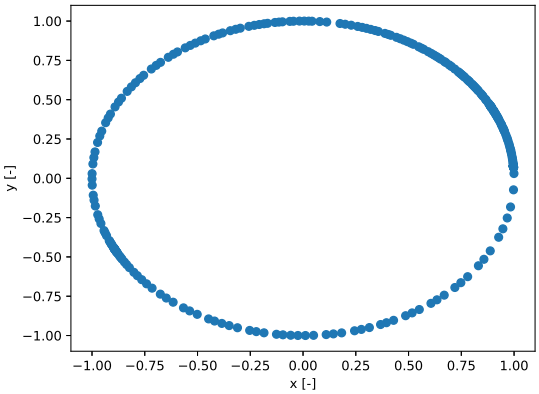

(d) Scatter graph to visualize the pointing direction of the azimuth angle for the 8 sensors averaging methods

Figure 10.5: The average of the measurements and single sensor measurements of test 3 in each direction while testing the complete sensor system with noise sources while rotating around z-axis

10.4. Case 4: Adding external noise source

In case 4 an additional noise source is added to the set-up and moved between two different places. The results can be found in Figure 10.6 where the error between the measured and calculated polar and azimuth angles and the EMF are displayed. The effect of the noise source diminishes if more sensors are used, which can be seen in the measurements of sensor 1 and the averaging method combinations *8 sensors* and *6 sensors* which are described in Table 10.2. This indicates the benefit of using multiple sensors.

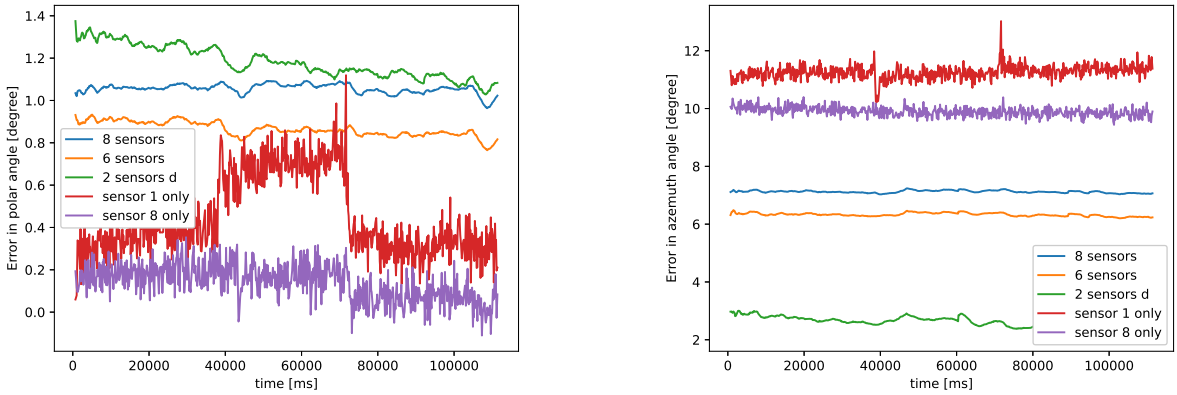

(a) Polar angle

(b) Azimuth angle

Figure 10.6: The error of the polar and azimuth angles of two single sensor measurements and three different combinations using the averaging method compared to the EMF while testing the complete sensor system with changing noise source. The x-direction of the sensors facing North

10.5. Test conclusion

Multiple conclusions can be made from the test results presented in Figures 10.1 to 10.6. First of all the requirement NMAG-1a-INSTR3 for a scientific instrument which states that the maximum sensitivity of the sensor system needs to be 0.5 nT is never met in the single measurements and the averaging method which was concluded in Chapters 6 and 7. A box-plot of the error between the EMF and measured data and calculated averages can be found in Figure 10.7. This figure shows that the median can be two to three orders of magnitude bigger than the maximum sensitivity. The maximum sensitivity for an attitude control sensor system is 50 nT as stated by requirement NMAG-1a-INSTR2. The range of the box-plots are still 0.5 to 1 orders of magnitudes bigger than the requirement for attitude control. The desired attitude accuracy of at least 3° as described in requirement NMAG-1a-INSTR5 is only achieved for the polar angles where the maximum error is 1.5°. The maximum detected error for the azimuth angle is 7.5° which is more than two times the desired accuracy as seen in Figure 10.6. One of the displayed averaging methods also complies to the 3° accuracy requirement for the azimuth angles which is the combination *2 sensors d*as presented in Table 10.2. The same can be observed in Figure 10.4 indicating that the accuracy requirement for pointing direction can be met with some sensor configurations. Although the pointing accuracy requirement can be met, the requirement NMAG-1a-INSTR6 which says the magnetic field accuracy of the system should be 50 nT is never met. The magnetic field accuracy varies with 0.5 and 2 orders of magnitude and thus indicates that the assumption made for the requirement in Section 2.1 was insufficient and the requirement should be dropped.

The second observation that can be made from Figure 10.7 is the effectiveness of using the averaging method. The range of the errors of the averaging method are lower in all directions if a combination of sensors is used compared to single sensor measurements if all single sensors measurements behave as expected. For example the 8 sensors is heavily influenced by the results of the sensor 1 measurements in the x- and y-direction as can be seen in Figure 10.3. Looking at the accuracy sensor 5 has the smallest error in both the x and y-direction (with an -3.8 and 720 % error compared to EMF respectively). Although sensor 5 has the biggest error in the z-direction (with an 2.7 % error compared to EMF) it still compensates for having the lowest error in the y-direction by >700 nT (>100% error compared to the EMF). This leads to the conclusion that the error of the averaging method is more consistent in all directions and is less sensitive to magnetic noises compared to single measurements. Figure 10.6 confirms this with filtering out the magnetic noise seen in the measurements of sensor 1. A single sensor can still have a better accuracy than using multiple sensors which happens with sensor 5 as shown in Figure 10.7.

The third observation relates to the time between measurements which varies between 0.11 and 0.22 seconds which is bigger than the 0.1 s (10 Hz) mentioned in requirement NMAG-1a-INSTR4. The time between measurements mentioned are for the complete 8 sensor system. The time increments will become smaller with a sensor system with less sensors. The most time consuming process in the used set-up is writing the data to a SD card with a time between 0.04 s and 0.08 s.

This all leads to the conclusion that the proposed system set-up in combination with the averaging method is not sufficient as a attitude sensor without further knowledge of the satellite system. If an analysis of the

noise behavior of the complete satellite system is performed then there might be a possibility to create a sensor system that conforms to the NMAG-1a-INSTR2 requirement.

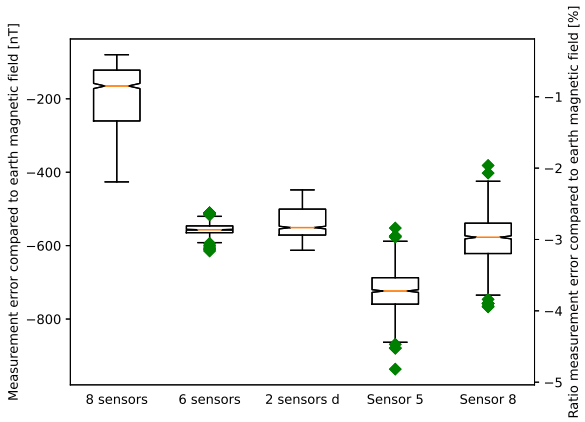

(a) x-direction

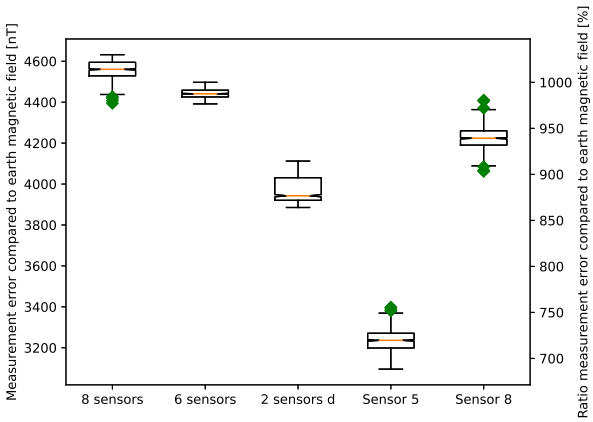

(b) y-direction

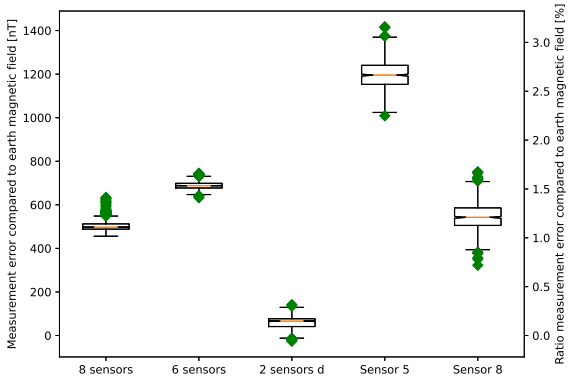

(c) z-direction

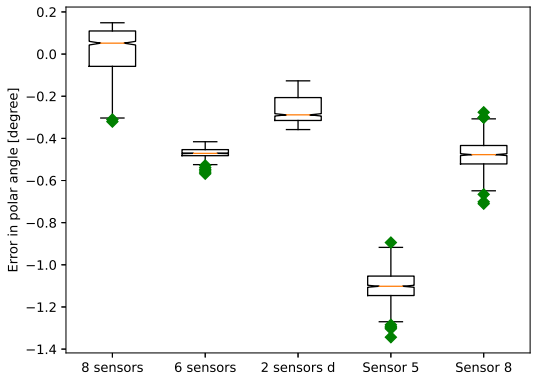

(d) Polar angle

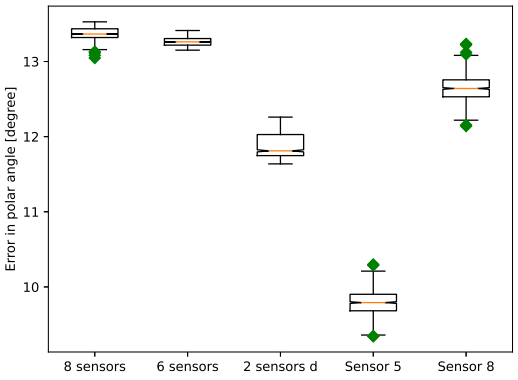

(e) Azimuth angle

Figure 10.7: Box plots of the error compared to the EMF and the averages of different combinations and two single sensor measurements from case 2 with x-direction pointing north

11

Conclusions and recommendations

This research was performed to answer the following question:

Is it possible to create a magnetic field instrument consisting of multiple magnetometers from low cost COTS components which can provide relevant data for attitude control and/or scientific data and can be positioned inside a satellite without special modifications?

Some of these points need to have some explanation. The low cost indicates a maximum cost of €2000 and €10000 for an attitude control and scientific instrument respectively. Special modifications indicate measurements placing the instrument on a boom and techniques that require extensive research.

Three related sub-questions were found to support the main question, which are the following:

- What is the effect of multiple sensors?
- Is there a number of sensors at which adding more won't affect the outcome?
- What is the effect of sensor placement?

The requirements for a sensor system to be an attitude control and/or scientific instrument is as follows. For both kind of systems (attitude or scientific) a measuring frequency of at least 10 Hz is preferred [NMAG-1a-INSTR4]. The sensitivity for an attitude control instrument needs to be 50 nT or less [NMAG-1a-INSTR2] and for a scientific instrument 0.5 nT or less [NMAG-1a-INSTR3]. The research was split in two related parts to answer the question. The two parts were software and hardware which were verified by a simulation and test respectively. The software includes the different methods devised to calculate the Earth magnetic field from the measurement data. The hardware includes the selection of components such as the sensors and the design of the sensor system. The hardware also includes the architecture of the system and the data management. The sensor placement with respect to the noise sources and the number of sensors used relates to both the software and the hardware.

11.1. Simulation

Two sensor measurements processing methods were explored for their effectiveness. The first method is called the averaging method which as its name implies averages the measured data of each sensor in the system. The second method uses a system of equations (SOE) to calculate the Earth magnetic field and the characteristics of the noise sources. These characteristics include the position of the noise sources in the satellite, the orientation of the noise sources and the dipole moment. This method is called the SOE method.

Most calculations during the simulations had an accuracy of more than 40 nT to 1200 nT. Both the methods are unable to consistently achieve the NMAG-1a-INSTR7 requirement for a scientific instrument which state that an accuracy of 0.5 nT is required. This means that the simulated accuracy of at least 3 orders of magnitude bigger than the requirement. The averaging method is able to comply to the NMAG-1a-INSTR6 for attitude control, which states that an accuracy of 50 nT is desired. There are also cases where the accuracy is multiple orders of magnitude bigger. The small set of arrangements that achieve the mentioned 50 nT accuracy requirement depend heavily on the placement of the sensors, noise sources and dipole strength of the

noise sources. Placing the sensors in one or more corners of the satellite is one of most promising configurations for the sensors because of two reasons. The first reason relates to the volume necessary for the sensors. The sensor needs to have a minimum distance from the closest noise source, this results in a sphere around the sensor that cannot contain electronic devices. If the sensors are placed in the corners of the satellite, then only an eighth of this sphere impacts the design of the satellite. The second reason is the symmetrical placing of the sensors which leads to a more accurate result due to the canceling of magnetic noise when sensors are on two sides of a noise source. The placement of eight sensors in each corner is not perfect and its effectiveness still depend on the noise source strength and configuration because a large noise source at 5 cm from a sensor can still have a large effect on the total results. The computational time for the averaging method was far below the 10 Hz allowed for the complete system with 6.78E-5 seconds per calculation for an eight sensor system.

The SOE method couldn't comply to the NMAG-1a-INSTR6 for attitude control except for situations where there are at least 3 times the number of sensors than the number of noise sources. This is physically not possible in a satellite system with multiple noise sources. The reason for the ratio between the high number of sensors needed versus the number of noise sources is the difference between unknowns and equations. The relation between necessary sensors and noise sources to get a determined system is as follows: $3 \cdot N_{sensors} \geq 6 \cdot N_{noisesources} + 3$. The SOE method will always use an undetermined SOE because more noise sources are present than sensors and therefore multiple possible solutions for the magnetic field will be found by the SOE method. The results were limited by using physical limitations such as the size of the satellite and the average of the sensor measurements. Even limiting the outcome by using the previous results was considered. All the limitations or a subset of them resulted in an absolute error worse or equal to the averaging method. In addition the computation time is very dependent on the number of sensors and number of noise sources with computational time ranging from 7 order of magnitude longer compared to the averaging method while using 1 sensor with 6 noise sources configuration to 8 order of magnitude longer compared to the averaging method using 8 sensors and 6 noise sources configuration. These computation times are far off from the desired 10 HZ for the complete system. Therefore the SOE method is not useful for a sensor system where the noise sources are completely unknown.

11.2. Test

The hardware chosen for the sensor system is a combination of an Arduino mega 2560, an AdafruitMicroSD card breakout board+, a multiplexer, a 12 V and a 9 V power source and eight LSM303d magnetic sensors. The LSM303d magnetic sensors are the heart of the system and were chosen for their sensitivity of 8 nT and price combination. This sensor system was tested in combination with a set of five noise sources in a satellite set-up which represents a 30 cm^3 cubesat. The individual sensors were placed in the eight corners of the test set-up.

The sensor system used was able to perform measurements at a frequency between 9.1 and 5 Hz. This doesn't comply to the 10 Hz minimum set as requirement but could be acceptable as an attitude control instrument if the desired 50 nT sensitivity was reached. Unfortunately the 50 nT sensitivity was not reached by the sensor system in combination with the averaging method, because the actual range of values of the complete system has a 0.5 to 1 order of magnitude difference. The accuracy requirement for attitude control NMAG-1a-INSTR5 states that an accuracy of 3 degrees or less should be achieved. This was achieved by the system for the polar angles with a maximum error of 1.4 degrees. The Azimuth angles had a maximum error of 7.5 degrees and thus do not comply to the 3 degree requirement. Only a couple of sensor configurations can get an accuracy of maximum 3 degrees.

During the tests, each individual measurement was compared to the results of the averaging method. The method was applied to different combinations of sensors. Both the individual measurement and the results of the averaging method were compared to the actual Earth magnetic field. The averaging method was able to produce better results than the individual sensor measurements when multiple sensors are used. The dependency on the measurements of a single sensor becomes less with an increase in number of sensors used.

Because the essential requirements for sensitivity, accuracy and measuring frequency are all not consistently achieved, it can be concluded that it is not possible to create a magnetic field instrument consisting of multiple magnetometers from cheap COTS components which can provide relevant data for attitude control and/or scientific data and can be positioned inside a satellite without special modifications with the methods and set-up presented in this research. Multiple sensors can improve the resulting Earth magnetic field mea-

surements compared to a single sensor especially in case of sensitivity. For the averaging method presented in the research it takes minimum 2 sensors to provide a better result than a well-placed single sensor.

Sensor placement is the most important part for designing the sensor system because a close noise source will largely influence the measurements of the complete sensor system even if measurements processing methods are used. Therefore systems with only one or two sensor perform better than a system with eight sensors if the averaging method is used. The SOE method while having a great potential needs more than eight sensors which is the maximum acceptable sensors to use.

11.3. Recommendations

One of the premises of the thesis was to be able to measure the Earth magnetic field without having the knowledge of the noise sources in a satellite. This knowledge however will improve the measurements of a single sensor and therefore should also improve the results of both presented measurement processing methods. In case of the SOE method it would reduce the number of unknowns drastically if only the locations of the noise sources were known. So less sensors are needed to achieve a determined system. This would also lead to an improved computational time.

Not every noise source is easily identified especially noise sources that use a varying current. An example of such a noise source are AC systems or systems that have an on and off state. A better understanding of these systems' electromagnetic field can be gained with current sensors in combination with self-learning programs to accurately define the noise caused by these fields. So it will be possible to determine the exact noise generation with the knowledge of the current. Such a self-learning program in combination with the SOE method could be able to identify the locations and direction of the noise sources so that the number of unknowns can be decreased.

Doing an analysis of the noise source also identifies the sources with the largest potential magnetic field and thus largest dipole. The placement of the sensors should be done based on this knowledge so that the sensors are placed at the largest distance possible to reduce their effect even if this would mean that a lower number of sensors are used.

A one dimensional Kallman filter was used for the computational methods. To increase the performance of the computational methods it is recommended to include an Extended Kallman filter.

The test set-up can be improved in multiple ways such as including more Arduinos to simulate different systems in a satellite or use a satellite component. A payload like a camera or a power system including solar cells can be used.

During calibration it became clear that the complete system in the satellite should be taken into account. In the thesis this was only done using a static test and should be extended with a rotational tool that is also used for the single sensor calibration. This tool should be built of materials with a low magnetic permeability

A

Requirements

code	Description	Value	Complaint	Comment
NAMG	The magnetic field instrument should be able to measure the Earth magnetic field in space			
NMAG-1	The magnetic field instrument should be able to measure the Earth magnetic field in space in a technical feasible manner			
NMAG-2	The magnetic field instrument should be able to measure the Earth magnetic field in space within constraints			
NMAG-1a	The magnetic field instrument should be able to measure both direction and the size of the magnetic field	-	yes	
NMAG-1b	The magnetic field instrument should be made using only COTS products	-	yes	
NMAG-1c	The magnetic field instrument should be able to fit in a microsat	-	yes	
NMAG-2a	The magnetic field instrument should have a low cost	-	yes	
NMAG-2b	The creation and testing of the instrument should comply with the designated deadlines	-		
NMAG-2c	The combined instrument and testing cost should not exceed €500	€30	yes	
NMAG-1a-INSTR1	The magnetic field instrument should have a measuring range of +/- 100 μT	200 μT	yes	
NMAG-1a-INSTR2	The magnetic field instrument should have a sensitivity of at maximum 50 nT if used for attitude control	>200 nT	no	
NMAG-1a-INSTR3	The magnetic field instrument should a sensitivity of at maximum 0.5 nT if used as a scientific instrument	>200 nT	no	
NMAG-1a-INSTR4	The magnetic field instrument should be able to preform at least 10 samples per second	9 Hz	no	
NMAG-1a-INSTR5	The magnetic field instrument should have an accuracy of at least 3 degrees if used for attitude control	2.9 - 7.5 degrees	yes/no	depends on the situation
NMAG-1a-INSTR6	The magnetic field instrument should have an accuracy of at least 50 nT if used for attitude control	>200 nT	no	Can be dropped, is to restrictive
NMAG-1a-INSTR7	The magnetic field instrument should have an accuracy of at least 0.5 nT if used as scientific instrument	>200 nT	no	
NMAG-2a-INSTR1	The magnetic field instrument should cost less the €10000 if it is used for scientific means	€220	yes	
NMAG-2a-INSTR2:	The magnetic field instrument should cost less the €2000 if it is used for attitude control	€220	yes	

B

Noise source configurations

The following tables show the noise source configurations for simulation set one and two. In these tables noise source four relates to the power system, noise source three relates to AC systems in the satellite and noise source two relates to the systems with a on/off state as discussed in Section 7.2.2

Table B.1: Noise source configuration 1

source number	x-location [m]	y-location [m]	z-location [m]	m [$\frac{N \cdot m}{T}$]	theta [rad]	phi [rad]	m_{vary} [$\frac{N \cdot m}{T}$]	f [$\frac{N \cdot m}{T}$]
1	0.165239	0.268888	0.00896286	0.0285454	1.50378	0.812377	-	-
2	0.212444	0.0376756	0.13705	-0.149546	1.49817	3.47635	-	3.70E-4
3	0.0872714	0.0621729	0.194743	0.0184896	1.37048	1.18008	2.805e-05	69.6207
4	0.153248	0.0154402	0.0835462	-0.0756331	1.41835	5.98223	-2.156E-4	-
5	0.267884	0.132243	0.202876	-0.0266717	1.47052	4.28269	-	-

Table B.2: Noise source configuration 2

source number	x-location [m]	y-location [m]	z-location [m]	m [$\frac{N \cdot m}{T}$]	theta [rad]	phi [rad]	m_{vary} [$\frac{N \cdot m}{T}$]	f [$\frac{N \cdot m}{T}$]
1	0.0340465	0.239881	0.0767977	-0.055855	1.26306	6.14476	-	-
2	0.292345	0.193669	0.00720341	-0.0988049	1.11193	3.78273	-	3.70E-4
3	0.21862	0.12438	0.0296178	0.131065	1.0144	5.24832	-2.242E-4	13.58
4	0.10544	0.211809	0.0901309	-0.0719674	0.917075	0.536432	-3.109E-4	-
5	0.212282	0.0739948	0.192257	-0.071142	1.01779	3.06802	-	-

Table B.3: Noise source configuration 3

source number	x-location [m]	y-location [m]	z-location [m]	m [$\frac{N \cdot m}{T}$]	theta [rad]	phi [rad]	m_{vary} [$\frac{N \cdot m}{T}$]	f [$\frac{N \cdot m}{T}$]
1	0.14838	0.298972	0.103962	0.0188361	0.357567	0.08737	-	-
2	0.0684249	0.122459	0.105529	-0.0585622	0.547704	3.70023	-	3.70E-4
3	0.0766422	0.231568	0.0436401	0.121957	1.13565	2.40642	1.058E-4	52.89
4	0.118899	0.228161	0.291799	0.0548437	1.56536	0.721429	4.484E-5	-
5	0.113195	0.0930028	0.272754	-0.0342159	1.53592	5.43152	-	-

Table B.4: Noise source configuration 4

source number	x-location [m]	y-location [m]	z-location [m]	m [$\frac{N \cdot m}{T}$]	theta [rad]	phi [rad]	m_{vary} [$\frac{N \cdot m}{T}$]	f [$\frac{N \cdot m}{T}$]
1	0.0606607	0.243109	0.260992	-0.154957	1.27015	0.503062	-	-
2	0.235364	0.21403	0.142928	0.0681349	0.826783	5.89047	-	3.70E-4
3	0.258161	0.198399	0.0240813	-0.136635	1.2261	6.01634	-9.961E-5	53.05
4	0.0981256	0.213147	0.0446311	-0.0239246	0.795877	3.42065	1.960E-4	-
5	0.0746581	0.0338703	0.0972073	0.0957807	1.51706	3.04567	-	-

C

Test results

C.1. Non-calibrated measurements without noise

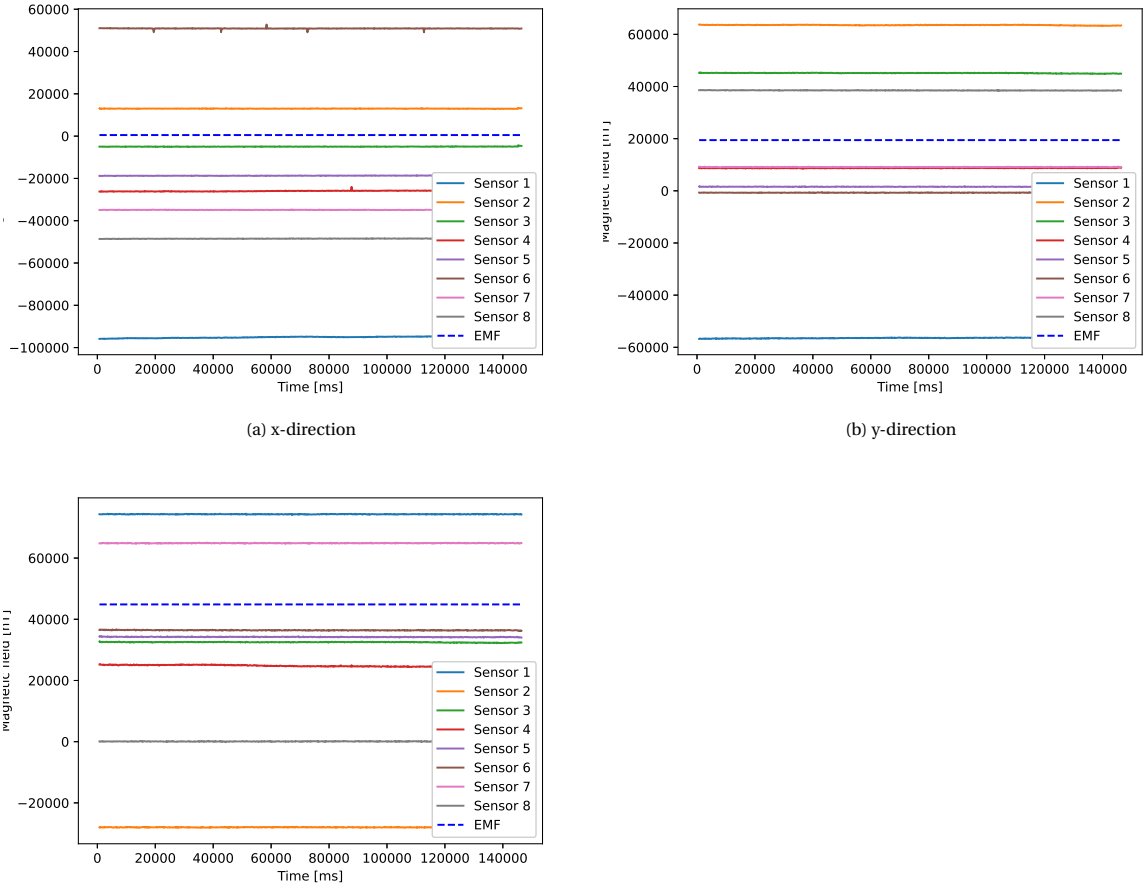

(a) x-direction

(b) y-direction

(c) z-direction

Figure C.1: The measurements of each sensor in each direction while testing the complete sensor system. The x-direction of the sensors are facing East

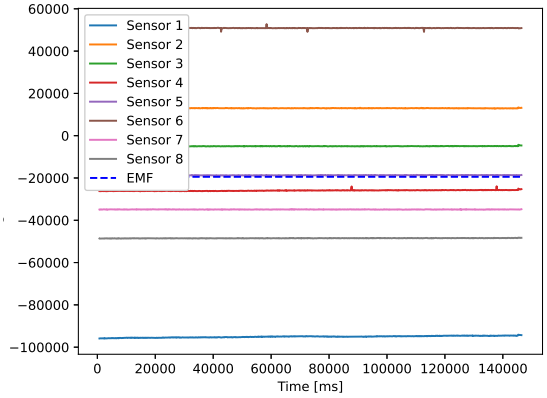

(a) x-direction

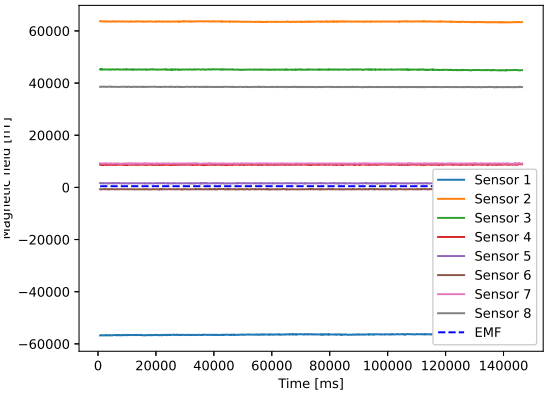

(b) y-direction

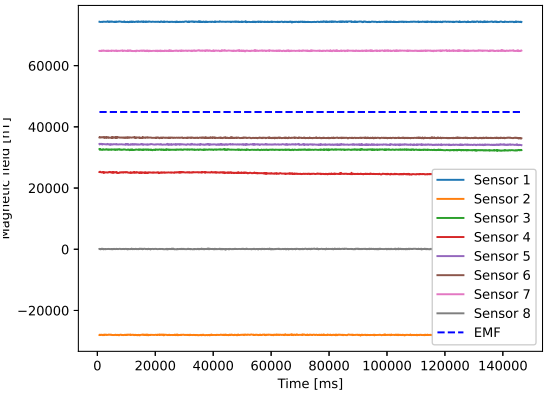

(c) z-direction

Figure C.2: The measurements of each sensor in each direction while testing the complete sensor system. The x-direction of the sensors are facing South

C.2. Calibrated measurements without noise

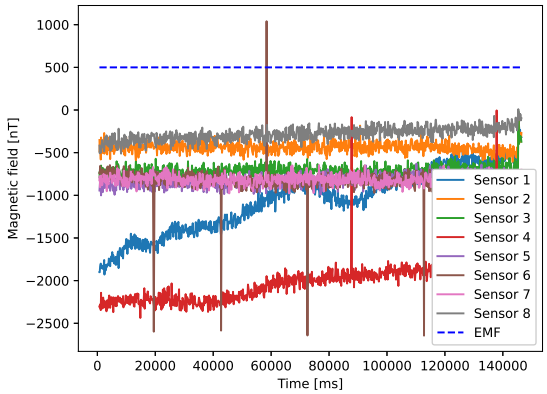

(a) x-direction

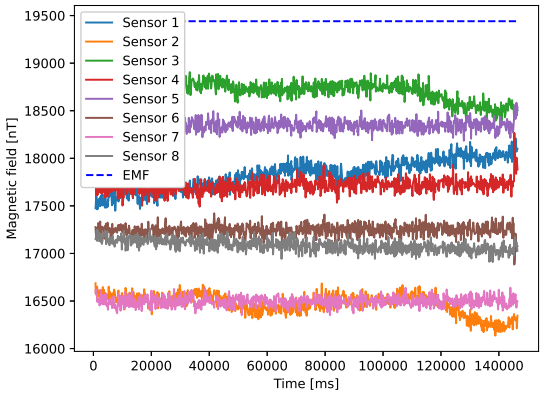

(b) y-direction

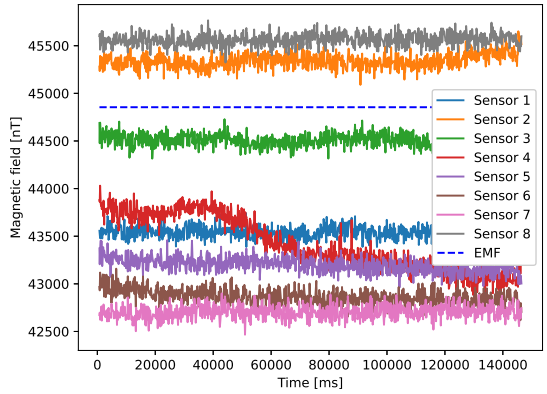

(c) z-direction

Figure C.3: The measurements of each sensor in each direction while testing the complete sensor system after calibration. The x-direction of the sensors facing West

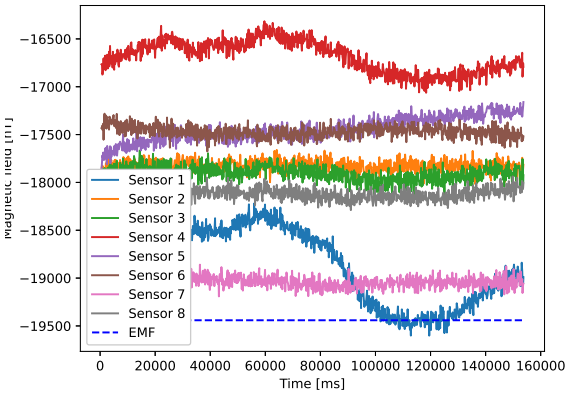

(a) x-direction

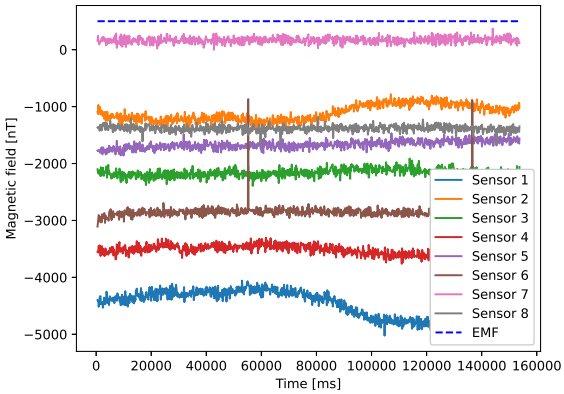

(b) y-direction

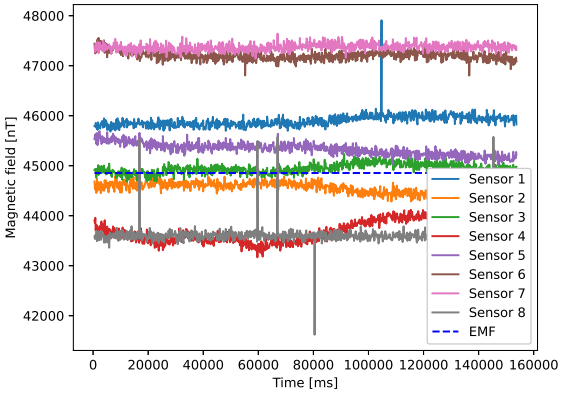

(c) z-direction

Figure C.4: The measurements of each sensor in each direction while testing the complete sensor system after calibration. The x-direction of the sensors facing South

Bibliography

[1] HAN Ke, WANG Hao, Tian XIANG, and JIN Zhonghe. Magnetometer compensation scheme and experimental results on zdps-1a pico-satellite. *Chinese Journal of Aeronautics*, 25(3):430–436, 2012.

[2] Supratik Banerjee. *Compressible turbulence in space and astrophysical plasmas: Analytical approach and in-situ data analysis for the solar wind*. PhD thesis, Paris 11, 2014.

[3] A Dandridge, AB Tveten, GH Sigel, EJ West, and TG Giallorenzi. Optical fibre magnetic field sensors. *Electronics Letters*, 16(11):408–409, 1980.

[4] Jozef Hudák, Josef Blažek, František Kmec, Katarína Draganová, and P Lukác. Multi-position static test of magnetometer from imu. *J. Electr. Eng*, 61(7):24–27, 2010.

[5] Mohan N Undeland, William P Robbins, and N Mohan. Power electronics. In *Converters, Applications, and Design*. John Whiley & Sons, 1995.

[6] NewSpace Systems. Newspace systems magnetometer, July, 2014. NMRM-Bn25o485 datasheet.

[7] DM Miles, IR Mann, M Ciurzynski, D Barona, BB Narod, JR Bennest, IP Pakhotin, A Kale, B Bruner, CDA Nokes, et al. A miniature, low-power scientific fluxgate magnetometer: A stepping-stone to cube-satellite constellation missions. *Journal of Geophysical Research: Space Physics*, 121(12):11–839, 2016.

[8] Eigil Friis-Christensen, H Lühr, and Gauthier Hulot. Swarm: A constellation to study the earth's magnetic field. *Earth, planets and space*, 58(4):351–358, 2006.

[9] Marina Díaz-Michelena. Small magnetic sensors for space applications. *Sensors*, 9(4):2271–2288, 2009.

[10] Mark L Psiaki. Global magnetometer-based spacecraft attitude and rate estimation. *Journal of Guidance, Control, and Dynamics*, 27(2):240–250, 2004.

[11] Hongliang Ma and Shijie Xu. Magnetometer-only attitude and angular velocity filtering estimation for attitude changing spacecraft. *Acta Astronautica*, 102:89–102, 2014.

[12] Nobuo Sugimura, Toshinori Kuwahara, and Kazuya Yoshida. Attitude determination and control system for nadir pointing using magnetorquer and magnetometer. In *2016 IEEE Aerospace Conference*, pages 1–12. IEEE, 2016.

[13] MARIO H ACUNA. The magsat precision vector magnetometer. *Johns Hopkins APL Technical Digest*, 1:210–213, 1980.

[14] Tian Xiang, Tao Meng, Hao Wang, Ke Han, and Zhong-He Jin. Design and on-orbit performance of the attitude determination and control system for the zdps-1a pico-satellite. *Acta Astronautica*, 77:182–196, 2012.

[15] A Balogh, To J Beek, RJ Forsyth, PC Hedgecock, RJ Marquedant, EJ Smith, DJ Southwood, and BT Tsurutani. The magnetic field investigation on the ulysses mission-instrumentation and preliminary scientific results. *Astronomy and Astrophysics Supplement Series*, 92:221–236, 1992.

[16] spaceflight101. Swarm – instrument overview, 2020.

[17] Klaus Krogsgaard. Compact vector magnetometer for pico satellites. 2003.

[18] P Volegov, A Matlachov, J Mosher, MA Espy, and RH Kraus Jr. Noise-free magnetoencephalography recordings of brain function. *Physics in Medicine & Biology*, 49(10):2117, 2004.

[19] T Katila. Principles and applications of squid sensors. In *Advances in biomagnetism*, pages 19–32. Springer, 1989.

[20] GS Waters and PD Francis. A nuclear magnetometer. *Journal of Scientific Instruments*, 35(3):88, 1958.

[21] GEM Systems. Short review of nuclear precession scalar magnetometers, 2020.

[22] Tim M Tierney, Niall Holmes, Stephanie Mellor, José David López, Gillian Roberts, Ryan M Hill, Elena Boto, James Leggett, Vishal Shah, Matthew J Brookes, et al. Optically pumped magnetometers: From quantum origins to multi-channel magnetoencephalography. *NeuroImage*, 2019.

[23] George B Hospodarsky. Spaced-based search coil magnetometers. *Journal of Geophysical Research: Space Physics*, 121(12):12–068, 2016.

[24] Christophe Coillot, Paul Leroy, and K Kuang. Induction magnetometers principle, modeling and ways of improvement. In *Magnetic Sensors—Principles and Applications*, number 1. InTech, 2012.

[25] Alfredo García-Arribas, Eduardo Fernández, and DD Cos. Thin-film magneto-impedance sensors. In *Magnetic Sensors-Development Trends and Applications*. InTech, 2017.

[26] Jinde Yin, Peiguang Yan, Hao Chen, Li Yu, Junfeng Jiang, Min Zhang, and Shuangchen Ruan. All-fiber-optic vector magnetometer based on anisotropic magnetism-manipulation of ferromagnetism nanoparticles. *Applied Physics Letters*, 110(23):231104, 2017.

[27] AKM. Ak09940 ultrahigh precision 3-axis electronic magnetometer, november, 2018. AK09940 datasheet.

[28] ST. Ultra compact high performance e-compass 3d accelerometer and 3d magnetometer module, June, 2012. LSM303D datasheet.

[29] ROHM. 3-axis digital magnetometer ic bm1422agmv, october, 2016. BM1422AGMV datasheet.

[30] ST. inemo inertial module: 3d accelerometer, 3d gyroscope, 3d magnetometer, March, 2015. LSM9DS1 datasheet.

[31] ST. Digital output magnetic sensor: ultra-low-power, high-performance 3-axis magnetometer, May, 2015. LIS3MDL datasheet.

[32] QST. 3-axis magnetic sensor qmc5883l, February, 2016. QMC5883L datasheet.

[33] Honeywell. 3-axis magnetic sensor hybrid hmc2003, march, 2011. HMC2003 datasheet.

[34] Thomas L Saaty. Decision making with the analytic hierarchy process. *International journal of services sciences*, 1(1):83–98, 2008.

[35] Paul Myers. Interfacing using serial protocols using spi and i2c. *Proc. ESP*, 2005:1–9, 2007.

[36] Storey Neil. *Electronics: A Systems Approach, 4/E*. Pearson Education Limited, 2009.

[37] NOAA. Compute earth's magnetic field values, 2020.